8-2019

Impact of Excitation-Inhibition Balance/Imbalance on Dynamics of Cortical Neural Networks

Vidit Agrawal
University of Arkansas, Fayetteville

Impact of Excitation-Inhibition Balance/Imbalance on Dynamics of Cortical Neural Networks

A dissertation submitted in partial fulfillment
of the requirements for the degree of
Doctor of Philosophy in Physics

by

Vidit Agrawal
Indian Institute of Science Education and Research Mohali
Integrated Bachelor of Science-Master of Science, 2014

August 2019
University of Arkansas-Fayetteville

This dissertation is approved for recommendation to the Graduate Council.

_____
Woodrow L. Shew, Ph.D.
Dissertation Director

_____
Pradeep Kumar, Ph.D.
Committee Member

_____
Yong Wang, Ph.D.
Committee Member

ABSTRACT

The purpose of this research is to study the implications of Excitation/Inhibition balance and imbalance on the dynamics of ongoing (spontaneous) neural activity in the cerebral cortex region of the brain.

The first research work addresses the question that why among the continuum of Excitation-Inhibition balance configurations, particular configuration should be favored? We calculate the entropy of neural network dynamics by studying an analytically tractable network of binary neurons. Our main result from this work is that the entropy maximizes at regime which is neither excitation-dominant nor inhibition-dominant but at the boundary of both. Along this boundary we see there is a trade-off between high and robust entropy. Weak synapse strengths yield entropy which is high but drops rapidly under parameter change. Strong synapse strengths, on the other hand yield a lower, but more robust, network entropy.

The second research work is motivated from experiments suggest that the cerebral cortex can also operate near a critical phase transition. It has been observed in many physical systems that the governing physical laws obey a fractal symmetry near critical phase transition. This symmetry exists irrespective of the observational length-scale. Thus, we hypothesize that the laws governing cortical dynamics may obey scale-change symmetry. We test and confirm this hypothesis using two different computational models. Further, we extend the transformational scheme show that as a mouse awakens from anesthesia, scale-change symmetry emerges.

The third research project is motivated by experimental observations from in motor cortex under modulation of inhibitory inputs. We found that low intensity increase (decrease) in overall inhibition in cortex causes decrease (increase) in spiking activity for some neurons. Even though, the population level activity largely unchanged. This behavior is paradoxical when

compared to the status quo that says that increase (decrease) inhibition should lead to decrease (increase) in neural spiking activity. We simulated similar dynamical change to inhibitory signal modulation in neural network model. We found that this paradoxical behavior arises due to sparse connectivity and inhomogeneity in inhibitory weights.

ACKNOWLEDGEMENTS

I want to thank my research advisor and dissertation director, Dr. Woodrow L. Shew for making my research experience productive and stimulating. Under his supervision, I learned how to define a research problem, find a solution to it, and finally publish the results. It is a great honor to be one of Dr. Shew's Ph.D. students and I really appreciate all the time he took in guiding me throughout the course of my doctoral studies. Besides my advisor, I would like to thank my dissertation committee members Dr. Pradeep Kumar and Dr. Yong Wang for their insightful comments and continuous encouragement.

Calculations in my research were performed on Trestles at the Arkansas High Performance Computing Center, which is funded through multiple National Science Foundation grants and the Arkansas Economic Development Commission. I would like to extend my humble gratitude towards them. I would like to thank my fellow lab mates Patrick Kells and Srimoy Chakraborty for their continuous help and collaborative efforts in research. I want to thank my research collaborators Dr. Daniel B. Larremore, Dr. Juan G. Restrepo, Dr. Thomas Knöpfel and Andrew B. Cowley, there feedback and discussions have been an important part of my learning process.

Special thanks to Sanghamitra Mandal, who was very important in the success of my PhD, for being the greatest source of my emotional strength and for sharing her excellent knowledge. Lastly, I would like to express my deepest gratitude to my parents and younger brother, who believed in me and supported me throughout my life. This dissertation would not have been possible without their warm love, continued patience and understanding.

DEDICATION

I would like to dedicate this dissertation to my parents Mr. Ramanuj Agarwal and Mrs. Snehlata Agarwal. All my past, present and future scientific or non-scientific contributions would not have been possible without their support.

TABLE OF CONTENTS

LIST OF FIGURES

CHAPTER 1 INTRODUCTION

1.1 Spontaneous Activity in Cerebral Cortex

The brain is one of the most complex physical systems which has captured the fascination of many scientists around the world. It is composed of many regions that perform different tasks that, in coherence, sense the world and control the bodily functions of all animals including humans. The cerebral cortex is the highly convoluted outer layer of cerebrum and covers over 2/3 of the human brain. It performs many important functions such as sensing and interpreting to various stimuli such as vision, hearing and touch, and generating a response such as motor functions. Also, it performs cognitive functions like thinking, perceiving, information processing and understanding languages.(Jones and Peters, 1984)

Traditionally, most neuroscience research has focused on the role of cerebral cortex in processing sensory input and creating a motor response. But, neurons in cerebral cortex are active even without the presence of a sensory input and even when the body is not moving. (Sanseverino *et al.*, 1973; Webb, 1976; Legendy and Salcman, 1985; Tsodyks *et al.*, 1999; Abeles, 2012). This is referred to as ongoing or spontaneous activity. At population level, dynamical patterns of the spontaneous activity are seen across the cortex. Examples of some studies done include, high-resolution optical imaging in cat's visual cortex (Arieli *et al.*, 1996), optical imaging in mice (Scott *et al.*, 2014; Gautam *et al.*, 2015) and in organotypic cultures (Shew *et al.*, 2009) and functional Magnetic Resonance Imaging (fMRI) studies in human brain (Fox, Snyder, *et al.*, 2006; Fox and Raichle, 2007). One reason that Studying spontaneous activity is of importance is that it has been intricately linked to stimulus-evoked activity. Researchers found that orientation maps constructed from spontaneous activity match with the ones seen in visual responses (Tsodyks *et al.*, 1999; Kenet *et al.*, 2003). Similar spatiotemporal

correlations are seen in visual cortex of animals while under no visual stimulus and observing natural scenes(Fiser, Chiu and Weliky, 2004). Others have found that population response to auditory and somatosensory stimuli similar to spontaneous activity(Luczak, Barthó and Harris, 2009). Moreover, the ongoing activity is said to contribute to large variability observed in stimulus responses(Arieli *et al.*, 1996; Azouz and Gray, 1999; Kisley and Gerstein, 1999). In itself, studying spontaneous activity has important consequences. For example, by analyzing spontaneous cortical activity recorded using fMRI scans of human brains, researchers have been able to distinguish between human dorsal and ventral attention systems.(Fox, Corbetta, *et al.*, 2006). Also, researchers have proposed that on a longer timescale spontaneous activity reflects past inputs and future responses.(Ohl, Scheich and Freeman, 2001; Yao *et al.*, 2007) The work we present here is primarily focused on understanding several dynamical aspects of spontaneous activity.

1.2 Excitation/Inhibition in Cortical Networks

Before we start with the discussion of network of neurons, it is essential to describe the neuron first. Ramón y Cajal described the basic principle of neural connections.(Ramón y Cajal, 1894) Dendrites receive signals via synapses from upstream neurons. When such an input signal is received it changes the membrane potential (potential difference across cell wall) or the receiving neuron. All the signals get integrated at the cell body and, if the membrane potential is increased above a certain threshold, then an action potential is generated. Action potentials are often referred to as spikes or firing of neuron. This action potential is a pulse like signal that is then conducted along the axon which send signal to downstream neurons. At the end of every axon is a synapse, the point of contact between two neurons. that the neurons in cerebral cortex can be classified into two broad classes in terms of their neurotransmitters. The excitatory

neurons release glutamergic neurotransmitters and inhibitory neurons that release GABAergic neurotransmitters.(Gutnick and Mody, 1995). As the names suggest an excitatory or inhibitory neuron send signal that increase or decrease the membrane potential of its downstream neurons. Each neuron in cerebral cortex receives approximately 10^4 synaptic inputs on its dendrites; many of these inputs are excitatory, many are inhibitory. These inputs compete with each other, often canceling each other, but occasionally excitatory input exceeds inhibitory input by enough to cause the neuron to fire.

The collective activity of a large network of neurons is very sensitive to the balance between these excitatory and inhibitory neurons that influence each other via a complex connectivity. The Excitation-Inhibition (E/I) balance is key to a healthy cerebral cortex. An E/I imbalance may lead to serious neurological disorders. Epilepsy is linked to decrease in inhibition, that may cause neurons to become over-amplified and lead to massive brain oscillatory activity.(Buckley and Holmes, 2016) Scientists have proposed that some forms of autism are caused by increased ratio of E/I.(Rubenstein and Merzenich, 2003; Nelson and Valakh, 2015). On the other hand increased inhibition is implicated in Down syndrome(Fernandez and Garner, 2007) and may silence cortical neurons.(Sitdikova *et al.*, 2014). Thalamocortical dysrhythmia which is responsible for conditions like depression and Parkinson's disease has been linked to increase in inhibition. (Llinás *et al.*, 1999). Alterations in GABA neurotransmitter system may be involved in the pathophysiology of schizophrenia.(Wassef, Baker and Kochan, 2003) In a healthy functioning cortex, this E/I balance is considered to be maintained carefully within a certain range. Researchers have shown in slices of ferret cortex via *in vitro* measurements that local cortical circuits operate through proportional balance of Excitation and Inhibition. This balance is said to be established through

local recurrent connections and generate self-sustaining activity that can be turned on and off by synaptic inputs.(Shu, Hasenstaub and McCormick, 2003) In rat somatosensory cortex via *in vivo* simultaneous intracellular recordings, other researchers have found continuous synchronization and correlations in strengths of excitatory and inhibitory inputs, during both spontaneous and sensory-evoked activity.(Okun and Lampl, 2008) From the perspective of physics of brain, previous works have shown many emergent phenomena in neural systems that depend on E/I balance. For example, information capacity, transmission and dynamical range maximizes when E/I is properly balanced.(Shew *et al.*, 2009, 2011; Larremore, Shew and Restrepo, 2011; Gautam *et al.*, 2015) However, small changes in E/I balance can occur naturally in healthy brains. For example, changes in alertness are associated with neuro-modulatory chemicals that alter the E/I balance(Harris and Thiele, 2011; Zagha and McCormick, 2014; Stringer *et al.*, 2016).

It becomes an interesting research question to alter the E/I balance and study the impact on the neural activity. Biologically, there are different ways researchers have altered the E/I balance in the neural systems and study its impact on neural activity. For example, by modifying relative number of excitatory and inhibitory neurons (Alvarez-Dolado *et al.*, 2006; Gogolla *et al.*, 2009; Chen and Dzakpasu, 2010), excitatory versus inhibitory synaptic strength(Zhang, Jiao and Sun, 2011), intrinsic neuronal excitability (Turrigiano, Abbott and Marder, 1994; Bacci, Huguenard and Prince, 2004; Maffei and Turrigiano, 2008), tone of neuromodulators(Bacci, Huguenard and Prince, 2004; Williams and Castner, 2006; Lucas-Meunier *et al.*, 2009; William Moreau *et al.*, 2009) and synapse-related proteins expression(Hines *et al.*, 2008; Terauchi *et al.*, 2010) In this thesis we report three projects, each aimed at understanding a different aspect of E/I balance and its impact on spontaneous neural activity. In two of the projects, we approach this goal primarily using computational models, in which direct control of the strengths and/or

numbers of E and I neurons are feasible. In the third project, we combine computational modeling with analysis of experimental data. In the experiments, drugs were used to alter the strength of inhibition in rat cortex.

1.3 Motivation

This dissertation focuses on the Excitation-Inhibition balance and imbalance in cortical neural networks. Specifically, we study it's impact on the collective dynamics of large networks of cortical neurons.

In the first project we study the Shannon entropy *H* (Shannon, 1948) calculated from spontaneous activity of a computational model of neural network. The motivation behind this project is to understand how brain would tune the strength of its excitatory and inhibitory synapses to achieve high and robust entropy. Researchers have argued for the benefits of high entropy as it would correspond to a larger repertoire of internal states to mediate internal information transfer.(Fagerholm *et al.*, 2016) High entropy has also been shown to occur with high mutual information between stimulus and response(Shew *et al.*, 2011; Fagerholm *et al.*, 2016) Under the manipulation of the numbers and strengths of excitatory and inhibitory synapses, our aim is to find that under what conditions one would expect the network activity to have high entropy. We further want to explore how the entropy would change under the fluctuation of synaptic strengths as it happens in real cortex.

The second project is motivated by experimental suggestions that under certain conditions cerebral cortex operates near criticality (i.e. near the critical point of a second order phase transition). The cortical activity under these conditions exhibits scale-invariant statistics.(Tagliazucchi *et al.*, 2012; Scott *et al.*, 2014) Criticality and Phase transition is a well-known phenomenon studied extensively in equilibrium and non-equilibrium physical

systems.(H. Eugene Stanley, 1971) In physical systems such as Ising Model, it has been shown that not only the network activity but the Hamiltonian is also scale invariant, at criticality. (Wilson, 1979) This has been shown via scale-transformation scheme using the mathematical framework of Renormalization Group. We present a hypothesis that, if a system is scale-invariant, then an appropriately chosen coarse-graining procedure will leave the governing laws unchanged and leave the system variables with identical statistics. This has possible implications in neuroscience as it will indicate that neural activity observed at different length scale is governed by the same laws. Independently, in studies done at different observational length scales researchers have shown that neural dynamics follow power-law statistics For example, in spatially-resolved measurements in animals(Scott *et al.*, 2014) and low-resolution measurements in humans(Tagliazucchi *et al.*, 2012). Since the neural dynamics at these length scales follow similar statistics the laws governing these dynamics might also be similar.

The motivation behind the third project stems from experimental observations of what happens to network activity after pharmacologically altering the E/I balance. These experiments are done on rat motor cortex where neural activity is recorded via multielectrode voltage measurements. The E/I balance is altered by administering drugs that promotes/block GABA receptors which is responsible for inhibitory signals between neurons. Traditional thinking about such inhibitory signal manipulation is that increasing/decreasing inhibition would decrease/increase the spiking rate of neurons. But, paradoxically, we found that some neurons exhibit behavior opposite to this traditional expectation. Some neurons fired much more when inhibition was increased. And some neurons fired much less when inhibition was suppressed. Surprisingly, the overall population activity, averaged across all neurons, stayed largely unchanged. Previous works have also reported that neurons behave in paradoxical manner under

signal modulation and the underlying reason has been indicated to be the inhomogeneity in network connectivity.(Song *et al.*, 2005; Garcia Del Molino *et al.*, 2017)

1.4 Dissertation Objectives

There are three main objectives of this dissertation;

1. Determine how noise/information capacity/entropy depend on E/I balance by analyzing the spontaneous activity in a computational model of network of Excitatory and Inhibitory neurons.
2. Test the hypothesis that dynamical rules governing the neural activity follow scale-change symmetry. What is the impact of E/I balance on that in a more realistic model and the implications of measuring scale-change symmetry of dynamical rules in cerebral cortex?
3. Determine the mechanism by which a cortical neuron generates a paradoxical change in firing rate under E/I imbalance. Even though, the population activity on average remains constant. What are the intrinsic network characteristics that may give rise to such behavior?

CHAPTER 2 ENTROPY FOR NETWORK OF EXCITATORY-INHIBITORY INTEGRATE-AND-FIRE NEURONS

Keywords: Neural networks; Phase transition; criticality; entropy

2.1 Introduction

The network of neurons in cerebral cortex displays rich and complex dynamics even when not engaged by any particular sensory or motor interaction with the external world.(Arieli *et al.*, 1996; Fox and Raichle, 2007) From one point of view, such ongoing internal dynamics are thought to mediate memory consolidation and other internal cognitive processes.(Han, Caporale and Dan, 2008; Luczak, Barthó and Harris, 2009; Berkes *et al.*, 2011; Miller *et al.*, 2014; Romano *et al.*, 2015) On the other hand, ongoing fluctuations in cortical network dynamics have often been considered a nuisance, imposing noisy fluctuations in neural response to sensory input.(Lee *et al.*, 1998; Averbeck, Latham and Pouget, 2006; Ecker *et al.*, 2014) In both of these contexts, it is important to understand the mechanisms that govern the fluctuations of ongoing cortical network dynamics. Here, we investigate the Shannon entropy of the network spike rate. In the context of internal cognitive processes, high entropy might be beneficial, corresponding to a larger repertoire of internal states to mediate internal information transfer.(Fagerholm *et al.*, 2016) When considered as noise, high entropy can be a hindrance to effective sensory coding.(Lee *et al.*, 1998; Averbeck, Latham and Pouget, 2006; Ecker *et al.*, 2014) Indeed, in principle, encoding of sensory input would be most reliable if the cortex was totally silent (low entropy) until the stimulus excited it. However, real cortex does not operate this way; it has many jobs to do beyond encoding sensory input and is never silent. Previous studies have shown that ongoing cortical dynamics with high entropy occurs together with high mutual information between stimulus and response(Shew *et al.*, 2011; Fagerholm *et al.*, 2016) suggesting that a large

repertoire of ongoing dynamical states may be necessary for a large repertoire of stimulus-evoked states.(Luczak, Barthó and Harris, 2009; Berkes *et al.*, 2011)

A crucial factor for determining the entropy of network dynamics in the cortex is the competition between two types of neurons: excitatory (E) and inhibitory (I). This is most apparent in previous experiments that pharmacologically manipulated the E/I balance.(Mao *et al.*, 2001; Shew *et al.*, 2011; Gautam *et al.*, 2015; Fagerholm *et al.*, 2016) Enhanced inhibition (GABA agonists) often results in a dynamical regime characterized by low firing rates and weak population-level correlations, while decreased inhibition (GABA antagonists) tends to result in a regime with higher firing rates and strong correlations. Two studies in particular have shown that entropy can be increased by tuning the E/I balance to the tipping point between these two distinct dynamical regimes.(Shew *et al.*, 2011; Fagerholm *et al.*, 2016) However, a more systematic understanding of how E/I balance impacts entropy is difficult to obtain experimentally because pharmacological manipulations are rather difficult to precisely control. Moreover, with a few interesting exceptions,(Chen and Dzakpasu, 2010; Hunt *et al.*, 2013) experiments do not vary the numbers of excitatory or inhibitory neurons. Computational models offer an alternative approach in which the number of excitatory and inhibitory neurons, as well as strength of excitatory and inhibitory synapses, can easily be controlled. Previous computational studies have addressed similar topics but typically have neglected inhibition(Shew *et al.*, 2011; Ferraz, Melo-Silva and Kihara, 2017) or have not considered the effects of changing the E/I ratio.(Scarpetta and de Candia, 2013; Yang, Zhou and Zhou, 2017) Thus, theoretical and experimental understanding of the relationship between the entropy of ongoing dynamics and the balance of excitation and inhibition—mediated by both relative strengths of excitatory and inhibitory synapses and relative numbers of excitatory and inhibitory cells—remains unresolved.

Here, we attempt to improve the theoretical understanding of entropy of ongoing dynamics by studying a network model of binary neurons in detail. We consider how entropy of the population firing rate depends on the fraction of inhibitory neurons α and the strengths of E and I interactions, W_E and W_I, respectively. We find maximal entropy near the tipping point between the low and high firing rate dynamical regimes, as seen in experiments.(Shew *et al.*, 2011) We also find that, for a given choice of W_E and W_I, the tipping point can be achieved by adjusting the value of α. This raises the question: among the different possible parameter configurations that place the system at the tipping point, why should one be favored over another? We find that there is a trade-off between high and robust network entropy: networks with weak synapses can achieve a high entropy when excitation and inhibition are balanced, but the entropy degrades significantly upon small deviations from the balanced state. On the other hand, networks with stronger synapses have a lower maximum entropy, but they are more robust to parameter changes. We also find that if E and I synaptic strengths are proportional to each other, as found in many experiments,(Wehr and Zador, 2003; Haider, 2006; Denève and Machens, 2016) then robust, high entropy requires a small fraction of I neurons (α near 0.1). In mammalian cortex, α has been found to be near 0.2 with remarkable consistency over the lifetime of an organism(Sahara *et al.*, 2012) and over different regions of cortex.(Hendry *et al.*, 1987; Meinecke and Peters, 1987) Our results suggest that mammalian cortex strikes a compromise with intermediate but robust entropy.

In what follows, we introduce and analyze the binary neuron model which both predicts and provides insight into the results of model numerical simulations.

2.2 Model and Theory

2.2.1 Binary Neuron Model

We explore the effects of excitation and inhibition balance on entropy using a simple, analytically tractable model. The model, studied previously in Ref. (Larremore *et al.*, 2014), consists of a network of N stochastic binary neurons, indexed $i = 1,2, \dots, N$. The state of neuron i at time t is denoted by x_i^t, which can take the values $x_i^t = 0$ if the neuron is resting and $x_i^t = 1$ if the neuron is spiking. Time is assumed to evolve in discrete steps $t = 0,1,2, \dots ..$ The evolution of each neuron's state is stochastic and depends on the states of other neurons at the previous time step,

$$x_i^{t+1} = \begin{cases} 1 \; with \; probability \; \eta + (1-\eta)\sigma\left(\sum_{j=1}^{N} \epsilon_j w_{ij} x_j^t\right) \\ 0 \; otherwise, \end{cases} \qquad 2\text{-}1$$

where $\epsilon_j = 1$ if neuron j is excitatory and $\epsilon_j = -1$ if neuron j is inhibitory. The strength of the synapse from neuron j to neuron i is $w_{ij} > 0$ and $w_{ij} = 0$ if neuron j does not connect to neuron i. The transfer function $\sigma(x) = \min[1, \max(0, x)]$ converts the input to neuron i into a probability. The constant $\eta = 1/(100N)$ represents independent spontaneous activation due to noise or external sources, resulting in one spike per 100 time steps among all neurons, on average. We note that other choices of η could cause quantitative changes in our results below, but we expect that our qualitative conclusions are not sensitive to moderate changes in η. For example, it is well known that noise tends to smooth out the sharpness of phase transitions like the one discussed below.(Williams-García *et al.*, 2014)

We consider Erdős-Rényi networks where a directed link is made independently from neuron j to neuron i with probability $k/(N-1)$ for all $i \neq j$. The parameter k is the expected

number of outgoing connections from each neuron. To control the relative number of excitatory and inhibitory neurons, we assign each neuron to be inhibitory with probability α and excitatory otherwise. Finally, we assume for simplicity that $w_{ij} = w_E$ for excitatory synapses (i.e., if $\epsilon_j = 1$) and $w_{ij} = w_I$ for inhibitory synapses (i.e., if $\epsilon_j = -1$) and define the effective excitatory weight as $W_E = kw_E$ and the effective inhibitory weight as $W_I = kw_I$. We interpret our model to represent a small patch of cortex, $100\ \mu m$ in scale, like a single cortical column. At these scales, it is a reasonable approximation to neglect distance-dependent differences in connectivity for excitatory and inhibitory neurons.(Song *et al.*, 2005)

The model is characterized by the parameters N, k, W_E, W_I, and α. For definiteness, in all simulations, we will consider, unless otherwise indicated, only the parameters $N = 10{,}000$ and $k = 100$ and study the population firing dynamics of the model as a function of (W_E, W_I, α). As a measure of collective network dynamics, we study the fraction of spiking neurons, or *network activity*, given by

$$S^t = \frac{1}{N}\sum_{i=1}^{N} x_i^t \qquad 2\text{-}2$$

In Ref. (Larremore *et al.*, 2014), it was found that the collective dynamics of the network is determined by the largest eigenvalue λ of the connection strength matrix A with entries $\{\epsilon_j w_{ij}\}_{i,j=1}^{N}$. Network activity saturates at a high value for $\lambda > 1$ and dies out or reaches a steady low value for $\lambda < 1$. At the tipping point between these two regimes, defined by $\lambda = 1$, excitation and inhibition are balanced such that network activity is characterized by large fluctuations that are effectively ceaseless (their lifetime scales exponentially with N).(Larremore *et al.*, 2014)

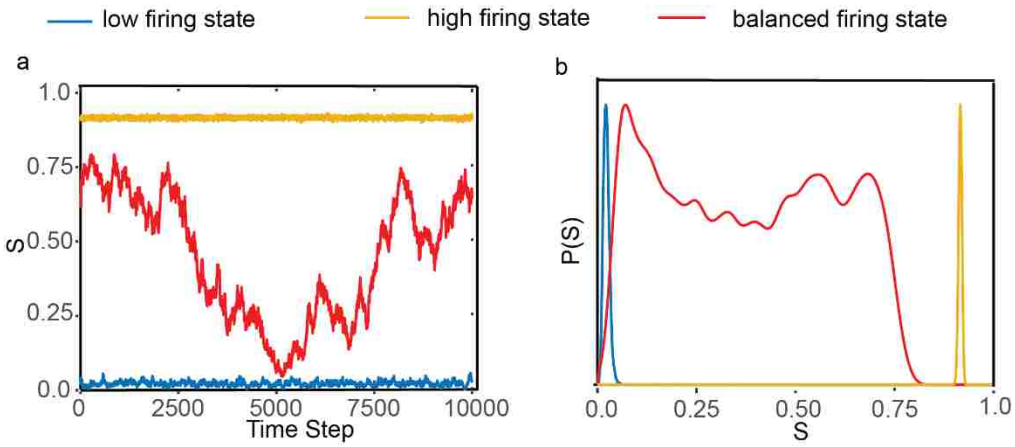

Figure 2-1 Network activity and dynamics of binary model. Time series of network activity (a) show diverse fluctuations when excitation and inhibition are balanced ($\lambda = 1$). Similarly, probability distributions (b) of network activity are broadest when $\lambda = 1$. All probability distributions have been normalized by their peak probability to facilitate comparison of their shapes. Dynamical parameters: $\alpha = 0.11$ (Blue), 0.1 (Red), 0.09 (Yellow); $W_E = W_I = 1.25$.

Figure 2-1 shows an example of the time series of network activity for these three regimes. For the Erdős-Rényi networks considered here, λ can be approximated by the expected row sum of A,

$$\lambda \approx kw_E(1-\alpha) - kw_I\alpha = W_E(1-\alpha) - W_I\alpha \qquad 2\text{-}3$$

With this approximation, then, the parameters that give $\lambda = 1$ form a 2-dimensional surface in the (W_E, W_I, α) parameter space.

2.2.2 Entropy

We consider the Shannon entropy of the time-series of network activity, which quantifies the size of the repertoire of accessible population firing rates. The network activity is discrete $\left(0, \frac{1}{N}, \frac{2}{N} \ldots 1\right)$. For a given set of network parameters (W_E, W_I, α), we consider the steady-state probability distribution of network activity $P(S)$ and the associated entropy,

$$H = -\sum_S P(S)\, log_2[P(S)] \qquad 2\text{-}4$$

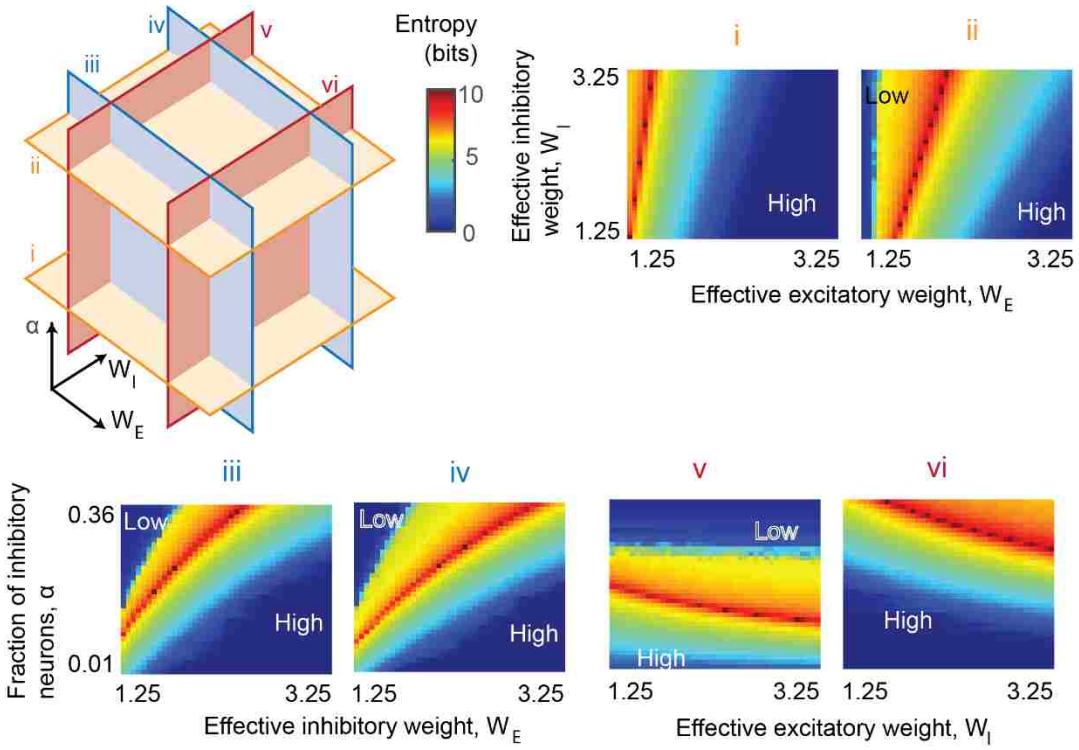

Figure 2-2 High entropy at the boundary between high and low firing regimes. Each panel shows how entropy (color) varies across a two-dimensional section of the three-dimensional $W_E - W_I - \alpha$ parameter space. The relative orientation of the six different sections is illustrated and labeled [(i)–(vi)] in the cartoon (left). For (i) and (ii), α is fixed at 0.1 and 0.2. For (iii) and (iv), W_I is fixed at 1.5 and 2.5. For (v) and (vi), W_E is fixed at 1.5 and 2.5. A curved critical surface in $W_E - W_I - \alpha$ space separates the high firing regime (H) from a low firing regime (L). Entropy is high along this regime boundary. Note that as I or E synapse strength increases, the width of the peak in entropy also increases, indicating increased robustness (decreased fragility).

where the sum runs over the allowed values $S = 0, \frac{1}{N}, \frac{2}{N}, \ldots, 1$. In practice, we estimate $P(S)$ numerically from a time series of S^t obtained from model simulations (Figure 2-1b).

2.3 Results

Our primary goal is to determine how the entropy of a network varies with the relative numbers of E and I neurons and the relative strength of E and I synapses. We first describe our results from numerical simulations of the binary model and then describe results from the theory. First, we show in Figure 2-1 that the system network activity visits the widest variety of states when excitation and inhibition are balanced at the tipping point between high and low firing rate

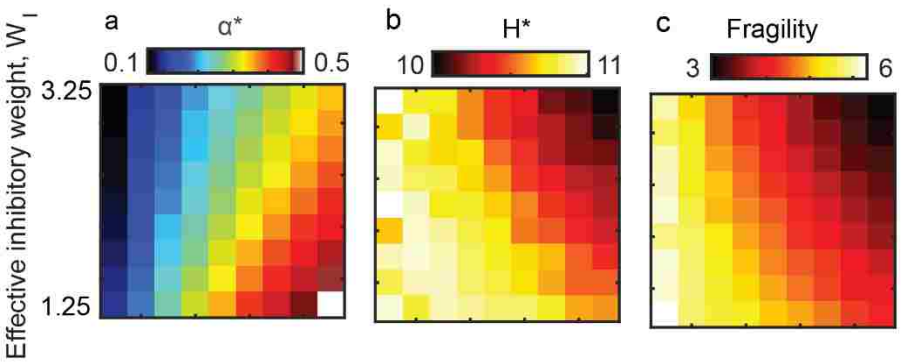

Figure 2-3 Trade-off between high entropy and robust entropy. (a) For each combination of W_E and W_I effective synaptic weights, we identify the critical fraction of inhibitory neurons (α^*) with the highest entropy. (b) Comparing all critical entropy H^* across the entire critical surface, entropy was highest for low W_E and W_I. (c) Highest fragility was also found for low W_E and W_I.

regimes. This is visible in time series (Figure 2-1a) as well as empirical distributions $P(S)$ of network activity (based on 10^4 time steps of simulation). Correspondingly, entropy H is greatest along the boundary between low and high firing regimes (Figure 2-2). In the three-dimensional (W_E, W_I, α) parameter space, this boundary forms a curved surface, which we henceforth refer to as the *maximum entropy surface*.

As discussed in Chapter 2.2.1, we expect that the transition from the low to the high firing regimes occurs at the *critical surface* of parameters where $\lambda = 1$. While we find this is usually an excellent approximation to our numerical results, the maximum entropy and critical surfaces differ slightly for high values of α, and therefore, we will only use the critical surface as a qualitative guide to the location of the maximum entropy surface.

To numerically identify the maximum entropy surface, for each fixed value of (W_E, W_I), we compute entropy across a wide range of values of α, finding the value α that maximizes (W_E, W_I, α). In Figure 2-3a, we show α^* as a function of W_E and W_I. As one might expect, higher values of W_E require a larger number of I neurons (higher α^*) in order to maintain a balanced network and vice versa. This agrees qualitatively with the estimate using the critical

surface, $\alpha^* \approx (W_E - 1)/(W_E + W_I)$ obtained from Eq. $\lambda \approx kw_E(1-\alpha) - kw_I\alpha = W_E(1-\alpha) - W_I\alpha$ 2-3 with $\lambda = 1$.

Having identified the parameters that characterize the maximum entropy surface, we next ask two questions. First, where on the surface is entropy highest? Second, where on the surface is entropy most robust? We consider the entropy to be robust if it does not drop dramatically when we make a small perturbation in W_E, W_I, and α away from the peak entropy surface. This approach is similar to other ways to quantify sensitivity to model parameters, such as Fisher information.(Lehmann and Casella, 1998) To quantify how much the entropy decreases if parameters are perturbed away from the maximum entropy surface, we define *fragility* $F(W_E, W_I)$ as follows. For a given pair of (W_E, W_I) values, we first calculate the entropy at the corresponding point on the maximum entropy surface, $H^* = H(W_E, W_I, \alpha^*)$. Then, we calculate the entropy at two points at a small distance δ above and below the surface, $H_{up} = H(W_E + \Delta W_E, W_I + \Delta W_I, \alpha + \Delta\alpha)$ and $H_{down} = H(W_E - \Delta W_E, W_I - \Delta W_I, \alpha - \Delta\alpha)$. The perturbations $\pm(\Delta W_E, \Delta W_I, \Delta\alpha)$ are defined to be normal to the maximum entropy surface, which will give the largest drop in entropy for a given perturbation size. The size of the perturbation was chosen to be small (Euclidean norm $\delta = 0.01$, about 1% variation in parameters) to emphasize that entropy can be quite sensitive to these parameter changes in certain parts of (W_E, W_I) space. Finally, we define *fragility* $F(W_E, W_I)$ as the mean of the entropy difference,

$$F(W_E, W_I) = \frac{\left(H^* - H_{up}\right) + (H^* - H_{down})}{2} \qquad 2\text{-}5$$

Our main results are in Figure 2-3b and Figure 2-3c. Figure 2-3b shows the entropy H^* on the maximum entropy surface as a function of the effective E and I weight W_E and W_I. Networks with weak effective synapse strengths (low values of W_E and W_I) can achieve a higher entropy H^* than networks with strong effective synapse strengths. However, as shown in Figure 2-3c,

high entropy comes at the cost of high fragility: networks with weak effective synapse strengths have the highest fragility, while networks with strong effective synapse strengths are the most robust. We note that while the variation in entropy H^* is relatively moderate across the range studied approximately 10%), the fragility ranges from 3 to 6, indicating that our 1% perturbation of parameters results in a dramatic drop in entropy of approximately 30% - 60%. One could argue that what matters are the final values of entropy after perturbation (i.e., H_{up} and H_{down}) rather than how much entropy drops due to perturbation (i.e., F). From this perspective, strong synapses are also better; H_{up} and H_{down} are lower for weak synapses than for strong synapses. This can be seen by subtracting Figure 2-3b and Figure 2-3c. We conclude that there is a trade-off between high and robust entropy, with stronger effective synapse strengths promoting lower but more robust entropy, and weaker effective synapse strengths promoting a high but fragile entropy.

Finally, we address the role of the fraction α of I neurons in promoting entropy robustness. We note that if the choices of E and I synapse strengths are constrained to be proportional to each other, as experiments suggest,(Wehr and Zador, 2003; Haider, 2006; Denève and Machens, 2016) then $W = W_E = bW_I$ and the estimate $\alpha \approx (W_E - 1)/(W_E + W_I)$ becomes $\alpha^* = \left(1 + \frac{1}{b}\right)^{-1}\left(1 - \frac{1}{W}\right)$. Thus, α^* is a monotonically increasing function of synapse strength W. Therefore, for such constrained networks, entropy and fragility decrease with the fraction of I neurons α. Thus, a small non-zero α, similar to that found in mammalian cortex, is needed to obtain high and robust entropy.

2.4 Discussion

Here, we have shown that Shannon entropy of neural network dynamics is sensitive to the structure of excitatory and inhibitory interactions. Generally, high entropy is obtained by

balancing E and I synaptic efficacy such that the system operates near the tipping point between two phases of network dynamics. Entropy is high all along this boundary, i.e., for a wide range of properly balanced E/I combinations. However, the regions within this boundary with the highest entropy are not robust; small variations in the synaptic strengths W_E, W_I and in the fraction of inhibitory neurons α could cause entropy to plummet, drastically reducing the accessible states and disrupting the functioning of the network. We found that entropy is more robust when the effective synaptic strengths are larger. Given that W_E, W_I, and α are inevitably somewhat variable during development, across brain regions, and across individuals,(Hendry *et al.*, 1987; Meinecke and Peters, 1987; Sahara *et al.*, 2012) robustness to W_E, W_I, and α variability may be important. For networks constrained such that $W_E \sim W_I$,(Wehr and Zador, 2003; Haider, 2006; Denève and Machens, 2016) our findings imply that a small, nonzero fraction $\alpha > 0$ of inhibitory neurons would result in a more robust network entropy. Our results suggest that a population of organisms with reliable and high entropy brains requires that small, nonzero fraction of neurons be inhibitory, which is consistent with what exists in mammalian cortex.(Hendry *et al.*, 1987; Meinecke and Peters, 1987; Sahara *et al.*, 2012)

Different parts of the space of models we explore here relate to several other models studied previously. The parts of parameter space with relatively weak $W_E \; and \; W_I$ and with $\alpha = 0.2$ are similar to models previously studied in the context of "criticality" in the cortex.(Larremore *et al.*, 2014) The parts of parameter space where $W_E \; and \; W_I$ are stronger may be related to the widely studied set of models referred to as "chaotic balanced'' networks.(Vreeswijk and Sompolinsky, 1998; Denève and Machens, 2016; Rubin, Abbott and Sompolinsky, 2017) A more detailed comparison of our model dynamics to previous models could bridge the study of the criticality hypothesis with that of chaotic balanced networks.

How might one experimentally test the results of our work? One way would be to measure changes in firing rate fluctuations in response to acute manipulation of excitatory or inhibitory synapses. Such manipulations can be made pharmacologically, for example.(Mao *et al.*, 2001; Shew *et al.*, 2011; Fagerholm *et al.*, 2016) Our work predicts two testable phenomena. First, if the cortex is on the high entropy surface discussed here, then any manipulation of excitation or inhibition will result in a drop in firing rate fluctuations. Conversely, if either excitatory or inhibitory manipulation results in an increase in firing rate entropy, this would suggest that the cortex is not operating on the high entropy surface. A second prediction from our work is that size of the drop in entropy due to a manipulation of inhibition or excitation will be correlated with the entropy before the manipulation. This prediction supposes that the cortex is sometimes operating with a weak-synapse E/I balance where entropy is higher and the drop in entropy would be greater and at other times is operating with a strong-synapse E/I balance where entropy is lower and the drop in entropy would be less.

Although high entropy is likely to be beneficial for certain functions of cerebral cortex, other functions might be better served by a low entropy condition. For example, as discussed in the introduction, lower entropy might improve sensory signal processing by increasing the signal-to-noise ratio. In this context, a small shift toward the lower firing side of the phase transition might be beneficial. Such temporary shifts can occur due to neuromodulation; for example, attention is known to shift cortical dynamics toward a regime with smaller collective fluctuations.(Harris and Thiele, 2011) However, a shift toward the high firing regime or too large a shift toward the extremely inhibition-dominant regime would likely be bad for function. Indeed, extreme deviation from well-balanced excitation and inhibition is implicated in a variety of brain disorders. For instance, when inhibition is sufficiently weak relative to excitation,

seizures occur, as in epilepsy.(Dichter and Ayala, 1987) Too much inhibition is associated with Down's syndrome.(Fernandez and Garner, 2007) Autism is also associated with imbalanced excitation and inhibition,(Rubenstein and Merzenich, 2003; Nelson and Valakh, 2015) both in terms of abnormal numbers of inhibitory neurons and strengths of synapses.(Gogolla *et al.*, 2009) Our work suggests that the dysfunction associated with these disorders may be, in part, due to abnormal entropy of cortical network dynamics.

If high entropy is a beneficial property for brain circuits, then the robust maximization of entropy could be a phenotypic target of evolution in the nervous system. Our results suggest that hitting this target requires neural circuits that include some inhibitory neurons and operate near the tipping point of a phase transition.

CHAPTER 3 SCALE INVARIANCE IN NEURAL NETWORK DYNAMICAL RULES: RENORMALIZATION GROUP APPROACH

3.1 Introduction

The ongoing collective population activity of neurons in cerebral cortex exhibits complex spatiotemporal fluctuations. This ongoing activity is responsible for the majority of the brains energy consumption(Buzsáki, Kaila and Raichle, 2007), is closely related to past experiences (Kenet *et al.*, 2003; Han, Caporale and Dan, 2008; Luczak, Barthó and Harris, 2009), contributes to memory consolidation (Ji and Wilson, 2007; Gupta *et al.*, 2010), and modulates ongoing cortical processing (Arieli *et al.*, 1996; Petersen *et al.*, 2003; Fox, Snyder, *et al.*, 2006; Fox *et al.*, 2007). Thus, understanding how ongoing cortical activity is organized is an important goal of systems neuroscience. Comparing ongoing cortical activity across diverse species, measured with different experimental methods over the past decade, a common phenomenon has been found with surprising consistency. The spatiotemporal sizes of ongoing fluctuations follow a specific statistical law; they are distributed according to a power-law probability density function with the same exponent near -1.5. This phenomenon has been observed in fMRI in humans (Tagliazucchi *et al.*, 2012; Haimovici *et al.*, 2013), MEG in humans (Shriki *et al.*, 2013), voltage imaging in mice (Scott *et al.*, 2014; Fagerholm *et al.*, 2016), multi-electrode electrophysiology in monkeys (Petermann *et al.*, 2009; Yu *et al.*, 2017), cats (Hahn *et al.*, 2017), rats (Gireesh and Plenz, 2008; Gautam *et al.*, 2015), and even turtles (Shew, Clawson, Pobst, Karimipanah, Nathaniel C. Wright, *et al.*, 2015; Clawson *et al.*, 2017) and *in vitro* brain-in-a-dish systems (Beggs and Plenz, 2003; Shew *et al.*, 2011). What can explain such shared phenomena observed across such diverse cortical systems, measured with differing spatial and temporal resolution?

One hypothesis is that the cerebral cortex can operate near the critical point of a phase transition (Beggs and Timme, 2012; Shew and Plenz, 2013; Hesse and Gross, 2014; Plenz, Niebur and Schuster, 2014). This hypothesis builds upon well-established physics of critical phase transitions; at criticality, multiple material properties are expected to be power-law distributed according to universal scaling laws that are insensitive to many details of the physical system (H E Stanley, 1971; H. Eugene Stanley, 1971; Wilson, 1975, 1979). From theory and computational modeling work, it is clear that neural systems can be tuned into a variety of different dynamical regimes or phases (e.g. asynchronous, oscillatory, bursting), often with distinct boundaries separating different regimes (Brunel, 2000; Haldeman and Beggs, 2005; Wang, Hilgetag and Zhou, 2011; Poil *et al.*, 2012; Gautam *et al.*, 2015). Similar to physical systems, near certain regime boundaries these neural models exhibit power-law distributed collective dynamics with the same power-law exponents, despite many detailed differences among models (Haldeman and Beggs, 2005; Wang, Hilgetag and Zhou, 2011; Gautam *et al.*, 2015). What does the physics of critical phenomena tell us about where this universality comes from?

Fundamental insight into the origins of universal critical phenomena in physical systems (and a Nobel Prize) came from the realization that the basic laws governing the system obey a peculiar symmetry. The laws are the same across different scales; they have scale-change symmetry. Critical phenomena, including power-law distributed observables, stem directly from this bizarre fractal symmetry of the governing physical laws (Wilson, 1975, 1979). Motivated by this basic fact about critical phenomena in physical systems, here we hypothesize that the governing laws for cortical dynamics also conform to scale-change symmetry. Despite more

than a decade of intense research on criticality in neural systems, this basic question has not been addressed. How does one go about testing this hypothesis?

Here, we develop an approach inspired by renormalization group theory, but with a focus on practical applicability to real neural data. Renormalization group theory is the mathematical approach used to understand scale-invariance at criticality in equilibrium physical systems (H. Eugene Stanley, 1971; Wilson, 1975, 1979; Stanley, 1999), and in certain non-equilibrium dynamical systems (Loreto *et al.*, 1995; Vespignani, Zapperi and Pietronero, 1995; Vespignani, Zapperi and Loreto, 1997; Tauber, 2014). However, renormalization group ideas have not been developed in the context of neural systems. In brief, the idea begins with a coarse-graining procedure which transforms all the system variables and governing laws at one spatiotemporal scale to new set of variables and laws at a coarser scale. If the system obeys the scale-change symmetry, then an appropriately chosen coarse-graining procedure will leave the governing laws unchanged and leave the system variables with identical statistics.

Here, we first applied our approach to two computational models, one simple, and the other more biologically realistic. For both models, we found that dynamical rules were indeed maximally scale-invariant when operating near a phase transition. Next, we applied our approach to experimental data. We found that, in the awake state, the apparent rules governing dynamics of mouse cerebral cortex were more scale-invariant than in the anesthetized state. This suggests that the unconscious cortex deviates further from criticality than does the conscious cortex.

3.2 Results

3.2.1 Simple Model

We developed our approach using a network of binary, probabilistic, excitable nodes similar to that used in previous studies of non-equilibrium critical phenomena in neural systems

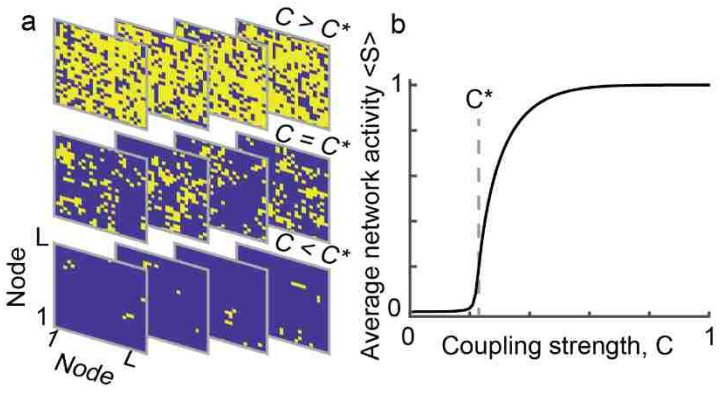

Figure 3-1 Phase Transition in a Simple Neural Model a. Each panel shows the two-dimensional lattice of nodes at a single time step. Each pixel represents one node (yellow, active; blue, inactive). A subset of the full lattice is shown for clarity. b. As coupling strength C increases a sharp increase in time-averaged network activity occurs at a critical coupling strength C^* near $C = 0.23$. S is averaged over 10^4 time steps excluding a transient period of 10^4 time steps.

(Haldeman and Beggs, 2005; Kinouchi and Copelli, 2006; Shew *et al.*, 2009; Larremore, Shew and Restrepo, 2011), but on a two-dimensional $L\ X\ L$ square lattice ($L = 400$) with nearest neighbor connections (including self). We interpret each node in the network as the aggregate state of a group of neurons, analogous to the signals measured using experimental techniques with somewhat coarse spatial resolution (e.g. local field potential (Petermann *et al.*, 2009), voltage imaging (Scott *et al.*, 2014), or functional magnetic resonance imaging (Tagliazucchi *et al.*, 2012; Haimovici *et al.*, 2013)). The state $X(t+1)$ of a node at time $t+1$ is either active (1) or inactive (0) depending on the number of neighbors $n(t)$ which were active at time t.

$$X(t+1) = \begin{cases} 1\ with\ probability\ \phi_n = 1-(1-C)^{n(t)}(1-p) \\ 0\ otherwise \end{cases} \quad 3\text{-}1$$

and C defines the strength of coupling between all connected pairs of nodes and p defines a probability of activation without any active neighbors ($p = 0.001$ unless stated otherwise). We interpret p as an external source of input to the neural system. The states of all the network nodes are updated synchronously. One way to characterize the collective network dynamics is by measuring the fraction of active nodes at a time, or network activity, given by $S(t) =$

$L^{-2}\sum_{i=1}^{L^2} X_i(t)$. By tuning the coupling strength, we tuned the model through a critical phase transition at $C = C^*$ separating a low-activity (small S) from a high-activity (large S) regime (Figure 3-1). Most of our results consider the range of C from 0.15 to 0.35.

Our first goal was to examine how the dynamical rules governing the system change when considered at different scales of observation. For this, we consider six activation probabilities $\phi_n = 1 - (1 - C)^{n(t)}(1 - p)$ with $n = 0, 1, 2, 3, 4, or\ 5$ ($n = 5$ means all 4 neighbors plus self). Together, these six probabilities completely specify the rules of the system dynamics (actually they over-specify the rules, which are completely specified by *C* and *p*, but over-specification can be helpful with noisy data). Importantly, we can estimate these probabilities directly from data, whether simulated or experimentally measured. For instance, ϕ_1 is estimated as the fraction of instances with $n(t) = 1$ that lead to activation at time $t + 1$. Based on 10^4 timesteps of data from the model (excluding the transient of duration 10^2 timesteps), we can estimate all six ϕ_n probabilities with precision ≤ 2% for 0.15 < *C* < 0.35 (except ϕ_0, which was less accurate for *C* > 0.3; see Supplementary materials SM Figure 3-1).

The scale-change symmetry at the heart of critical phenomena in physical systems suggests that the ϕ_n could be invariant across observational scales when *C* equals its critical value *C**, but not if *C* deviates from *C**. The next step towards testing this possibility was to identify an appropriate coarse-graining renormalization transformation to map one observational scale onto a coarser scale.

3.2.2 Coarse-graining scheme

Motivated by the limited spatiotemporal resolution of typical experimental data and real-space block renormalization schemes originally used to gain insight on critical phenomena in physical systems (H. Eugene Stanley, 1971; Wilson, 1979; Kadanoff, 1993), we devised a

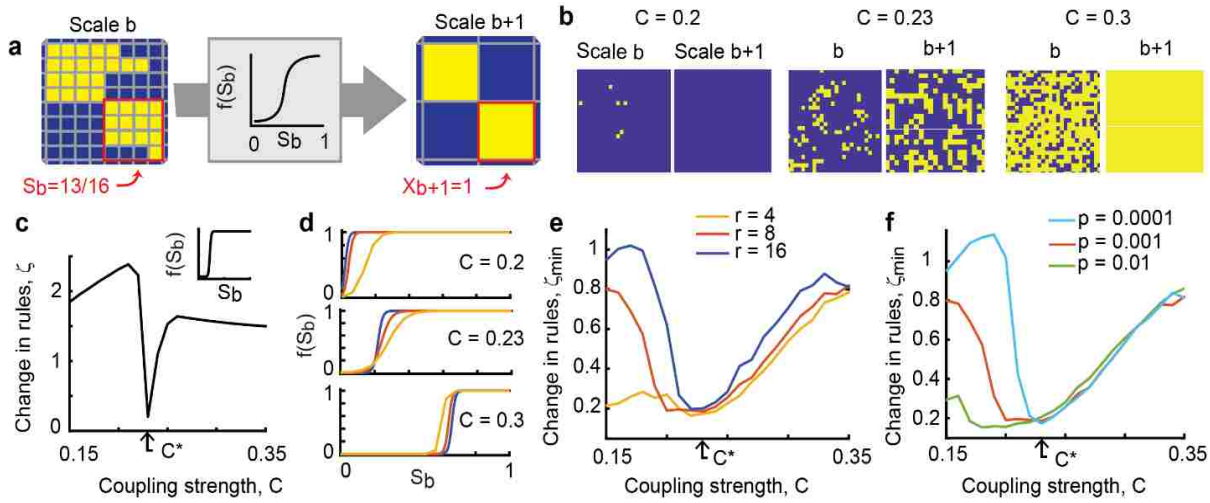

Figure 3-2 Scale-Invariance of Dynamical Rules Peaks at Criticality. a. Cartoon illustration of coarse-graining scheme. Each block of nodes at fine scale b is transformed probabilistically to one node at the coarse scale $b + 1$. b. Examples of activity snapshots before and after coarse graining. c. Upon coarse graining, the dynamical rules change the least (ζ is minimal) at criticality. Inset shows the coarse-graining transformation function with $(k; x_0) = (76; 0.22)$. Block size was $r = 8$. d. Shown are optimal coarse-graining functions for three C values and six block sizes (legend in e. specifies different values of r and τ). e. Using the optimal coarse-graining function for each C resulted in the strongest scale-invariance of dynamical rules, i.e., lowest ζ_{min} around $C = C^*$. This result held for multiple choices of block size and duration (see legend). f. The valley in ζ_{min} as a function of coupling strength C became broader as p was increased. For a–e $p = 0.001$.

spatiotemporal transformation scheme described as follows. Each $r \times r \times \tau$ spatiotemporal block of nodes ($r \times r$ in space and of duration τ) at scale b transforms into a single node at coarser scale $b + 1$. Thus, an $L \times L \times T$ lattice at observational scale b transforms into a coarse $L/r \times L/r \times T/\tau$ lattice at observational length scale $b + 1$, as illustrated for r = 4 and τ = 1 in Figure 3-2a, b. The state X_{b+1} of a coarse node depends on the average state $S_b = \tau^{-1} r^{-2} \sum_{i=1}^{\tau r^2} X_b^i$ of the corresponding τr^2 nodes at the finer scale according to

$$X_{b+1} = \begin{cases} 1 & with\ probability\ f(S_b) = \left[1 + exp\left(-k(S_b - x_0)\right)\right]^{-1}, \\ 0 & otherwise. \end{cases} \quad 3\text{-}2$$

By tuning the transformation parameters k and x_0, we can explore a family of logistic function coarse-graining procedures including majority rules and other previously studied functions.

Similar coarse graining schemes have been used in previous work on deep learning (Hinton and Salakhutdinov, 2006).

To quantify the change in the dynamical rules due to coarse-graining, we define a parameter ζ

$$\zeta = \sum_{n=0}^{5} |\phi_n^b - \phi_n^{b+1}| \qquad 3\text{-}3$$

where ϕ_n^b is the activation probability estimate at scale b and ϕ_n^{b+1} is the activation probability estimate at the coarser scale $b+1$. Note that root mean squared differences or any other monotonic function of the differences of ϕ_n^b and ϕ_n^{b+1} would not change our following conclusions. We ran the model for a range of coupling strengths $0.15 < C < 0.35$, simulating 10^4 timesteps for each C. In line with expectations from critical phenomena in physical systems, we found that ζ was minimized for C near $C^* = 0.23$ (Figure 3-2c). This result was obtained using transformation parameters $k = 76$, $x_0 = 0.22$, and block size $r \times r \times \tau = 8 \times 8 \times 1$ (Figure 3-2c, inset). This means that the dynamical rules governing the network activity are least changed at C^*.

However, some caution is appropriate; if a different transformation function f was used, perhaps the minimum ζ would occur at a different C. Therefore, to draw a more definitive conclusion, we next systematically searched the two-dimensional space of all possible f functions, seeking the function that minimizes ζ for each C independently. We found that, when using such optimal f functions, the dynamical rules remained most scale invariant (i.e. lowest ζ) for C near C^* (Figure 3-2d, e). Thus, our first conclusion is that scale invariance of the governing laws at criticality - one of the most fundamental concepts of critical phenomena in physical systems - can also manifest in neural systems.

We also verified our results for coarse graining blocks with different spatial sizes $r = 4, 8, 16$ (Figure 3-2d, e), and durations $\tau = 1, 2, 4, 8$ (Figure 3-2d, e), and different levels of noise $p = 10^{-2}, 10^{-3}, 10^{-4}$ (Figure 3-2f). Optimal x_0 increased with *C* and *r*; optimal *k* increased with *r* and was lowest near *C* = *C** (Figure 3-2d). Changes in r, τ, and p did not qualitatively change our conclusion that coarse graining causes the least change in the dynamical rules near criticality. However, increasing p, decreasing r, and increasing τ all had the effect of broadening the minimum in ζ_{min} and shifting the minimum towards slightly smaller values of C. For increasing p, this shift in the minimal C may be due to the phase transition becoming 'smeared out', less sharp with increased noise (Williams-García *et al.*, 2014), but further investigation is needed to test this possibility. We chose a range of $0.15 < C < 0.35$ because at lower values ($C < 0.15$) the rates of activity became so small that our estimates of the ϕ_n became poor due to subsampling, which made ζ_{min} an unreliable measure (see supplementary materials SM Figure 3-2). A skeptical reader may note that $\boldsymbol{\zeta}$ is not zero at criticality for our model; the scale-invariance we observe is imperfect. Why might this be? In the calculation of ζ, we found that the largest contribution to ζ came from the ϕ_0 term in the sum, which represents spontaneous activation of a node. This is because the coarse graining procedure tends to cause periods with very low S at scale b to become $S = 0$ at scale $b + 1$, thus creating excessive apparent spontaneous activation at scale $b + 1$. When ζ is calculated by excluding ϕ_0 it still minimizes for C near C^* but with a much lower value of ζ indicating higher degree of scale invariance for the dynamical rules governing interactions, i.e. those with $n > 0$ (see supplementary materials SM Figure 3-3).

3.2.3 Realistic Model

The abstract binary model we have discussed so far is simple to interpret and directly comparable to previous work on critical phenomena in neural systems using similar models. Moreover, it is relatively similar to models of spreading dynamics in previous renormalization group studies (e.g. sand piles (Vespignani, Zapperi and Pietronero, 1995) and forest fires (Loreto *et al.*, 1995)). In this sense, it is not terribly surprising that our simple conformed to scale-change symmetry of governing rules, which is expected from theory of critical phenomena. However, our simple binary model is not very biologically realistic. For example, the dynamics of real cerebral cortex never exhibit a sustained high firing regime as we see in the simple model with $C > C^*$. In reality, if the excitability of real cortex is enhanced (or other parameters analogous to C are enhanced) the dynamics tend to exhibit large, repetitive bursts of activity that are suppressed by depressive adaptive mechanisms before reaching a sustained high firing regime (Shew *et al.*, 2009; Gautam *et al.*, 2015). Indeed, activity-dependent adaptive effects can act to make the critical regime more robust (Levina, Herrmann and Geisel, 2007; Shew, Clawson, Pobst, Karimipanah, Nathaniel C. Wright, *et al.*, 2015), which could make the possibility of scale invariant dynamical rules even more plausible in real brains. Next, we set out to test our ideas in a more realistic model of a neural network that generates more realistic network activity. Similar to other recent model studies (Gautam *et al.*, 2015; di Santo *et al.*, 2018), the phase transition we examine in our more realistic model separates an asynchronous phase from an oscillatory ordered phase, which better matches experimental observations.

Building on our simple model; we kept binary, probabilistic, integrate-and-fire neurons on a two-dimensional square lattice ($LXL = 160X160$), but now we introduced inhibitory neurons (20% of all neurons), spike-frequency adaptation, refractoriness, and different distance-

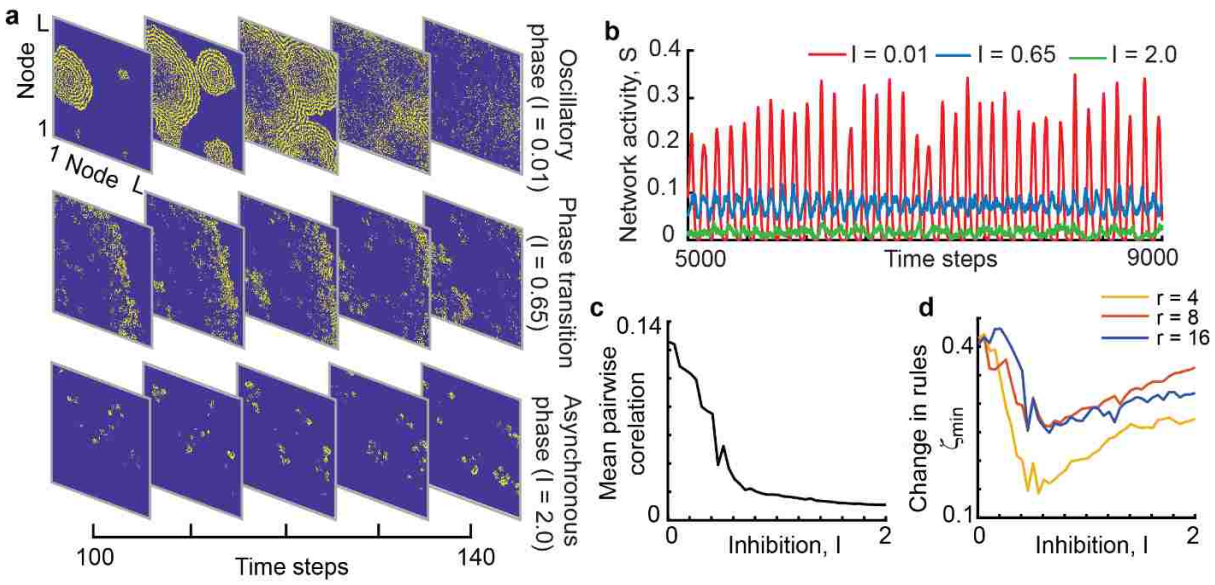

Figure 3-3 Scale-Invariance of Dynamical Rules Peaks at Phase Transition in a More Biologically Plausible Model. a. Each panel shows the two-dimensional lattice of neurons at a single time step. Each pixel represents one neuron (yellow, active; blue, inactive). The spatio-temporal dynamics was limited to small scales for strong inhibition ($I = 2.0$, bottom row), exhibited massive propagating waves and oscillations for weak inhibition ($I = 0.01$, top row), and had more complexity near the transition between these extremes ($I = 0.65$, middle row). b. Time series of network activity reveals the prominent oscillatory activity of the weak inhibition regime (red). c. As inhibition is increased, the boundary of the oscillatory regime near $I = 0.65$ (dashed line) is revealed by the drop in mean pairwise correlations. d. Scale-invariance of dynamical rules peaked (ζ_{min} is minimal) near the onset of the oscillatory regime. This held for blocks with different spatial sizes and durations (see legend).

dependent connectivity for excitatory and inhibitory neurons. At each time t, the binary state $X_i(t) = 1$ with probability $p_i(t)$, where

$$p_i(t) = \begin{cases} 1 \ \ for \ \ \chi_i(t)h_i(t)^{-1} \geq 1 \\ \chi_i(t)h_i(t)^{-1} \ \ for \ \ 0 \leq \chi_i(t)h_i(t)^{-1} < 1 \\ 0 \ \ for \ \ \chi_i(t)h_i(t)^{-1} < 0 \end{cases} \qquad 3\text{-}4$$

Input from other neurons is $\chi_i(t) = \sum_{j \neq i} W_{ij}X_j(t-1)$ and the activity-dependent adaptation is modeled by $h_i(t) = \sum_{t'=t-\tau}^{t} X_i(t')$ where $\tau = 80$. If this sum is zero, we set h to 1. At each time step a neuron can also be activated due to external sources with probability $p_{ext} = 0.001$ (treated independently of p_i). After a neuron fires, its state is set to 0 for a refractory period of 1 time step. The default synaptic weight matrix W is constructed with long-range inhibition relative to

shorter-range excitation. Weights of inhibitory synapses were $W_I(d) = -I * \exp\left(-\frac{d}{C_I}\right)^2$ and excitatory synapses were $W_E(d) = E * \exp\left(-\frac{d}{C_E}\right)^2$ where d is the distance from the presynaptic neuron to the postsynaptic neuron. We consider $C_I = 3$ and $C_E = 2$ (in units of lattice spacing) and fixed excitatory input strength $E = 1$. By tuning the inhibitory input strength oscillatory firing state (high mean pairwise correlation) from asynchronous low firing (low mean pairwise correlation) regime (Figure 3-3**Error! Reference source not found.**a, b, c).

Like the simple model, we found that ζ_{min} is minimized near the phase transition (Figure 3-3**Error! Reference source not found.**d). We emphasize that this more realistic model is outside the bounds of well-understood critical phenomena in physics. While it shares some features with simple models of spreading dynamics (e.g. excitable nodes with refractory periods), the presence of inhibition and nonlocal connectivity make it quite different from these previously studied models. Thus, there is no guarantee that the phase transition we consider here has anything to do with criticality. In this sense, it is substantially more surprising that we observe minimal scale-change of dynamical rules near this phase transition. For the results in Figure 3-3**Error! Reference source not found.**d, we only considered ϕ_n with $n = 1, 2, 3, 4$ for ζ calculation, because ϕ_0 tended to be most prone to error as discussed above (see supplementary materials SM Figure 3-3). We did not include ϕ_5 because the refractory period precluded the occurrence of ϕ_5 at scale b.

So far, we have applied our approach to spike data from our two models. However, many experimentally measured signals are continuous and more closely related to membrane potential, particularly at the larger spatial scales (e.g. LFP, fMRI, EEG, voltage imaging, wide-field calcium imaging). How might we apply our approach to such continuous signals? To address this

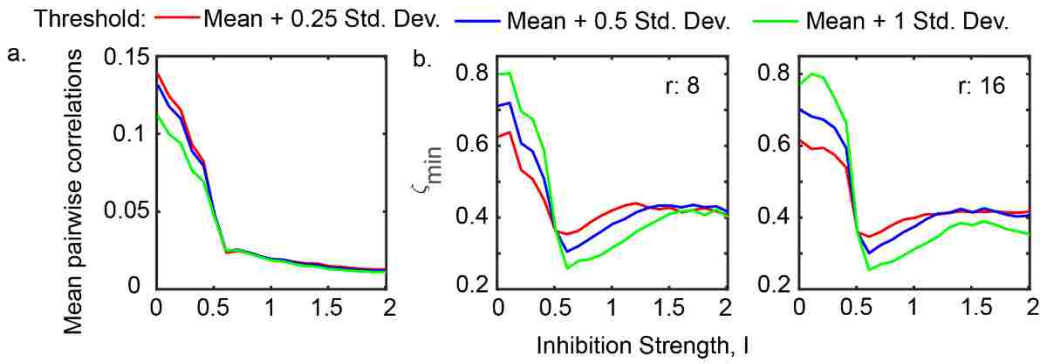

Figure 3-4 Applying Our Approach to Continuous Synaptic Input. a. Mean pairwise correlations of binarized membrane potential for the realistic model. b. Change in dynamical rules ζ_{min} governing the binarized membrane potential as a function of inhibition strength I for $r = 8$ (left), $r = 16$ (right), and different binarization thresholds (color). For all the cases shown $\tau = 1$ and network size, $L\ X\ L = 160X160$.

question, here, we first used our more realistic model. We generated a continuous signal from the model, using the 'membrane potential' from the model neurons. We defined the membrane potential of the i^{th} neuron to be $\chi_i(t)h_i(t)^{-1}$, as defined above. Next, we binarized the continuous membrane potential signal. Following a previously established approach (Tagliazucchi *et al.*, 2012; Scott *et al.*, 2014), we defined time points of activation when the voltage imaging time course crossed above a threshold of 0.5 standard deviations (SD) beyond the mean from below (results consistent for different thresholds 0.25 SD and 1 SD) (Figure 3-4). We found that, like the spike data presented above, this binarized continuous signal also supported our main claim: minimal ζ_{min} near the phase transition.

3.2.4 Mouse cerebral cortex

One advantage of our approach is that it can readily be applied to experimental data, provided the data has sufficient spatial resolution and coverage. Here, we demonstrate this for measurements of cerebral cortex in a mouse awakening from anesthesia. Previous work (Scott *et al.*, 2014) with this data suggested that as the mouse awakens the cortical dynamics transitioned from a supercritical regime, similar to the oscillatory regime in our realistic model, towards

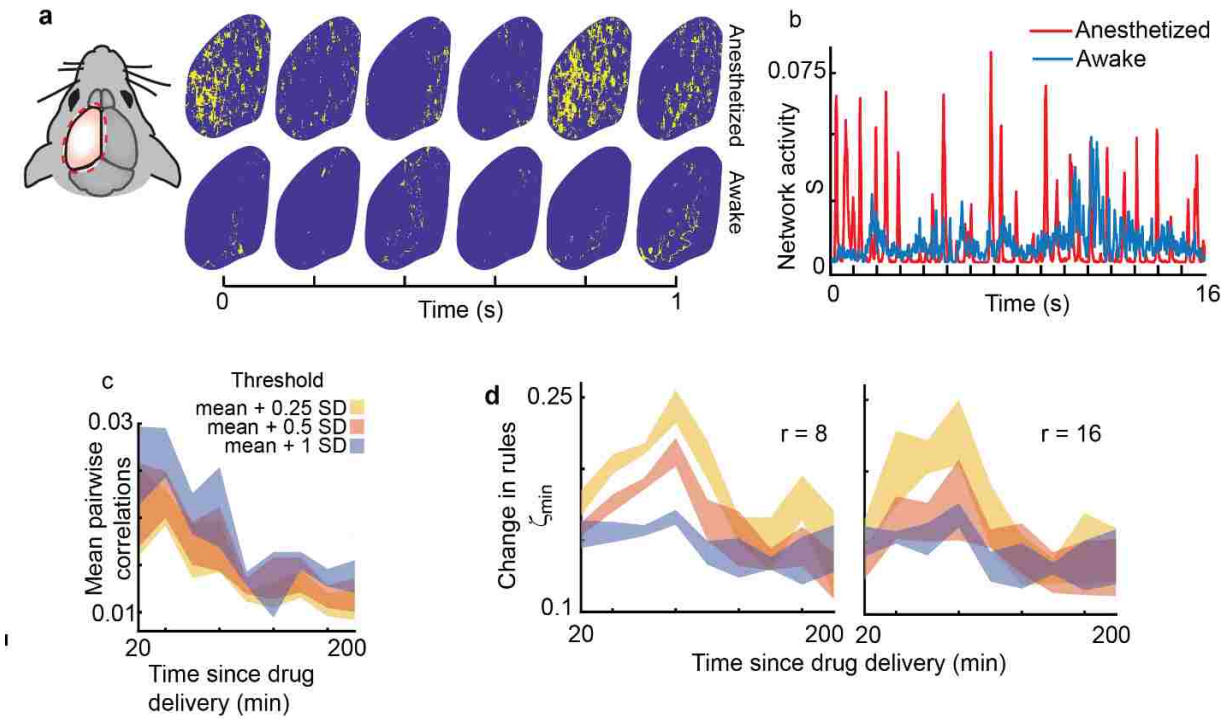

Figure 3-5 Increase in Scale-Invariance of Cortical Dynamical Rules as Mouse Awakens a. Genetically encoded voltage-sensitive fluorescence imaging was done to measure the spatiotemporal dynamics across one hemisphere of mouse cortex as it awoke from anesthesia. Each panel shows a snapshot of binarized activity (yellow, active; blue, inactive). The signal of each pixel arises from many neurons within $33X33\ \mu m^2$ area. b. Time series of binary network activity datasets. Under anesthesia (red), the dynamics exhibited relatively large-scale bursts, whereas the awake dynamics (blue) tended to be more diverse. c. Mean pairwise correlation decreases as the mouse awakens. d. Scale-invariance of dynamical rules increases (ζ_{min} decreases) as the mouse awakens. Results were qualitatively consistent for three different binarization thresholds (yellow, red, and blue) and two different coarse graining block sizes ($r = 8$ and 16).

criticality.(See supplementary materials section 3.4.2 for experimental methods) The brain activity was measured over the dorsal surface of nearly an entire hemisphere of mouse cortex with high spatial resolution using genetically-encoded voltage-sensitive fluorescence imaging. Each dataset was acquired during 1 min with 50 Hz sample rate and $33 \times 33\ \mu m^2$ per pixel spatial resolution. Multiple such 1 min recordings were performed over a period of 200 minutes as the mouse awoke. Each pixel represents the aggregate activity of many neurons within cortical layers 2 and 3. This voltage imaging signal is a continuous signal. To apply our approach, we followed the same binarization approach described above for the membrane

potential analysis of the realistic model (Figure 3-4). We converted each pixel voltage time series into binary form (Figure 3-5a). For each pixel and each 1 min recording, time points of activation were defined at times when the voltage imaging time course crossed above a threshold of 0.5 standard deviations (SD) beyond the mean from below (results consistent for different thresholds 0.25 SD and 1 SD).

Under the effect of anesthesia, we found that the mouse exhibited synchronous burst firing, similar to the oscillatory regime of our realistic model. As the mouse woke up, more asynchronous firing was observed (Figure 3-5b), similar to the activity near the onset of the oscillatory regime of our realistic model. This change manifested as a decrease in pairwise correlations as the mouse awoke from anesthesia (Figure 3-5c). Next, we assumed nearest neighbor interactions among pixels and proceeded to estimate the activation probabilities ϕ_n^b. Then, we applied our course-graining procedure and estimated ϕ_n^{b+1}. As with our analysis of the realistic model only 4 activation probabilities, $n = 1, 2, 3\ 4$ were used to estimate ζ_{min}. We found that ζ_{min} decreased as the mouse awoke from anesthesia. This finding demonstrates that the rules governing cerebral cortex dynamics approach scale-change symmetry during the transition from anesthetized to awake.

We note that, for higher values of τ, there was increased noise in the trend relating ζ_{min} to time since drug delivery. As τ increases, we are left with fewer time points with which we estimate the rules ϕ_n and calculate ζ_{min}. This decrease in samples may be responsible for poorer estimates of the rules ϕ_n and a noisier ζ_{min} versus time trend. Future studies with longer duration experimental recordings could better test this possibility.

3.2.5 Relating rules to dynamics

The approach we have developed here offers a new way to learn about whether a system is operating near criticality by examining how the rules governing dynamics change with scale. In contrast, the traditional way to assess whether a system is near criticality is by examining the dynamics, rather than the rules. For instance, the experimental data we analyze here (Figure 3-5) has previously been shown to exhibit dynamics that are consistent with an approach to criticality as the mouse wakes up (Scott *et al.*, 2014; Fagerholm *et al.*, 2016). This claim was largely based on examining cascades of propagating neural activity, often called neuronal avalanches. At criticality, theory predicts that different sizes of avalanches occur with probability that is related to size according to a power law with exponent near -1.5. In contrast, in the ordered phase (like the oscillatory phase in our realistic model) avalanche sizes are expected to deviate from a power law distribution, with very large cascades becoming more prominent. When Scott et al. analyzed our experimental data, they found that the anesthetized state was consistent with an ordered phase, while the awake state was more consistent with criticality. This finding is consistent with our conclusion that scale-change symmetry increases as the mouse wakes up. However, we emphasize that a power law distribution of avalanche sizes is certainly not equivalent to our finding of scale-change symmetry of rules. Indeed, power law distributions of observed dynamics can arise due to mechanisms that are totally unrelated to criticality (Sornette, 1998; Reed and Hughes, 2002; Mitzenmacher, 2003; Beggs and Timme, 2012; Stumpf and Porter, 2012). If criticality is responsible for a power law distribution of an observable, then we would expect to also find scale-change symmetry of rules. To clarify how scale-change symmetry of rules is related to power law avalanche size distributions, we studied our models further. We examined avalanche size distributions for the simple model as C was tuned through C* and for

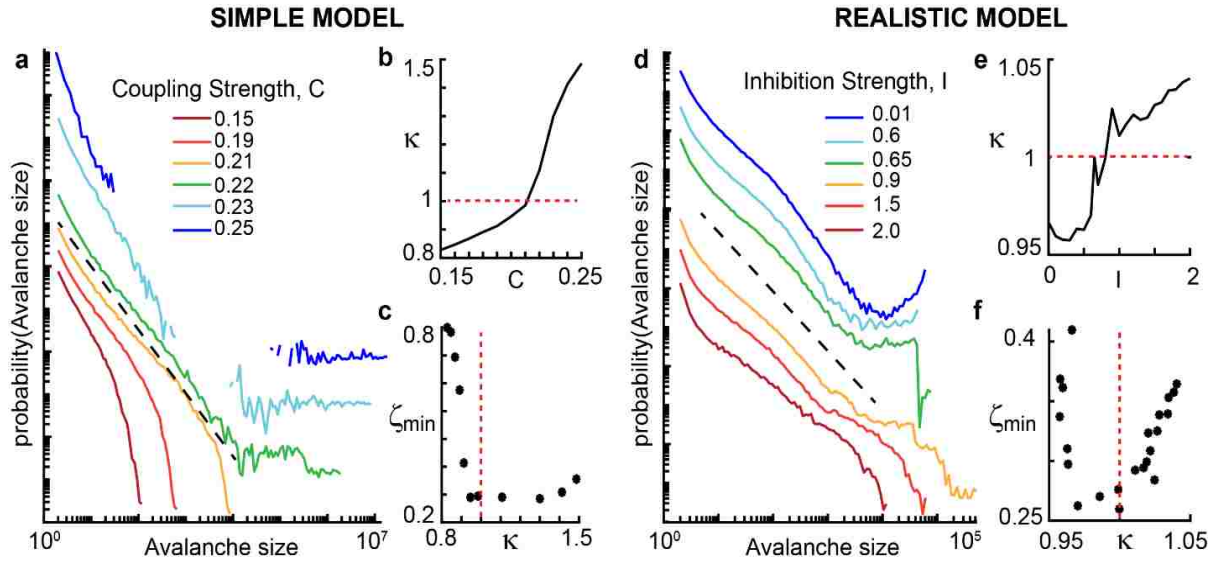

Figure 3-6 Scale-Invariance of Rules Versus Avalanche Size Distributions. a. Shown are avalanche size distributions obtained from the simple model with different values of coupling, c. The probability for large avalanches is prominent for strong coupling and dramatically lower for weak coupling. Distributions are shifted vertically for visual comparison. Black dashed line indicates a power law with exponent 1.5. b. The parameter k measures deviation between a measured avalanche size distribution and 1.5 power law. Near $C = C^*$, we found minimal deviation from power law ($k = 1$). c. We found minimal change in rules ζ_{min} near $k = 1$. d. For the realistic model, avalanche size distributions exhibited high probability for large avalanches when inhibition was small (blue) and approximate power law distributions for stronger inhibition. e. Near the onset of the oscillatory phase, we found the smallest deviation from power law (k near 1). f. Change in rules ζ_{min} was minimal near $k = 1$.

the more realistic model as inhibition (I) was tuned from strong (I = 2) to weak (I = 0.01). We used the previously developed measure κ to quantify deviation from a power law (Shew *et al.*, 2009; Scott *et al.*, 2014). In brief, κ = 1 for a perfect match to the reference power law with exponent -1.5, κ > 1 when large avalanches become prominent (as expected in the ordered phase), and κ < 1 when large avalanches become rare (as expected in the asynchronous phase). Further description of κ is given in the supplementary materials section 3.4.3.

As expected for the simple model, we found that the distribution of avalanche sizes was close to a power law (κ near 1) when C was tuned near C* (Figure 3-6a, b). Thus, in this case, ζ_{min} was also smallest near κ = 1 (Figure 3-6c). Comparing κ and ζ_{min}, we found that κ is more

sensitive to changes in C for C > C*, while ζ_{min} is more sensitive for C < C*. For the more complex model, the oscillatory regime (low inhibition) showed a clear bump in the tail of the avalanche distributions similar to previous studies of dynamics in the ordered (supercritical) phase (Figure 3-6d). As inhibition was tuned from weak to strong, the avalanche size distributions did approach approximate, but rather imperfect power laws. The changes in avalanche distributions we observed for increasing inhibition is similar to what has been shown previously for our experimental data as the mouse wakes up (Scott *et al.*, 2014). Despite the imperfect power laws found in the realistic model, we computed κ and found a clear tendency for minimal ζ_{min} near κ = 1 (Figure 3-6e, f). These results demonstrate a close relationship between avalanche statistics and the scale-change symmetry of rules governing a neural system.

3.3 Discussion

Here we have shown that in neural network models, the rules that govern the system behavior obtain a degree of scale-change symmetry that is most pronounced when the system operates near criticality. In the spirit of renormalization group theory in physical systems, our approach offers a potential explanation of why diverse neural systems can exhibit very similar critical phenomena.

Another useful outcome of our work is that the tools we develop provide a way to assess whether a change in system dynamics takes the system closer to or further from criticality. Our approach complements traditional approaches for seeking evidence for criticality based on power-laws and scaling relations. Such power-law distributions constitute necessary, but insufficient evidence for the criticality hypothesis (Klaus, Yu and Plenz, 2011; Beggs and Timme, 2012; Stumpf and Porter, 2012). Our results suggest that a change towards criticality should be accompanied by an increase in scale invariance of effective dynamical rules. To be

more specific, considering our model work (both models, Figure 3-2Figure 3-3 andFigure 3-4), it is clear that, for a wide range of parameters (C or I) around criticality, a decrease in ζ does not happen unless the parameters have been tuned toward criticality – tuning C towards C* (Figure 3-2) or tuning I towards the value that corresponds to the onset of oscillations (FigureFigure 3-3 andFigure 3-4). However, for a given observed decrease in ζ_{min}, we cannot make precise conclusions about how much closer to criticality the system has shifted. This is not possible considering the quantitative differences in the shape of the ζ_{min} vs C and ζ_{min} vs I curves and how they depend on the details of analysis parameters (e.g. block size). The stronger conclusions that can be made are about 1) the direction of change, and 2) about the relative size of changes within one system. For example, our methods could be used to ascertain which kinds of pharmacological manipulations result in a bigger shift away or towards criticality in a single system with consistent measurement tools. This is an important value of our approach – measuring relative changes in proximity to criticality.

Limitations of study. One limitation of our approach is that it currently requires binary data (Figure 3-1, Figure 3-2 andFigure 3-3) or binarization of continuous data (Figure 3-4 and Figure 3-5). Although spike data is well suited to a binary approach, it would be useful for future work to generalize the approach to continuous data, which is more common in experiments. However, we emphasize that our results based on binarization of continuous data from our realistic model (Figure 3-4) were qualitatively consistent with our results based on spikes. This suggests that the binarization of continuous data provides a useful strategy for studying scale-change symmetry of dynamical rules.

Another limitation of our approach is that we have based our assessment of scale-change symmetry ζ_{min} on one step of renormalization. Renormalization group theory, in contrast,

emphasizes that many steps of renormalization may be required before true scale invariance is found. Each step of renormalization is thought to remove irrelevant details that could corrupt scale invariance. This fact may contribute to why our scale-change measure ζ_{min} is not very close to zero even when our simple model is at criticality. However, the fact that we do find a prominent minimum in ζ_{min} near criticality indicates that we can detect the scale-change symmetry in spite of only performing one step of renormalization. This is important, because, when working with real data from finite systems, it is not plausible to do many steps of coarse graining especially with a large block size.

We also note that there are some trivial types of scale-change symmetry that we are not interested in and have not highlighted in our results above. For instance, for a completely saturated system – all neurons firing at every time step – the dynamics and rules would be identical upon coarse graining. The coarse level would still be completely saturated. Likewise, a completely silent network would also exhibit such trivial scale-invariance. These trivial types of invariance are not the subject of our work but should be noted for completeness.

Our initial application of our approach to experimental data provided interesting results. We showed that scale-invariance of the rules governing cortical network dynamics increased during the transition from unconsciousness to consciousness. This finding is in line with other recent work that suggests the anesthetized cortex deviates from critical dynamics and approaches criticality as it wakes up (Scott *et al.*, 2014; Bellay *et al.*, 2015; Fagerholm *et al.*, 2016) . A recent coarse-graining study of experimental data obtained in hippocampus also revealed interesting scaling, in line with the scale-change symmetry we report here (Meshulam *et al.*, 2018). Our finding raises interesting questions about the functional consequences of scale invariant rules. What does it mean that local interactions, say among cortical columns, are

governed by the same rules as larger scale interactions, say among cortical regions? We expect that our approach will be useful for future studies of these questions and how the dynamical rules

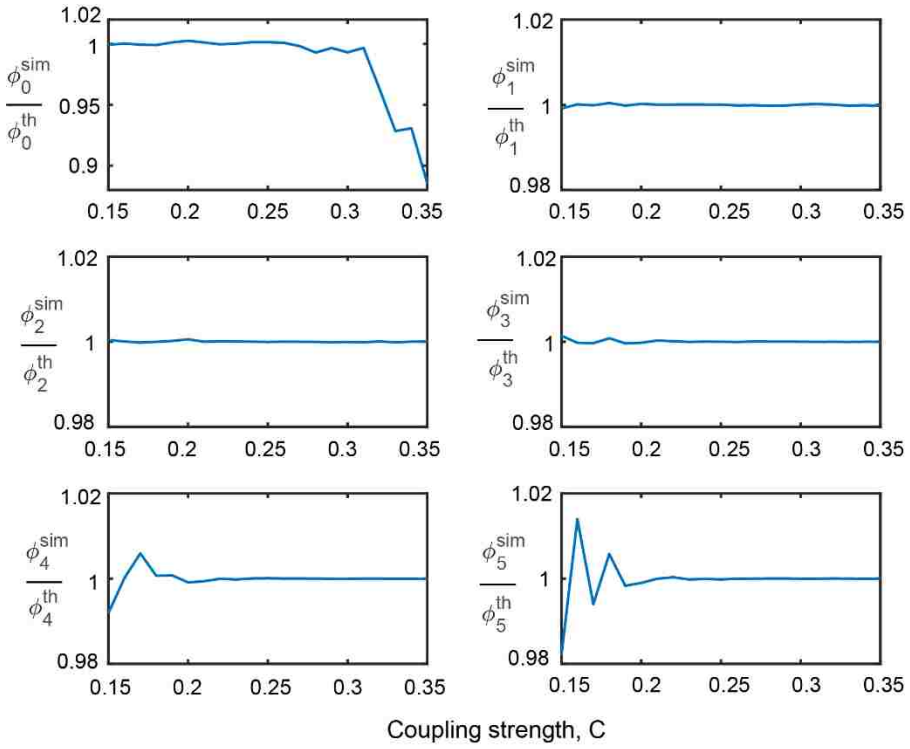

governing brain dynamics differ across scales and brain states.

3.4 Supplementary Materials

3.4.1 Figures

SM Figure 3-1. Estimation accuracy of dynamical rules by comparing ϕ estimated from simulation data vs analytically calculated value. ϕ estimated from network activity data for 10^4 timesteps after 10^2 transient timesteps at coupling strength $0.15 < C < 0.35$. All calculations done for Network size, L X L = 400 X400 and p = 0.001.

In SM Figure 3-1**Error! Reference source not found.Error! Reference source not found.** we show the accuracy of estimating rules ϕ (Related to Figure 3-2 in Section 3.2.2). To test the accuracy of estimation of ϕ_n we took network activity data for 10^4 timesteps after 10^2 transient timesteps at coupling strength $0.15 < C < 0.35$. We compared the activation probability estimated from the simulation ϕ_n^{sim} to analytically calculated $\phi_n^{th} = 1 -$

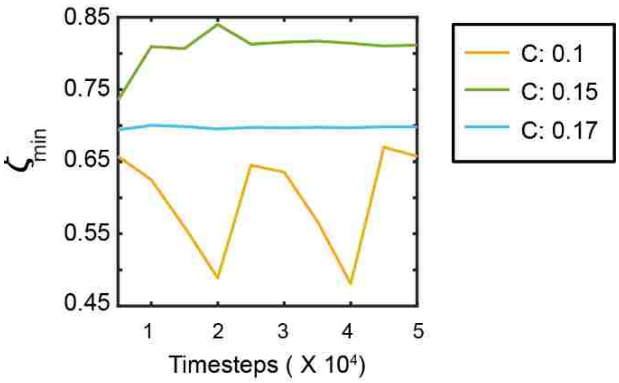

$(1-C)^n(1-p)$ at each C value. Our accuracy is better than 2% for all ϕ_n in the range $0.15 < C < 0.35$ except ϕ_0 where the accuracy is around 2% for $C > 0.3$.

SM Figure 3-2 dependency of rule-change $\zeta_{\min}$ on simulation timesteps. $\zeta_{\min}$ values calculated using data from simulations with varying numbers of timesteps at coupling strengths, $C = 0.1$ (yellow), $C = 0.15$ (green), $C = 0.17$ (cyan). All calculations done for Network size, $L\ X\ L = 400\ X\ 400, r = 8\ and\ p = 0.001$.

In SM Figure 3-2 we show the dependency of rule-change ζ_{min} on simulation timesteps. (Related to Figure 3-2 in the Section 3.2.2) Shown are ζ_{min} *values* calculated using data from simulations with varying numbers of timesteps at coupling strengths, $C = 0.1$ (yellow), $C = 0.15$ (green), $C = 0.17$ (cyan). When the network activity is too low, the estimation of a consistent ζ_{min} require data from increased simulation timesteps

In SM Figure 3-3 we show the alternative estimation of ζ_{min} by excluding ϕ_0. (Related to Figure 3-2 in Section 3.2.2) Shown is the change in dynamical rules ζ_{min} based on excluding ϕ_0. $r = 4$ (blue); $r = 8$ (green); $r = 16$ (red). All calculations are done for network size, $LXL = 400X400$, $r = 8$ and $p = 0.001$. A major contribution to ζ_{min} comes from the difference in ϕ_0 when the network activity is transformed from observational length scale b to $b + 1$. The main reason behind this are the cases when the transformation scheme probabilistically transforms a partially active block of nodes to an inactive node at one timestep and at next timestep partially active block of nodes do changes only slightly but is transformed to an active node. Even with the 5 activation probabilities ϕ_n for $n = 1,2,3,4,5$, ζ_{min} still minimize at C near the critical point C^*.

SM Figure 3-3 Change in dynamical rules ζ_{min} based on excluding ϕ_0. $r = 4$ (blue); $r = 8$ (green); $r = 16$ (red). All calculations are done for network size, $LXL = 400X400$, $r = 8$ and $p = 0.001$.

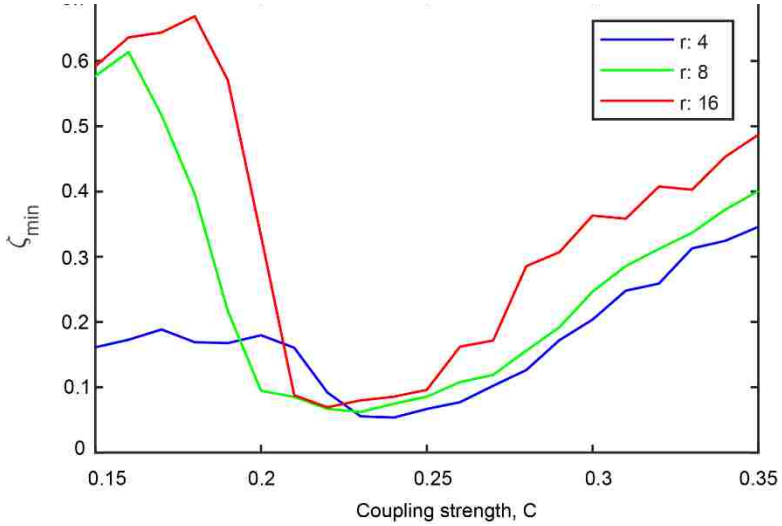

3.4.2 Experimental Methods

Animal experiments were performed in accordance with the National Institutes of Health guidelines for animal research and were approved by the Institutional Animal Care and Use

Committees of the RIKEN Wako Research Center (Japan).The following methods for obtaining the experimental data in **Error! Reference source not found.** have been reported in previous publications as described previously (Akemann *et al.*, 2012; Scott *et al.*, 2014). We describe them again here. In utero electroporation was performed on the mouse (day E15) with the pCAG-VSFP Butterfly 1.2 plasmid. This resulted in expression of the voltage indicator Butterfly 1.2 in pyramidal cells in cortical layers 2/3 of one hemisphere. For imaging, the skull was thinned and a head-post implanted 2-6 months following electroporation. Three days following head-post implantation the imaging measurements reported here were performed. The mouse was first anesthetized (pentobarbital 0.9 g/kg i.p.), then head-fixed, and imaged with a dual emission wide-field epifluorescence microscope (halogen excitation). The voltage imaging signal was the ratio of mKate2 to mCitrine fluorescence, taken after offset subtraction and equalization of heartbeat- related modulation of fluorescence. Between consecutive 1 min imaging periods were 1 min pauses. Preprocessing of voltage signals included baseline normalization by the average over the duration of each recording, spatial and temporal smoothing, and high-pass filtering at 0.5 Hz.

*3.4.3 Avalanche size distributions and **K** calculation*

The following methods for defining avalanches and computing κ (Figure 3-6) have been reported in previous publications (Tagliazucchi *et al.*, 2012; Scott *et al.*, 2014; Fagerholm *et al.*, 2016). First, avalanches were defined as spatiotemporally contiguous clusters of active pixels. Clusters of active pixels were identified in each frame, based on the detection of connected pixels in a coactive first neighbors graph. Avalanches were then defined as starting with the activation of a previously inactive cluster, continuing while 1 contiguous cluster was active in the next time point. Avalanche size probability density distributions (Figure 3-2a, d) were calculated by

counting the number of avalanches in each size bin and normalizing by the total number of avalanches and bin size. Avalanche size probability distributions were compared with a power law with exponent -1.5 using a measure called K, first developed in our previous work (Shew et al., 2009). First, the measured distribution is recast as a cumulative density function (CDF), called $F(\beta)$, which specifies the fraction of measured cluster sizes $s < \beta$. Then a reference CDF is created corresponding to a perfect -1.5 power law, called $F_{NA}(\beta)$

$$F_{NA}(\beta) = \left(1 - \sqrt{\frac{1}{L}}\right)^{-1} \left(1 - \sqrt{\frac{1}{\beta}}\right) \quad 3\text{-}5$$

for $l < s < L$, where l is the smallest avalanche size considered and L is the largest. A nonparametric measure, K, is defined to quantify the difference between the measured avalanche size CDF, $F(\beta)$, and the theoretical reference CDF, $F_{NA}(\beta)$, as

$$K = 1 + \frac{1}{m}\sum_{k=1}^{m}\left(F_{NA}(\beta_k) - F(\beta_k)\right) \quad 3\text{-}6$$

where β_k are $m = 10$ avalanche sizes logarithmically spaced between l and L. When computing K, avalanches below a minimum size, x_{min}, were excluded. The rationale for this is that some measurement noise is inevitable and likely to be uncorrelated across pixels, resulting in some small "noise cascades."

CHAPTER 4 INHOMOGENEITY IN INHIBITORY SYNAPSES LEADS TO PARADOXICAL CHANGE IN NEURONAL ACTIVITY

4.1 Introduction

In mammals, brain regions such as cortex and hippocampus, consist of subpopulations of excitatory and inhibitory neurons. (Jones, 1986; Amaral and Witter, 2004). The inhibitory neurons release neuro-transmitter GABA and comprise approximately 20% of cortical neuronal population.(Meinecke and Peters, 1987). The rest of the neuronal population in cortex are excitatory. The interplay of excitation and inhibition is crucial in shaping spontaneous (Haider, 2006; Okun and Lampl, 2008; Atallah and Scanziani, 2009) and sensory-evoked cortical activity. (Swadlow, 1988; Anderson, Carandini and Ferster, 2000; Monier *et al.*, 2003; Wehr and Zador, 2003; Tan *et al.*, 2004; Wilent and Contreras, 2005; Wu *et al.*, 2008; Poo and Isaacson, 2009; Isaacson and Scanziani, 2011). The balance between excitatory and inhibitory stimulus has been proposed to underlie learning and adaptation dependent changes in stimulus driven responses. (Froemke, 2015; Shew, Clawson, Pobst, Karimipanah, Nathaniel C Wright, *et al.*, 2015). Here we present a study where we manipulate the excitation-inhibition (E/I) balance in motor cortex of awake mice by pharmacologically altering inhibitory interactions.

What do we expect to happen if we alter inhibition? On one hand, there are many experiments where pharmacologically enhanced inhibition (GABA agonists) results in low firing rates and decreased inhibition (GABA antagonists) often leads to high firing rates.(Mao *et al.*, 2001; Shew *et al.*, 2011; Gautam *et al.*, 2015; Fagerholm *et al.*, 2016). But there are other studies that show that this might not always be true. Theoretically, it has been shown that, if the recurrent connections among the excitatory neurons are strong enough to make the excitatory network unstable when feedback inhibition is removed, then, selectively, increasing the direct

external inhibitory input to the inhibitory neurons can lead to increase in their firing rates.(Tsodyks *et al.*, 1997) This was referred to as a paradoxical response, because it is opposite of the change expected based on most previous experiments. A recent experiment showed using optogenetic manipulation that suppressing/activating inhibition and excitation can sometimes produce paradoxical changes in neural activity and corresponding differences in behavior of different individual animals.(Briguglio *et al.*, 2018). In another study researchers have shown that the external activation of a population that directly inhibits a second population can trigger a positive response or a negative response of the latter depending on the sensory input. These counterintuitive phenomena rely on the presence of multiple populations of inhibitory interneurons and nonlinear responses to input.(Garcia Del Molino *et al.*, 2017)

In our experiments, we observed that pharmacological manipulations of inhibition with low drug concentrations can lead to paradoxical changes neural dynamics. We found that the overall population firing rate remained largely constant, while the individual neurons had diverse changes in firing rate. A fraction of neurons (increase/decrease) firing rate when the inhibition (decrease/increase), i.e. a non-paradoxical, expected change. However, certain other neurons had a paradoxical change in their firing rates. By paradoxical change we mean that these neurons actually (decrease/increase) in response to (decrease/increase) in overall inhibition in the neural system. Here we examined both experimental data and a computational model to quantify and understand this paradoxical change in neural activity.

Based on our model, we argue that the reason behind the paradoxical behavior might be due to differences among neurons and synapses. In particular, inhomogeneity in the strength of inhibitory synapses seems to be an important feature. Based on previous work, it is not surprising that such inhomogeneity should exist. For example, researchers have used

comprehensive large-scale profiling of cortical neurons to differentiate 15 major types of inhibitory neurons, each with its own characteristic input-output connectivity profile.(Jiang *et al.*, 2015). It has also been shown that the local cortical circuity differs significantly from a random network. Especially, the distribution of synaptic connection strength can be fitted by a lognormal distribution. (Song *et al.*, 2005). In fact, at many physiological and anatomical levels in the brain, the distribution of numerous parameters such as synaptic weights, neuronal firing rates and number of synaptic contacts between neurons, is strongly skewed with a heavy tail.(Buzsáki and Mizuseki, 2014) Recent mouse brain network studies(Wang, Sporns and Burkhalter, 2012; Oh *et al.*, 2014) and retrograde labelling studies in macaques(Markov *et al.*, 2014) have shown that that, in a given cortical area, a minority of strong inputs are mixed with large numbers of weak inputs. Thus, inhomogeneity of neural properties is not controversial. However, it is less obvious how inhomogeneity of network properties might lead to paradoxical response to changes in inhibition. We will explain this new result below.

The outline of this study is as follows. First, we first analyzed how the neuronal activity recorded from motor cortex of awake mice change under the effect of drugs which alter inhibitory signaling, namely, bicuculine (suppresses inhibition) and muscimol (enhances inhibition). We show that under low drug concentration, for certain neurons the dynamical activity changes paradoxically, opposite to rest of the neurons. Next, we present a computational model consisting of integrate-and-fire neurons with excitatory and inhibitory synapses. In this model we successfully simulated the paradoxical neural behavior as we see in the experiments. Finally, we analyzed the network motifs in the computational model that lead to the paradoxical change in some neurons. We found that these neurons are connected to pre-synaptic neurons via strong inhibitory synapses. Thus, when the presynaptic neuron behaves non-paradoxically (e.g.

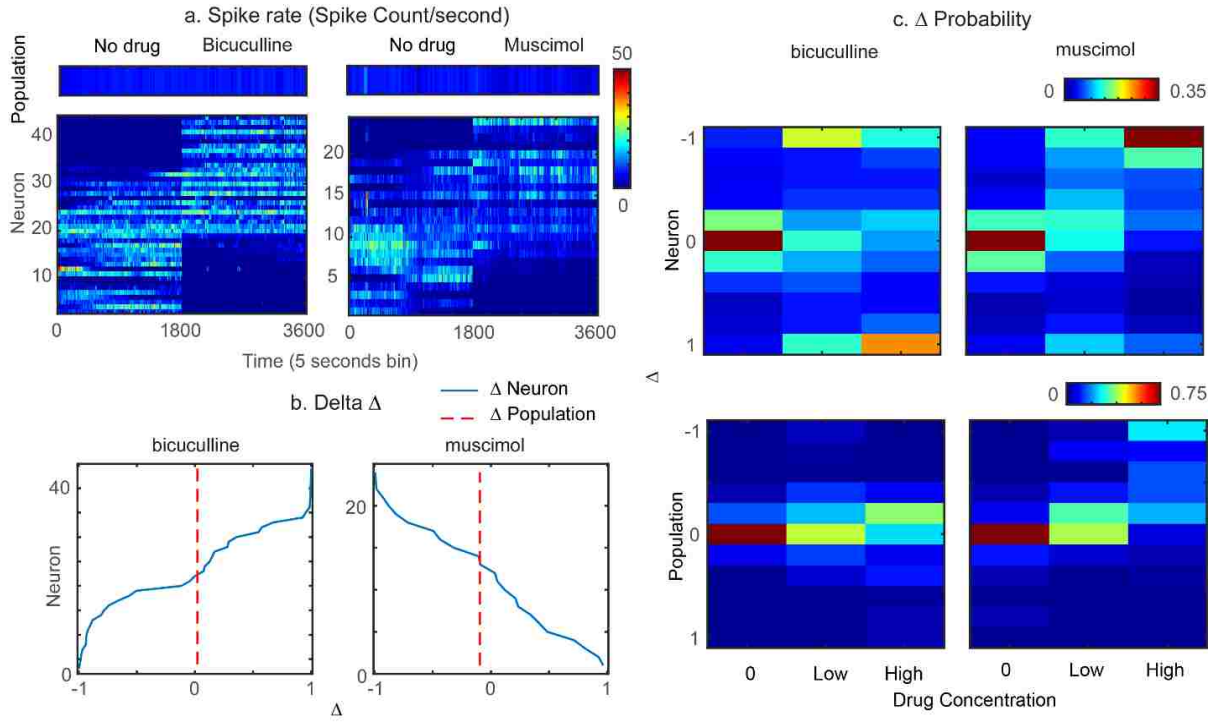

Figure 4-1 Diverse response to inhibition modulation in motor cortex. a) Single neuron and population spike rate as a function of time. Each row of the image represents a single neuron spike rate time series. Spike rate calculated over 5 seconds bin. b) Neuronal and Population Delta Δ. Data for a) and b) taken from Rat#3, with bicuculine 20uM concentration and muscimol 40uM concentration. c) Probability distribution of Delta Δ, as a function of concentration. The zero concentration Delta Δ is calculated by splitting the 'sham' reading in two halves and r_1 and r_0 calculated over them. Similarly, the low and high concentration Delta Δ values are calculated by splitting the 'drug' reading in two halves and thus r_1 is calculated from drug readings and r_0 from 'no drug' reading. The probability distribution of Delta Δ for zero concentration is calculated using all the experiments. For the low and high concentration, probability distribution of Delta Δ is calculated over experiments as mentioned in supplementary materials Section 4.4.2. Number of Neurons: Low concentration bicuculline- 747; muscimol- 633. High concentration bicuculline- 697; muscimol- 568.

decreasing firing when inhibition is increased), the post synaptic neuron experiences much less inhibition and paradoxically increases its firing.

4.2 Results

4.2.1 Experimental Results

The results of our study are based on interesting observations from electrophysiological recordings from motor cortex in awake rats (see supplementary materials 4.4.2). We recorded

neural spiking activity for 30 min before and 30 min after administering bicuculine (muscimol) to inhibit (promote) the GABA receptors, responsible for inhibitory input to neurons. We note, there is was a break between recordings to give the drugs time to reach a steady state. Inhibiting (promoting) GABA receptors to decrease (increase) inhibitory signals to neurons lead to diverse range of changes in neural dynamical activity. We quantify the spiking activity of neurons by calculating the spike rate, r which is the count of number of times a neuron spikes in a given time interval (5 seconds, for current analysis).

In Figure 4-1 we show the change in the neuronal and population spike rate under the effect of Inhibitory signal modulating drugs. We can see that under the effect of bicuculine ($20\mu M$ concentration) a fraction of neurons show increase in their spike rate whereas under muscimol ($40\mu M$ concentration) a fraction of neurons show decrease in spike rate. This dynamical behavior is an expected outcome for the corresponding inhibitory signal modulation. As an intuitive explanation, one would expect the neurons to fire more if more of its inhibitory input signals are blocked and vice-versa. But, interestingly for a fraction of neurons, increasing (decreasing) inhibitory signaling leads to increase (decrease) in their spike rate. Due to these paradoxically behaving neurons the overall population spike rate for these neurons remains largely unchanged. To quantify the changes in spike rate, we defined a parameter Δ calculated as,

$$\Delta = \frac{r_1 - r_0}{r_1 + r_0} \qquad 4\text{-}1$$

where r_1 is mean spike rate calculated after a change in inhibitory signaling. And r_0 is mean spike rate calculated before the change in inhibition. Δ will be $> 0 (< 0)$ if the spike rate increases (decreases) under the effect of the drug. In Figure 4-1b we show the Δ calculated for the spike rates shown in Figure 4-1a. We see that for the population the Δ value is close to 0

under both kind of drugs, whereas for individual neurons, a diverse range of Δ values are seen from -1 to 1.

It is important to mention that the results presented till now are with low drug concentrations. We went ahead to estimate the Δ values from a total of 49 experiments in 3 rats for a range of drug concentrations both for bicuculine and muscimol. To get statistically consistent results, we calculated the probability of a neuron or population of neurons to have a particular Δ value from many recordings done over low drug concentrations (≤ 80 μM) and high drug concentrations ($>$ 80 μM). Since firing rates also change in time without any drug manipulations, we also did a control analysis to obtain zero concentration Δ values by splitting the sham recording into two halves and then calculating Δ using them. In Figure 4-1c We present the results for the estimated $\Delta\, probability$ as a function of drug concentration. A key finding from this analysis was that as we increase the drug concentration the paradoxical change in neuronal spike rate gets less prominent, i.e. neurons behave in the traditionally expected way for large drug concentrations. Consequently, for large drug concentrations, the overall population spike rate does not remain steady; it increases (decreases) considerably under bicuculine (muscimol). These experimental findings motivated us to find what makes these cortical neurons to behave paradoxically. We simulated a model of neural network to answer this question.

4.2.2 Computational Model

We built upon a simple model, studied previously in Ref. (Larremore, Shew and Restrepo, 2011). The model consists of a network of *N* stochastic binary neurons, indexed $i = 1,2 \ldots, N$. The state of neuron *i* at time *t* is denoted by $x_i(t)$, which can take the values $x_i(t) = 0$ if the neuron is resting and $x_i(t) = 1$ if the neuron is spiking. Time is assumed to evolve in

discrete steps $t = 0,1,2$ .... The evolution of each neuron's state is stochastic and depends on the states of other neurons at the previous time step,

$$x_i(t) = \begin{cases} 1 \; with \; probability \; \sigma\left(\left[\eta + \sum_{j=1}^{N} w_{ij} x_j(t-1)\right]\right) \\ 0 \; otherwise \end{cases} \quad 4\text{-}2$$

where σ(x) constrains x to be between 0 and 1; $\sigma(x) = 0 \; for \; x \leq 0, \; \sigma(x) = 1 \; for \; x \geq 1, and \; \sigma(x) = x \; for \; 0 < x < 1$. The sum represents input from other neurons which fired at time $t - 1$ and external input to the network is represented by the constant $\eta = 0.8$.

The NXN matrix W models the network structure and synapse weights. The strength of the synapse from neuron j to neuron i is, $w_{ij} = w_E > 0$ for excitatory synapse, $w_{ij} = w_I < 0$ for inhibitory synapse and $w_{ij} = 0$ if neuron j does not connect to neuron i. The matrix W was constructed in four steps. First, an NXN matrix of numbers was drawn from a uniform distribution with entries between 0 and 1. Second, inhibitory neurons were designated by multiplying 20% of the columns of W by -1. Third, 99% of the inputs for each neuron were set to zero (i.e. disconnected), to provide sparse connectivity of 1%. The entire matrix was divided by a constant such that the largest eigenvalue of the matrix was 1, which ensures that the network dynamics are stable (neither growing, nor decaying in time, on average), as studied in previous work(Larremore, Shew and Restrepo, 2011; Larremore *et al.*, 2014). To mimic the inhibitory signal modulation in the network model, we multiply the inhibitory weights by inhibitory signal modulation factor, I. Thus, transforming inhibitory weights as follows: $w_I \rightarrow w_I * I$. Similar effects as bicuculine administration (block inhibitory signals) are recreated by choosing $I < 1$ and as muscimol administration (promote inhibitory signals) by choosing $I > 1$. To calculate the Δ probability for a fixed inhibitory modulation factor Δ values are generated for 100 random network realizations.

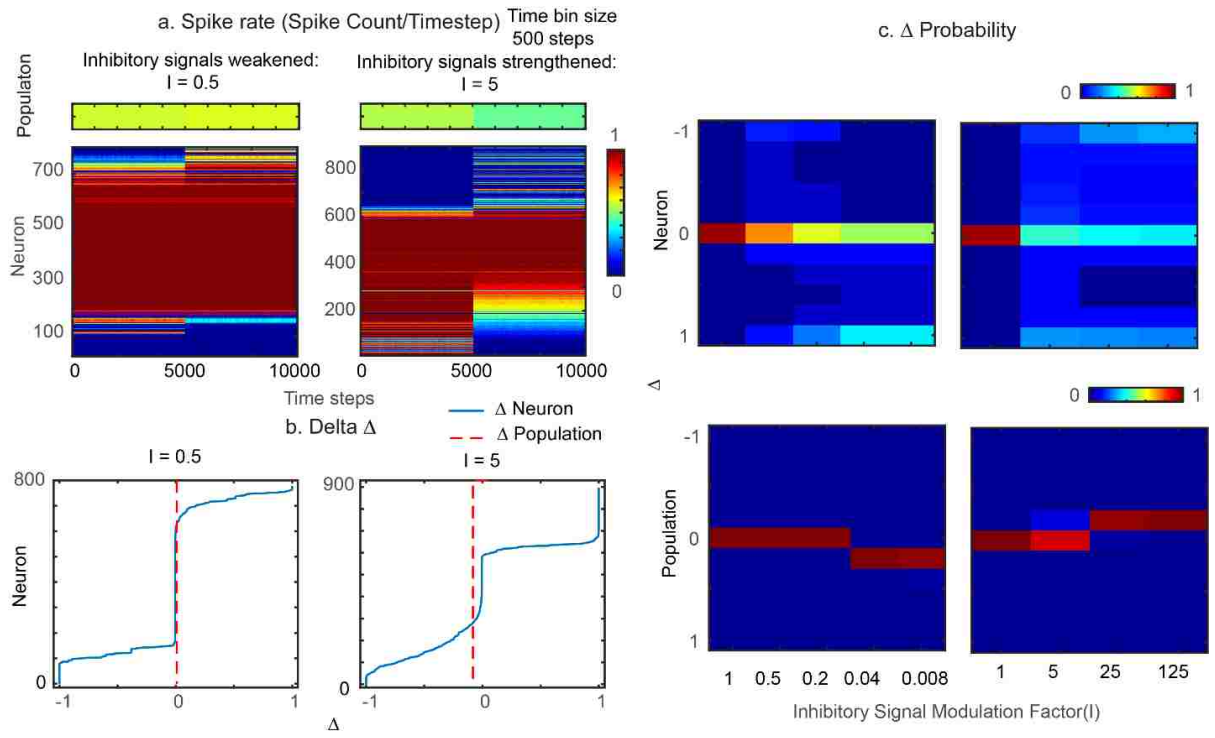

Figure 4-2 Diverse responses to inhibition modulation in neural network model. For two kinds of inhibition modulation, weakened, $I = 0.5$ and strengthened, $I = 5$, a) neuronal and population Spike rate, b) neuronal and population Delta Δ, and c) probability distribution of Delta Δ, as a function of concentration. Probability is calculated using Delta Δ values from 100 random network realizations at each Inhibitory Signal Modulation factor. Spike rate is calculated using spike data over 500 timesteps bin. All calculations are done for network size N=1000, connection probability $p=0.01$ and external noise $\eta=0.8$.

We found that this simple model did not result in any paradoxical changes in firing rate (Section 4.4.1 SM Figure 4-1). To obtain paradoxical changes we found that we needed greater inhomogeneity among the neurons and synapses. We create heterogeneity in the inhibitory synapses across the network by increasing the strength of synapse for a randomly selected fraction of inhibitory neurons. Inhibition is modeled as the negative entries w_I of weight matrix W. We randomly select $\alpha * \mathrm{N}$ inhibitory columns in W and set the entries to be $\beta * w_{ij}$, $\alpha = 0.5$ and $\beta = 50$. The model was run for 10^4 time steps. Spike rate time series were constructed using time bins of duration 500 timesteps.

After adding this inhomogeneity, we obtained model behavior similar to the experimental results. The spike rate change under inhibitory signal modulation is diverse at neuronal level. The overall population spike rate is balanced out and undergo only slight change for low degree of modulation (Figure 4-2a, b). A fraction of neurons behaves conventionally and increase (decrease) the spike rate when the inhibitory signal in the network is weakened (strengthened) and a fraction of neurons have paradoxically opposite change in their spike rate. In Figure 4-2c we show the Δ probability as a function of inhibitory modulation factor. In accordance to the experimental findings we see that for I closer to 1 i.e. weak inhibitory signal modulation paradoxical change in neuronal spiking activity is prominently seen which declines at very low or very high values of I. Consequently, significant change in population spike rate only occur at strong inhibitory signal modulation. We also estimated Δ probability as a function of I by considering other variations of the computational model parameters. In supplementary materials Section 4.4.1 **Error! Reference source not found.** we show models with dense connectivity, low noise or homogeneous inhibitory weights. Results for all the variations verified that the model discussed above has the best agreement with the experimental results.

4.2.3 Network Motifs

We showed that paradoxical change in the neural dynamics can be achieved through network connectivity that has inhomogeneity in the strength of inhibitory synapses. But we did not yet explain why such connectivity gives rise to spike rate increase (decrease) on increasing (decreasing) the overall inhibitory signal strength. We address this question by asking what is different about the input to the paradoxically behaving neurons compared to any randomly chosen neuron in the network. To do so, we first define the network motifs of two-level inputs to a target neuron. We define the target neuron to be one that undergoes a strong paradoxical

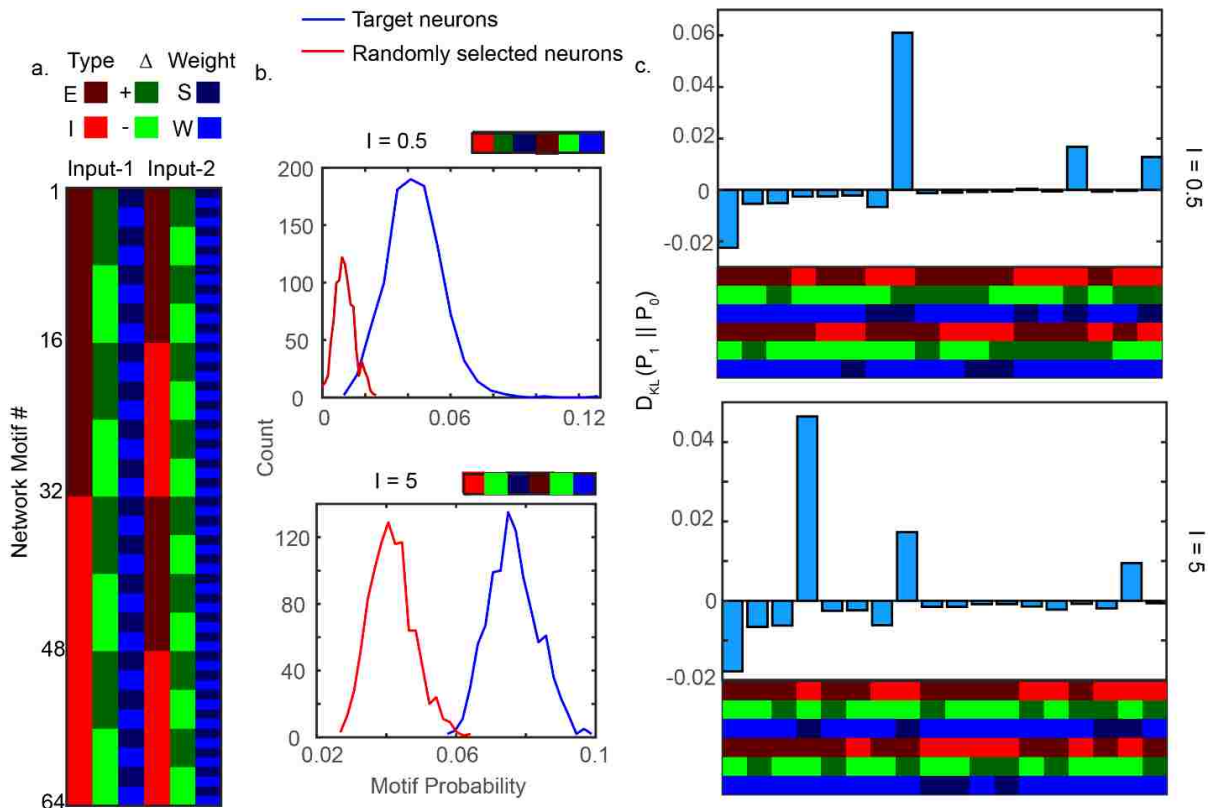

Figure 4-3 a) All possible Input Motifs. b) Considering 1000 realizations of our model, paradoxical neurons showed a distribution of motif probabilities. Shown here are distributions for two such motifs: Input1(Inh: Δ+: Strong weight)-Input2(Ext: Δ-: weak weight) $I = 0.5$ [top] and Input1(Inh: Δ-: Strong weight)-Input2(Ext: Δ-: weak weight) $I = 5$ [bottom]. c) Each bar represents the difference (Kullback–Leibler (KL) divergence) in motif probability averaged over 1000 model realizations. Shown are a subset of all 64 possible motifs, including those that account for the top 95% of the Motif probabilities. Motif Probabilities are estimated for 1000 random trials.

change and satisfies, $\Delta > 0.5\ for\ I = 5$ or $\Delta < -0.5\ for\ I = 0.5$. We define the network motif as follows,

$$Input\ Neuron\ 2 \rightarrow Input\ Neuron\ 1 \rightarrow Target\ Neuron$$

We characterize 6 properties in a network motif represented as $(N^1; \Delta^1; W^1; N^2; \Delta^2; W^2)$, where N^i is the type of input neuron, inhibitory (Inh) or excitatory (Ext); Δ^i is the Delta value of the input neuron, positive (+) or negative(-); and W^i is the strength of the input synapse, Strong (s) or Weak (w). The superscript $i = 1$ represents the presynaptic neuron to the target neuron, Input Neuron 1. Superscript $i = 2$ represents the presynaptic neuron to Input Neuron 1. Since all 6

properties each can have 2 possible states, we have 64 network motifs that will describe all the possible inputs into a neuron (see Figure 4-3a**Error! Reference source not found.**).

Next, we quantified how often each motif occurred for paradoxical neurons and compared this to the motif occurrence probability for any randomly chosen neuron, keeping the number same to avoid sampling bias.

For one realization of our model, we typically found about 10% paradoxically behaving neurons. We ran simulations for 1000 random network realizations to gain statistical significance. In **Error! Reference source not found.**b we show motif probability count distribution for 2 example network motifs, one for each kind of inhibitory signal modulation. It can be seen that for inhibitory signal modulation $I = 0.5$ the network motif $(Inh^1; +^1; s^1; Exc^2; -^1; w^2)$ has count distributions with very low overlap for target neurons and randomly selected neurons. This indicate that this particular network motif is specifically associated to neurons that show paradoxical dynamical change, i.e. have $\Delta < 0$. Similarly, for the case of, $I = 5$ kind of modulation the network motif we show $(Inh^1; -^1; s^1; Exc^2; -^1; w^2)$ network motif being specifically associated to neurons that have $\Delta > 0$.

To estimate the difference in inputs to target neurons and any random neuron in the network, we calculate Kullback–Leibler (KL) divergence for each possible motif,

$$D_{KL}\,(P_1 \,||\, P_0) = \; P_1\, log\, \frac{P_0}{P_1} \qquad 4\text{-}3$$

where P_1 and P_0 are mean motif probabilities for target neurons and randomly selected neurons respectively. In Figure 4-3c we show the KL-divergence for the most important network motifs (those that constitute 95% of all inputs to target neurons). It can be clearly seen that the network motifs that has highest KL-divergence are $(Inh^1; +^1; s^1; Exc^2; -^1; w^2)$ and $(Inh^1; -^1; s^1; Exc^2; -^1; w^2)$ for inhibitory signal modulations $I = 0.5$ and $I = 5$, respectively.

One key observation from these motifs is that the strong inhibitory input is essential to the paradoxical change in target neurons. Consider, $I = 0.5$, the spike rate of the presynaptic neuron with strong inhibitory input to the target neuron increases. Since this input is much larger than any other input, it immediately decreases the spike rate for target neuron. Hence, the inhomogeneity in inhibitory synapse becomes a key factor in target neurons changing spike rate paradoxically different to rest of the neurons. Similarly, on $I = 5$, the strong inhibitory input neuron gets shut down by increased inhibition. This will allow the target neuron to increase its spike rate based on the rest of its inputs.

We also performed t-test between motif probabilities for target neurons and randomly selected neurons to test which network motifs are differ with statistical significance. (see Supplementary Materials Section 4.4.1 **Error! Reference source not found.Error! Reference source not found.**) We found that many motifs had statistically significant differences in occurrence probabilities. But the motifs with the most extreme differences had strong inhibition presynaptic to the paradoxical neuron.

4.3 Discussion

Here we have shown that inhibitory modulation in neural network leads to paradoxical dynamical activity in a fraction of neurons. If the overall strength of inhibitory signal is (increased/decreased), most of the neurons (decrease/increase) their neural activity, as one would expect in a uniformly connected network. But a fraction of neurons responds in opposite direction and (increase/decrease) their neural activity. This paradoxical behavior is less common for strong inhibitory modulation. Moreover, the population spike rate only changes at high strength inhibitory modulation. The paradoxical behavior in some neurons acts as a balancing mechanism to maintain fixed population firing rate.

One interesting implication of these observations relates to homeostasis of network level activity(Turrigiano, 2011; Hengen *et al.*, 2013) . This is the idea that various mechanisms in the brain may act to maintain the firing rate of the neural population within certain healthy bounds. Our findings suggest that paradoxical changes in firing may serve as such a homeostatic mechanism in response to small changes in the balance of excitation and inhibition. To our knowledge this mechanism of population firing rate homeostasis has not previously been reported.

Going beyond our experimental measurements, our modeling efforts reveal a more detailed possible explanation of the paradoxical changes in firing rate. We have presented a network model of integrate and fire neurons with inhibitory and excitatory synapses. We model the connections between the neurons as Erdős-Rényi random network. Each link in the network represents a synapse from an (excitatory/inhibitory) pre-synaptic neuron to a post-synaptic neuron. The weight of the link of the link represents the synaptic strength. The dynamical behavior of the network model is qualitative similar to the behavior in the experimental recordings. We altered the inhibitory signals by multiplying all the inhibitory weights by a constant factor, which was > 1, for increase in inhibition and < 1, for decrease in inhibition. The key components of this network model are sparse connectivity, high external noise and inhomogeneity in inhibitory synaptic strength. Apart from these conditions, we follow 80:20 ratio of inhibitory and excitatory neurons as seen in many real neural systems. The excitatory weights are drawn from a uniform random distribution with limits [0,1]. This shows that the neurons can exhibit paradoxical dynamical behavior with homogenous excitatory weights. The sparse connectivity along with inhomogeneous inhibitory weights spanning multiple orders of

magnitude were essential for the neurons the ability to change their dynamics paradoxically and maintain the overall population firing rate.

Do these structures favor certain kind of network motifs? We address this question by estimating the network motif counts for all possible two-level input to neurons in the network. For a given neuron, the first level is the direct input by a pre-synaptic neuron. The spiking rate of this neuron is directly or indirectly proportional to the input depending on whether it's inhibitory or excitatory in nature. The second level is the pre-synaptic neuron to first level input and it indirectly affects the activity of the neuron. The second level neuron affects the spiking activity of first level input neuron which in turn affect spiking activity of the given neuron. We compared the neuron with strong paradoxical change to a random neuron in the network. We looked at two-level input motifs for both cases and estimated the probabilities of different two-level input motifs present in the network. To quantify the difference between paradoxical neurons and other neurons, we computed the Kullback–Leibler (KL) divergence between their motif probabilities. Our results clearly indicated that the neurons that undergoes paradoxical dynamical change have a strong inhibitory input neuron. We see that increasing network level inhibition reduced the spiking activity of this strong inhibitory input neuron. Similarly, decreasing network level inhibition leads to the strong inhibitory neuron increase its spiking rate. Since, this inhibitory input is much stronger than the rest of inputs, it becomes the deciding factor. If this strong input neuron fires the post-synaptic neuron will definitely not fire. Hence, the post-synaptic neuron exhibits the paradoxical change in spiking activity when the rest of the network not.

The results of our model suggest a new role for inhomogeneous network structure, particularly among inhibitory neurons, in firing rate homeostasis of cortical neural networks.

4.4 Supplementary Materials

4.4.1 Figures

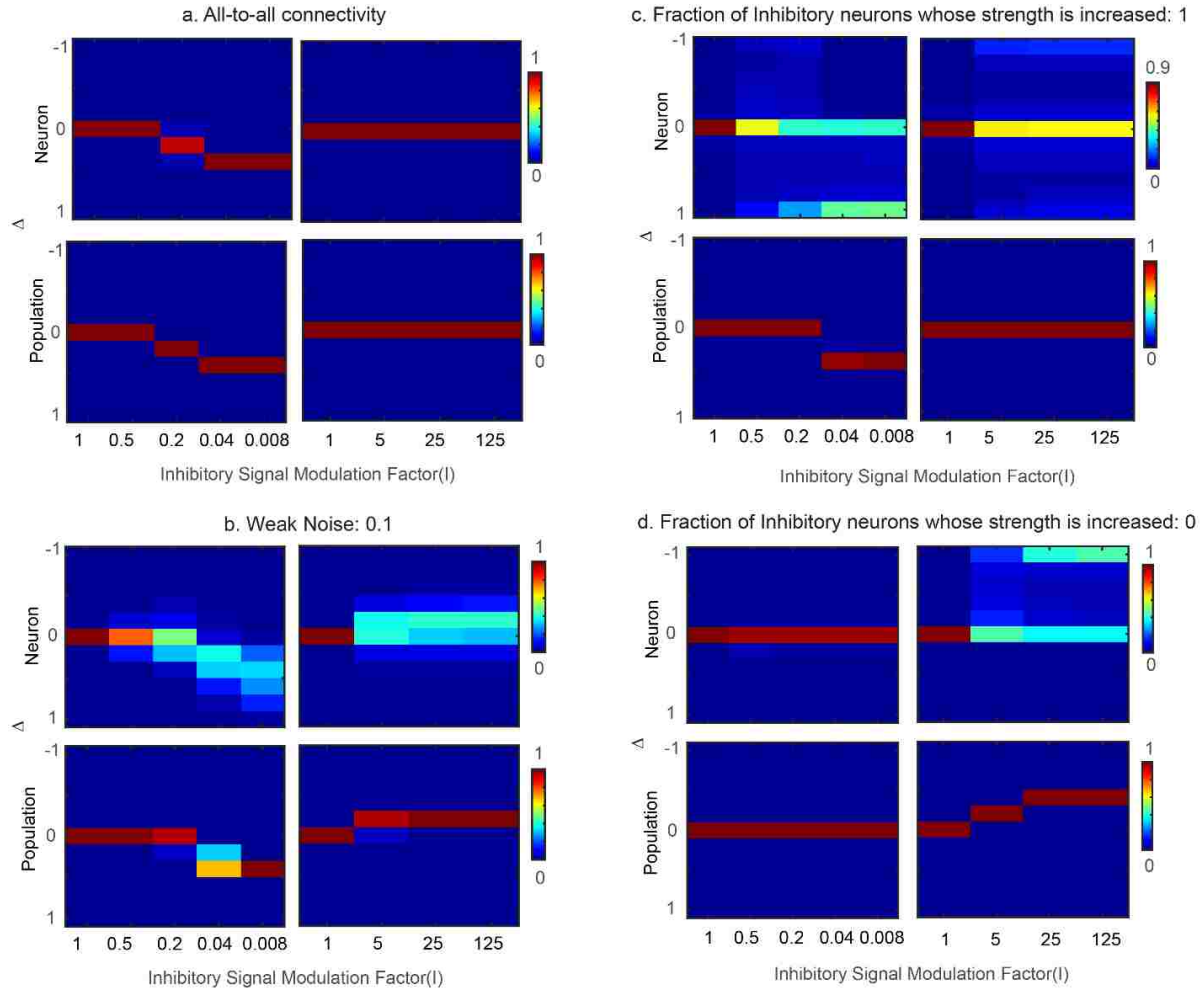

SM Figure 4-1 *Δ* probability as a function of Inhibitory signal modulation factor. a. This model has all-to-all connectivity instead of sparse connectivity (1%). b. This model has weaker noise of 0.1 instead of 0.8. c. In this model all of the inhibitory neurons have their strength increased by a factor of 100 instead of having a fraction of them having strong weight and rest with weak weights. d. In this model all inhibitory neurons homogeneously have weak weights. Model parameters: N: 1000; 80%:20% ratio of Excitatory: Inhibitory neurons; 100 network realizations used to calculate probability at each Inhibitory signal modulation factor.

In SM Figure 4-1 we show the Δ probability as a function of Inhibitory signal modulation factor (Related to Section Computational Model4.2.2). We show 4 different model that are same as the model presented in Section 4.2.2 except for one parameter. a. This model has all-to-all

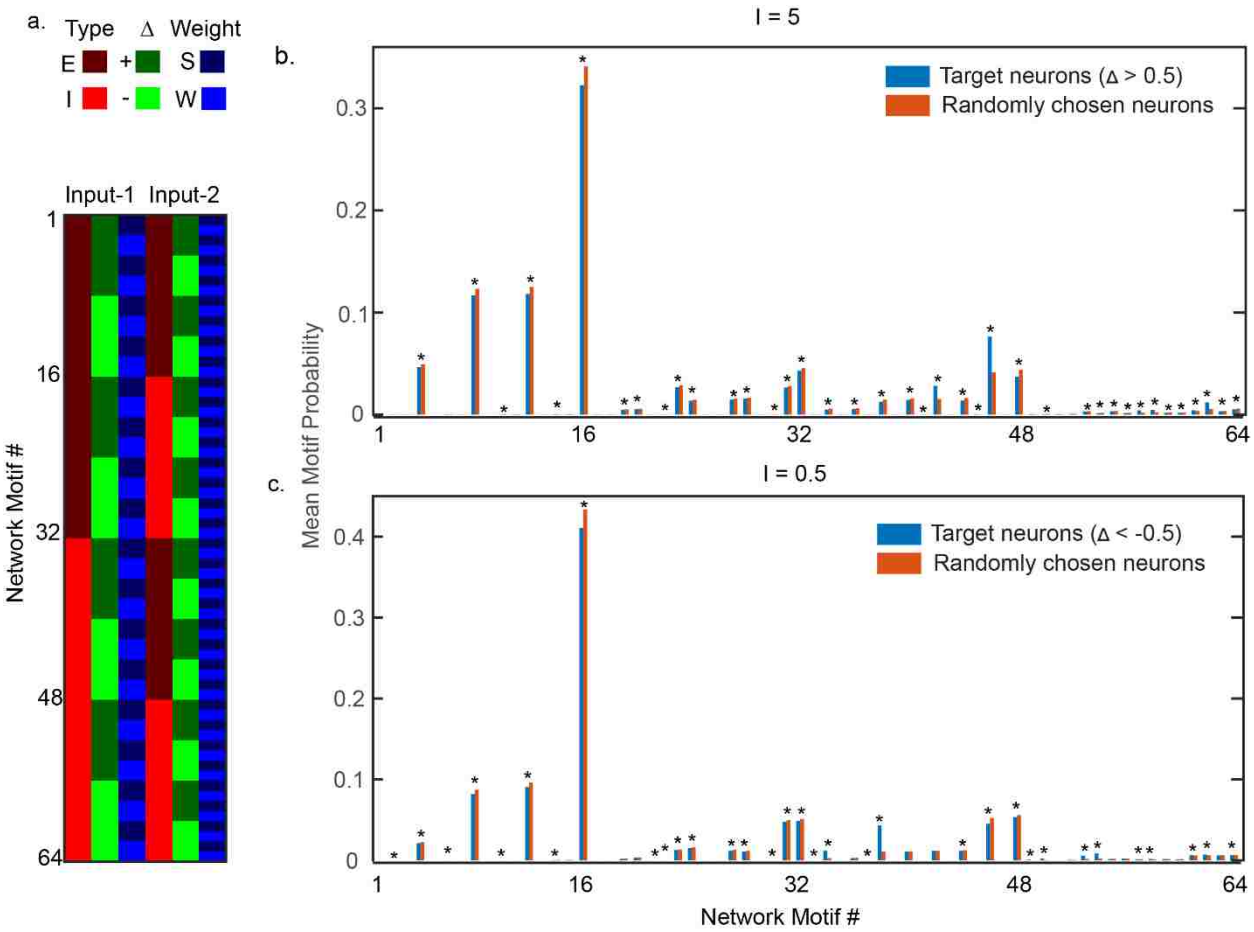

SM Figure 4-2 network motifs and the corresponding mean motif probabilities for both target neurons and randomly chosen neurons. We show results for both kinds of inhibitory signal modulation factor $I = 5$ and $I = 0.5$. We consider 1000 random network realizations and calculate motif probabilities. Further we performed t-test for all the network motifs to check motif probabilities for target neurons and randomly chosen neurons are different with statistically significance ($p < 10^{-3}$).

connectivity instead of sparse connectivity (1%). b. This model has weaker noise of 0.1 instead of 0.8. c. In this model all of the inhibitory neurons have their strength increased by a factor of 100 instead of having a fraction of them having strong weight and rest with weak weights. d. In this model all inhibitory neurons homogeneously have weak weights. Model parameters: N: 1000; 80%:20% ratio of Excitatory: Inhibitory neurons; 100 network realizations used to calculate probability at each Inhibitory signal modulation factor.

In **Error! Reference source not found.** we show the network motifs and the corresponding mean motif probabilities for both target neurons and randomly chosen neurons.

(Related to the section 4.2.3). We show results for both kinds of inhibitory signal modulation factor $I = 5$ and $I = 0.5$. We consider 1000 random network realizations and calculate motif probabilities. Further we performed t-test for all the network motifs to check motif probabilities for target neurons and randomly chosen neurons are different with statistically significance ($p < 10^{-3}$).

4.4.2 Experimental Methods

Animals: All procedures were carried out in accordance with the recommendations in the Guide for the Care and Use of Laboratory Animals of the National Institutes of Health and approved by University of Arkansas Institutional Animal Care and Use Committee (protocol #14048). We studied adult male rats ($n = 3$, Rattus Norvegicus, Sprague-Dawley outbred, Harlan Laboratories, TX, USA). Given the animal-to-animal variability and complexity of the data analysis, there is no feasible way to pre-specify either an effect size or a good number of experiments. We found that 3 animals (approximately 40 recordings per animal) for each condition were sufficient to obtain significant results, accounting for multiple comparisons.

Electrophysiology: Microelectrode array were chronically implanted with shank tips at a depth of $1300\ \mu m$ from the pia, thus targeting most electrodes to deep cortical layers of primary motor cortex. We used (Buzsaki32-CM32, Neuronexus), which has electrodes that are spaced more densely in space. The electrode arrays were oriented such that the plane of electrodes was perpendicular to the dorsal surface and parallel to the midline. The electrodes spanned $1.4\ mm$ in the rostrocaudal direction, centered at a point $0.5\ mm$ caudal from bregma and $2\ mm$ lateral from midline. The probe position was chosen deliberately to sample from neurons that are associated with a wide range of different body motions. Considering previous intracortical micro-stimulation studies the region we sampled is involved in many aspects of body movement

including hip flexion, trunk movements, pronation, wrist extension, elbow flexion, neck movement, and vibrissa movement(Kolb and Tees, 1990). The Buzsaki type probes were chosen for with the goal of improving spike sorting(Rossant *et al.*, 2016). In addition, the rats had a microcannula included in the chronic implant for local drug delivery (26GA guide cannula, 33GA injection cannula, Plastics One, Roanoke, VA, USA). The guide cannula was implanted with its tip touching, but not penetrating the cortical surface about $500\ \mu m$ from the point where the electrodes were inserted. Broadband recordings ($30\ min$ duration) of extracellular voltage fluctuations were performed with $30\ kHz$ sample rate (Cerebus, Blackrock Microsystems). Signals were digitized by a lightweight circuit ($1\ cm$ from implant) and then transmitted via a commutator to the recording system. The wire between the rat and the commutator was spring-supported, such that minimal vertical forces were applied to the rat when the rats head was at a natural height relative to the stage, thus facilitating free movement of the rat.

Pharmacology: Small volumes ($1-2\ \mu L, 2\mu L/min$ for $5\ or\ 10\ min$) of drug (muscimol or bicuculline methiodide) dissolved in sterile saline or just saline (sham condition) was injected through the microcannula. The injection was done using a syringe pump (Bioanalytical Systems, Inc., IN, USA). Bicuculline is a $GABA_A$ antagonist(Curtis *et al.*, 1970) and, Muscimol is a $GABA_A$ agonist(Frølund *et al.*, 2002). Multiple concentrations were tested for both muscimol and bicuculline including $20, 40, 80, 160, 320, 640\ and\ 1280\ \mu M$ μM. A 'sham' reading was taken along with each 'drug' recording. In **Error! Reference source not found.**c, the low drug concentration includes $20, 40\ and\ 80\ \mu M$ (reading taken over 20 experiments) for both muscimol and bicuculline methiodide. The high drug concentration includes $160, 320, 640\ and\ 1280\ \mu M$ (reading taken over 23 experiments) for both muscimol and bicuculline methiodide.

4.4.3 Data-analysis and Spike Sorting

Spike sorting was done with the kilosort software (https://github.com/cortex-lab/KiloSort), which was developed for electrode arrays with many closely spaced recording sites, like our Buzsaki style probes, as described recently(Rossant *et al.*, 2016). The spike sorting to convert electrophysiological recording to spike times data is done using MATLAB software. Each set of 'control' and 'drug' recording files were merged before spike sorting was performed.

The files are in '.ns5' format and 'mergeNSxNeV('x','y')' command is used to merge files located at paths 'x' and 'y'. Next, the '.ns5' file is converted to '.dat' file using code 'make_dat_file.m'. Following 3 files are copied to the current working directory; 'config_patrick.m', 'make_patrickChannelmap.m' and 'master_patrick.m'. In codefile 'config_patrick.m' datafile name is added to variable 'opsfbinary'. Next, in codefile 'master_patrick.m' datafile paths are added to variables 'fpath' and 'pathtoConfigfile'. At last we run the 'master_patrick.m' code.

At this point the spikes are sorted and we are ready to perform manual curation step to assess the quality of spikes. For this we open 'Anaconda prompt window' and go to the working directory. Next enter commands 'activate phy' and 'phy template-gui params.py'. This will open a Template-GUI (Graphic user interface) where we look at the spike events. The Template-GUI consist of several interactive plotting windows called Views. The manual curation step is guided by following link: https://github.com/kwikteam/phy-contrib/blob/master/docs/template-gui.md. The aim of manual curation step is a) See if the activity is noise, then deselect them b) Identify cases when the algorithm thought the spikes came from two neurons but are really from same neuron, then merge them, c) Identify cases when the algorithm thought the spikes came from one neuron but in reality, they are from different neurons, then split them.

To perform these tasks, we use these different views, ‘ClusterView’, ‘WaveformView’, ‘FeatureTemplateView’, ‘SimilarityView’, ‘CorrelogramView’, ‘AmplitudeView’.
The ‘ClusterView’ gives the ‘cluster id’, number of spikes ‘n_spikes’, channel with largest amplitude events ‘channel’ and depth of that channel ‘depth’. We select a cluster by clicking on it, the different views will show the properties corresponding to that cluster. The first thing to check is that is this cluster noise or not. A complete give-away would be ‘WaveformView’ showing all channels having same symmetrical bump. Along with that the ‘AmplitudeView’ will have vertical concentrated streak of points rather than a more uniform distribution. These clusters are directly marked as noise, either by ‘Ctrl+Alt+n’ or from the Wizard option in the toolbar.

If not noise, we need to identify if any of the channels in ‘WaveformView’ has a waveform that looks like a typical spike (hyperpolarization and then depolarization). This would require some practice on part of the user, so it is advisable to look through different clusters to get a feeling for a good waveform. In many cases there might not be a good spike on any of the channel. Since the implant we used had vertical channels close by and horizontal channels far apart, so a spike activity recorded at a given channels might also show at nearby channels but with reduced amplitude but not at horizontally next channels. One can toggle between the average waveform to individual waveform by the key ‘W’. Since, this step is highly subjective, it is advisable to be try two different strategies on same dataset, once be conservative in choosing good spike and once be quite open to select. One should go over all the clusters to first sort out noise and not noise clusters and then go back to first one for further analysis.

Next, we have to check for clusters that are wrongly ‘split’ or ‘merged’ by the automatic sorting step. First let’s see if any wrongly merged clusters, in the CorrelogramView if the central bin is not zeros then it’s an indicator that two clusters are merged together. The reason being if a

neuron fires then it cannot fire again during the refractory period. If one sees a spike in the cluster during this time it is coming from another neuron. To split the cluster in two look at the 'FeatureView', the different panels show the different principal components of the cluster of spikes. Go to the panel that shows two distinct groups most clearly, encircle one of the groups by holding down 'Ctrl and left click'. It will create a polygon around the group you would like to isolate. Once happy with the selection press 'K', this will successfully separate the two waveforms into two separate clusters. You can undo your selection 'Ctrl + right click' will undo your selection. Next, we look for clusters that are split wrongly by the sorting algorithm. For, this once we select a cluster from 'ClusterView', we go on to select one from 'SimilarityView' as well. In similarity view the similarity score will also be given and any cluster with score above 0.8 would be a candidate for merging. After selecting the two clusters, the judgement for merging them would be made by looking at the 'CorrelogramView', 'WaveformView' and the 'FeatureView'. The 'CorrelogramView' now will also have a cross-correlogram that shows the cross correlation between the cluster from 'ClusterView' and its similar cluster selected from 'SimilarityView'. A zero in central bin would be an indicator that the two split clusters might come from same neuron. Next, we look at the 'FeatureView' and 'WavefromView' and if get convincing proof that the two clusters are sufficiently overlapping in terms for both coming from same channels and having similar principle components plots, then we can merge them. To merge the two clusters, we go to the toolbar option 'Wizard' or press 'G'.

The final check that is an optional step but might be important when doing further analysis using the data is to clean out the noisy components. While looking at the 'AmplitudeView' and 'WaveformView' for good clusters one might find cases where there is noise mixed as well. This might happen if there some disturbance while recording the data. In

FeatureView these noises would show up as separate groups that can be easily seen. We cut out those groups by procedure described above for splitting, to clean the good clusters as much as possible. If for any cluster that you marked as noise and you want it to be in Good spikes category, then select it and press ‘Ctrl+G’. It is highly advisable to keep saving the progress either through the option in toolbar or by pressing ‘Ctrl+S’. The final data is saved in the files, ‘spike_times.npy’, ‘spike_clusters.npy’ and ‘cluster_group.tsv’. Run ‘check_spikes.m’ to get the final datasets containing label of neurons and corresponding time of spikes. This data is used to calculate the spike rate for different neurons for further analysis.

CHAPTER 5 CONCLUSION

In conclusion I would like to summarize all the 3 projects discussed above. Further, I will describe some of the main limitations and possible future directions one can take from each of the studies.

In the **first project**, we studied the impact of E/I balance on the entropy of ongoing or spontaneous spiking activity of network of neurons. We presented a model of a sparse random network of neurons with excitatory and inhibitory connections. We show that high entropy neural network dynamics requires balance of excitatory and inhibitory synaptic strength. This point is near the tipping point of the network dynamics, one side of which lies the excitation dominant high activity regime and other side lies the low-activity inhibition dominant regime. The entropy is high for any balanced configuration of excitatory and inhibitory weights that can be achieved either by changing the number of connections or by changing the strength of connections. However, the stability to fluctuations in synaptic strength varies for different configurations. We show that strong synaptic weights lead to robust entropy which need not be the highest, and weak weights lead to higher but fragile entropy neural dynamics. In the evolutionary context this becomes an interesting question as the robustness to excitatory and inhibitory parameter changes may be important.

This leads to two important predictions regarding the state of the cortex. First, if the cortex operates at the high entropy surface regime then change of excitation or inhibition will lead to less fluctuating firing rates, either high or low. On the other hand, if the fluctuations in firing rates increase after excitatory or inhibitory manipulation then the cortex is not operating on the high entropy surface regime. Also, if the drop in entropy is larger (smaller) after excitatory or inhibitory manipulations then, the cortex might be operating with weak (strong) synapse E/I

balance. A possible limitation of this work is that we presented a binary model of integrate-and fire neurons where the network dynamics is analytically well-defined. A more realistic model would be required to further test this idea that matches real cortical dynamics. Further, experimental testing is required to test our results. Both of these points also potential directions one can take. There are possible challenges in finding a realistic model as there is no certainty that dynamics could be as well defined and also the synaptic strengths might not be constant. Experimentally, one would test these ideas by acute pharmacological manipulation of excitatory or inhibitory synapses and measure the changes in firing rate fluctuations.

In the **second project**, we tested a well-known phenomenon of scale-invariance of dynamical rules, but in the context of neuroscience. Scale invariance has been widely studied in many equilibrium and non-equilibrium physical systems. The most famous example is the Ising Model where the network activity was scale-invariant and so was the Hamiltonian that governed it. This was shown under the framework of mathematical tool known as Renormalization Group. Motivated by this example and others, we presented a coarse-graining scheme applied to 2-dimenisioal lattice and estimated the change in the dynamical rules that govern the dynamics of the neural system. We found the scale-change symmetry is most prominent near the critical point that divides the high-activity and low-activity dynamical regime.

We further verified our hypothesis in a more realistic model of neural system that include features such as adaptation and distance dependent connectivity. For this model, the tipping point was between a highly- correlated oscillating neural activity and low-correlation low level activity. The cortical activity is usually recorded as a continuous signal rather than a binary state (active or inactive) signal. So, we simulated continuous signal by measuring the synaptic input and created binary data by point-processing the continuous signal. This procedure was in line

with previous studies that recorded large scale cortical activity. Here also, we found similar results as seen for binary spiking activity data.

Finally, we extended the transformational scheme to spontaneous activity recorded from mice cortex as it wakes up from anesthesia. Other results indicate that as the mouse wakes up the rules that govern its cortical dynamics achieve higher scale-symmetry. This was in line with previous studies. In a way our coarse-graining scheme presents an alternative method to test the critical hypothesis in real cortical system. We verified this fact by comparing our scale-symmetry parameter to existing methodology used by researchers. A possible limitation to this study is that we only test data collected from one mice study. Cortical data that on which such coarse-graining scheme can be applied are rare. This opens doors for both experimentalist and physicists to further explore this idea. Further, the coarse-graining scheme we devised is only limited to binary data. This would make for an interesting challenge for researchers to try and devise a coarse-graining scheme directly applied to continuous signal that can further be used on experimental data.

In the **third project**, we explored an interesting observation in spontaneous cortical activity in mice, after pharmacological manipulations of inhibition. The status quo response to an inhibition manipulation is to have an inverse effect on neural activity. We found that on increasing the inhibitory signal the spiking rate for some neurons also increased and vice-versa. Interestingly, the overall population level spiking rate was more or less constant, this point towards an internal defense mechanism in neural systems by which it keeps the neural state the same under small fluctuations in inhibition. On further analysis we found that this paradoxical behavior was more prevalent for low concentration of drug that manipulates inhibition, than for higher concentrations.

We simulated a network model of integrate-and-fire neurons with sparse and random connectivity, along with excitatory and inhibitory connections. We aimed at simulating qualitatively similar paradoxical change in neurons under manipulation of inhibitory signaling. We found that paradoxical behavior was due to inhomogeneity in network structure, more precisely in the distribution of inhibitory weights. The presence of few strong inhibitory connections in a network of weak excitatory and inhibitory connections created network motifs that lead to some neurons behave paradoxically compared to the rest of the network. Observing paradoxical behavior in one series of experiments is, understandably, not enough. But it does present a new perspective to look at the paradoxical response to signal manipulation seen in other studies. Further, experimentation is required to measure the strength of signals received by neurons that show paradoxical behavior.

REFERENCES

Abeles, M. (2012) *Local cortical circuits: An electrophysiological study*. Springer Science & Business Media.

Akemann, W. *et al.* (2012) 'Imaging neural circuit dynamics with a voltage-sensitive fluorescent protein', *Journal of Neurophysiology*, 108(8), pp. 2323–2337. doi: 10.1152/jn.00452.2012.

Alvarez-Dolado, M. *et al.* (2006) 'Cortical Inhibition Modified by Embryonic Neural Precursors Grafted into the Postnatal Brain', *The Journal of Neuroscience*, 26(28), p. 7380 LP-7389. doi: 10.1523/JNEUROSCI.1540-06.2006.

Amaral, D. G. and Witter, M. P. (2004) 'CHAPTER 21 - Hippocampal formation', in George Paxinos (ed.) *The rat nervous system*. 3rd edn. Academic Press, pp. 635–704. doi: 10.1016/B978-012547638-6/50022-5.

Anderson, J. S., Carandini, M. and Ferster, D. (2000) 'Orientation Tuning of Input Conductance, Excitation, and Inhibition in Cat Primary Visual Cortex', *Journal of Neurophysiology*. American Physiological Society, 84(2), pp. 909–926. doi: 10.1152/jn.2000.84.2.909.

Arieli, A. *et al.* (1996) 'Dynamics of Ongoing Activity: Explanation of the Large Variability in Evoked Cortical Responses', *Science*. AAAS, 273(5283), pp. 1868–1871. doi: 10.1126/science.273.5283.1868.

Atallah, B. V and Scanziani, M. (2009) 'Instantaneous modulation of gamma oscillation frequency by balancing excitation with inhibition', *Neuron*, 62(4), pp. 566–577. doi: 10.1016/j.neuron.2009.04.027.

Averbeck, B. B., Latham, P. E. and Pouget, A. (2006) 'Neural correlations, population coding and computation', *Nature Reviews Neuroscience*, 7(5), pp. 358–366. doi: 10.1038/nrn1888.

Azouz, R. and Gray, C. M. (1999) 'Cellular Mechanisms Contributing to Response Variability of Cortical Neurons In Vivo', *The Journal of Neuroscience*, 19(6), p. 2209 LP-2223. doi: 10.1523/JNEUROSCI.19-06-02209.1999.

Bacci, A., Huguenard, J. R. and Prince, D. A. (2004) 'Long-lasting self-inhibition of neocortical interneurons mediated by endocannabinoids', *Nature*. Macmillan Magazines Ltd., 431, p. 312. doi: 10.1038/nature02913.

Beggs, J. M. and Plenz, D. (2003) 'Neuronal avalanches in neocortical circuits.', *The Journal of neuroscience : the official journal of the Society for Neuroscience*, 23(35), pp. 11167–77.

Beggs, J. M. and Timme, N. (2012) 'Being critical of criticality in the brain.', *Frontiers in physiology*, 3, p. 163. doi: 10.3389/fphys.2012.00163.

Bellay, T. *et al.* (2015) 'Irregular spiking of pyramidal neurons organizes as scale-invariant neuronal avalanches in the awake state', *eLife*, 4(JULY 2015), pp. 1–25. doi: 10.7554/eLife.07224.

Berkes, P. *et al.* (2011) ‘Spontaneous Cortical Activity Reveals Hallmarks of an Optimal Internal Model of the Environment’, *Science*, 331(6013), pp. 83–87. doi: 10.1126/science.1195870ga.

Briguglio, J. J. *et al.* (2018) ‘Cortical Neural Activity Predicts Sensory Acuity Under Optogenetic Manipulation’, *The Journal of Neuroscience*, 38(8), p. 2094 LP-2105. doi: 10.1523/JNEUROSCI.2457-17.2017.

Brunel, N. (2000) ‘Dynamics of networks of randomly connected excitatory and inhibitory spiking neurons’, *Journal of Physiology-Paris*, 94(5–6), pp. 445–463. doi: 10.1016/S0928-4257(00)01084-6.

Buckley, A. W. and Holmes, G. L. (2016) ‘Epilepsy and autism’, *Cold Spring Harbor perspectives in medicine*. Cold Spring Harbor Laboratory Press, 6(4), p. a022749. doi: 10.1101/cshperspect.a022749.

Buzsáki, G., Kaila, K. and Raichle, M. (2007) ‘Inhibition and brain work.’, *Neuron*, 56(5), pp. 771–783. doi: 10.1016/j.neuron.2007.11.008.

Buzsáki, G. and Mizuseki, K. (2014) ‘The log-dynamic brain: How skewed distributions affect network operations’, *Nature Reviews Neuroscience*. Nature Publishing Group, 15(4), pp. 264–278. doi: 10.1038/nrn3687.

Chen, X. and Dzakpasu, R. (2010) ‘Observed network dynamics from altering the balance between excitatory and inhibitory neurons in cultured networks’, *Physical Review E - Statistical, Nonlinear, and Soft Matter Physics*, 82(3), pp. 1–8. doi: 10.1103/PhysRevE.82.031907.

Clawson, W. P. *et al.* (2017) ‘Adaptation towards scale-free dynamics improves cortical stimulus discrimination at the cost of reduced detection’, *PLOS Computational Biology*. Edited by C. C. Hilgetag, 13(5), p. e1005574. doi: 10.1371/journal.pcbi.1005574.

Curtis, D. R. *et al.* (1970) ‘GABA, bicuculline and central inhibition.’, *Nature*, 226(5252), pp. 1222–4.

Denève, S. and Machens, C. K. (2016) ‘Efficient codes and balanced networks’, *Nature Neuroscience*, 19(3), pp. 375–382. doi: 10.1038/nn.4243.

Dichter, M. A. and Ayala, G. F. (1987) ‘Cellular mechanisms of epilepsy: A status report’, *Science*, 237(4811), pp. 157–164. doi: 10.1126/science.3037700.

Ecker, A. S. *et al.* (2014) ‘State dependence of noise correlations in macaque primary visual cortex’, *Neuron*. Elsevier Inc., 82(1), pp. 235–248. doi: 10.1016/j.neuron.2014.02.006.

Fagerholm, E. D. *et al.* (2016) ‘Cortical Entropy, Mutual Information and Scale-Free Dynamics in Waking Mice’, *Cerebral Cortex*, 26(10), pp. 3945–3952. doi: 10.1093/cercor/bhw200.

Fernandez, F. and Garner, C. C. (2007) ‘Over-inhibition: a model for developmental intellectual disability’, *Trends in Neurosciences*, 30(10), pp. 497–503. doi: 10.1016/j.tins.2007.07.005.

Ferraz, M. S. A., Melo-Silva, H. L. C. and Kihara, A. H. (2017) ‘Optimizing information processing in neuronal networks beyond critical states’, *PLoS ONE*, 12(9), pp. 1–12. doi: 10.1371/journal.pone.0184367.

Fiser, J., Chiu, C. and Weliky, M. (2004) ‘Small modulation of ongoing cortical dynamics by sensory input during natural vision’, *Nature*. Macmillan Magazines Ltd., 431, p. 573. Available at: https://doi.org/10.1038/nature02907.

Fox, M. D., Snyder, A. Z., *et al.* (2006) ‘Coherent spontaneous activity accounts for trial-to-trial variability in human evoked brain responses.’, *Nature neuroscience*, 9(1), pp. 23–5. doi: 10.1038/nn1616.

Fox, M. D., Corbetta, M., *et al.* (2006) ‘Spontaneous neuronal activity distinguishes human dorsal and ventral attention systems’, *Proceedings of the National Academy of Sciences*, 103(26), p. 10046 LP-10051. doi: 10.1073/pnas.0604187103.

Fox, M. D. *et al.* (2007) ‘Intrinsic fluctuations within cortical systems account for intertrial variability in human behavior.’, *Neuron*, 56(1), pp. 171–84. doi: 10.1016/j.neuron.2007.08.023.

Fox, M. D. and Raichle, M. E. (2007) ‘Spontaneous fluctuations in brain activity observed with functional magnetic resonance imaging’, *Nature Reviews Neuroscience*, 8(9), pp. 700–711. doi: 10.1038/nrn2201.

Froemke, R. C. (2015) ‘Plasticity of cortical excitatory-inhibitory balance’, *Annual review of neuroscience*. 2015/04/09, 38, pp. 195–219. doi: 10.1146/annurev-neuro-071714-034002.

Frølund, B. *et al.* (2002) ‘GABA(A) receptor ligands and their therapeutic potentials.’, *Current topics in medicinal chemistry*, 2(8), pp. 817–32. doi: 10.2174/1568026023393525.

Garcia Del Molino, L. C. *et al.* (2017) ‘Paradoxical response reversal of top-down modulation in cortical circuits with three interneuron types’, *eLife*. Center for Neural Science, New York University, New York, United States., 6. doi: 10.7554/eLife.29742.

Gautam, S. H. *et al.* (2015) ‘Maximizing Sensory Dynamic Range by Tuning the Cortical State to Criticality’, *PLoS Computational Biology*, 11(12), pp. 1–15. doi: 10.1371/journal.pcbi.1004576.

Gireesh, E. and Plenz, D. (2008) ‘Neuronal avalanches organize as nested theta- and beta/gamma-oscillations during development of cortical layer 2/3.’, *Proceedings of the National Academy of Sciences of the United States of America*, 105(21), pp. 7576–81. doi: 10.1073/pnas.0800537105.

Gogolla, N. *et al.* (2009) ‘Common circuit defect of excitatory-inhibitory balance in mouse models of autism’, *Journal of Neurodevelopmental disorders*, 1, pp. 172–181. doi: 10.1007/s11689-009-9023-x.

Gupta, A. S. *et al.* (2010) ‘Hippocampal replay is not a simple function of experience.’, *Neuron*. Elsevier Ltd, 65(5), pp. 695–705. doi: 10.1016/j.neuron.2010.01.034.

Gutnick, M. J. and Mody, I. (1995) *The Cortical Neuron*. New York: Oxford University Press. doi: 10.1093/acprof:oso/9780195083309.001.0001.

Hahn, G. *et al.* (2017) 'Spontaneous cortical activity is transiently poised close to criticality', pp. 1–29.

Haider, B. (2006) 'Neocortical Network Activity In Vivo Is Generated through a Dynamic Balance of Excitation and Inhibition', *Journal of Neuroscience*, 26(17), pp. 4535–4545. doi: 10.1523/JNEUROSCI.5297-05.2006.

Haimovici, A. *et al.* (2013) 'Brain organization into resting state networks emerges at criticality on a model of the human connectome', *Physical Review Letters*, 110(17), pp. 1–4. doi: 10.1103/PhysRevLett.110.178101.

Haldeman, C. and Beggs, J. M. (2005) 'Critical Branching Captures Activity in Living Neural Networks and Maximizes the Number of Metastable States', *Physical Review Letters*, 94(5). doi: 10.1103/PhysRevLett.94.058101.

Han, F., Caporale, N. and Dan, Y. (2008) 'Reverberation of Recent Visual Experience in Spontaneous Cortical Waves', *Neuron*. Elsevier Inc., 60(2), pp. 321–327. doi: 10.1016/j.neuron.2008.08.026.

Harris, K. D. and Thiele, A. (2011) 'Cortical state and attention', *Nature Reviews Neuroscience*. Nature Publishing Group, 12(9), pp. 509–523. doi: 10.1038/nrn3084.

Hendry, S. H. *et al.* (1987) 'Numbers and proportions of GABA-immunoreactive neurons in different areas of monkey cerebral cortex.', *The Journal of neuroscience : the official journal of the Society for Neuroscience*, 7(5), pp. 1503–19. doi: 10.1523/JNEUROSCI.07-05-01503.1987.

Hengen, K. B. *et al.* (2013) 'Firing Rate Homeostasis in Visual Cortex of Freely Behaving Rodents', *Neuron*. Elsevier, 80(2), pp. 335–342. doi: 10.1016/j.neuron.2013.08.038.

Hesse, J. and Gross, T. (2014) 'Self-organized criticality as a fundamental property of neural systems', *Frontiers in Systems Neuroscience*, 8(September), pp. 1–14. doi: 10.3389/fnsys.2014.00166.

Hines, R. M. *et al.* (2008) 'Synaptic Imbalance, Stereotypies, and Impaired Social Interactions in Mice with Altered Neuroligin 2 Expression', *The Journal of Neuroscience*, 28(24), p. 6055 LP-6067. doi: 10.1523/JNEUROSCI.0032-08.2008.

Hinton, G. E. and Salakhutdinov, R. R. (2006) 'Reducing the dimensionality of data with neural networks.', *Science*, 313(5786), p. 504.

Hunt, R. F. *et al.* (2013) 'GABA progenitors grafted into the adult epileptic brain control seizures and abnormal behavior', *Nature Neuroscience*. Nature Publishing Group, 16(6), pp. 692–697. doi: 10.1038/nn.3392.

Isaacson, J. S. and Scanziani, M. (2011) 'How inhibition shapes cortical activity', *Neuron*, 72(2),

pp. 231–243. doi: 10.1016/j.neuron.2011.09.027.

Ji, D. and Wilson, M. A. (2007) ‘Coordinated memory replay in the visual cortex and hippocampus during sleep.’, *Nature neuroscience*, 10(1), pp. 100–7. doi: 10.1038/nn1825.

Jiang, X. *et al.* (2015) ‘Principles of connectivity among morphologically defined cell types in adult neocortex’, *Science (New York, N.Y.)*, 350(6264), pp. aac9462-aac9462. doi: 10.1126/science.aac9462.

Jones, E. G. (1986) ‘Connectivity of the primate sensory-motor cortex’, in *Sensory-motor areas and aspects of cortical connectivity*. Springer, pp. 113–183.

Jones, E. G. and Peters, A. (eds) (1984) *Cerebral Cortex*. 1st edn. Springer.

Kadanoff, L. P. (1993) *From Order To Chaos: Essays: Critical, Chaotic and Otherwise*. World Scientific.

Kenet, T. *et al.* (2003) ‘Spontaneously emerging cortical representations of visual attributes’, *Nature*, 425(6961), pp. 954–956.

Kinouchi, O. and Copelli, M. (2006) ‘Optimal dynamical range of excitable networks at criticality’, *Nature Physics*, 2(5), pp. 348–351. doi: 10.1038/nphys289.

Kisley, M. A. and Gerstein, G. L. (1999) ‘Trial-to-Trial Variability and State-Dependent Modulation of Auditory-Evoked Responses in Cortex’, *The Journal of Neuroscience*, 19(23), p. 10451 LP-10460. doi: 10.1523/JNEUROSCI.19-23-10451.1999.

Klaus, A., Yu, S. and Plenz, D. (2011) ‘Statistical analyses support power law distributions found in neuronal avalanches.’, *PloS one*, 6(5), p. e19779. doi: 10.1371/journal.pone.0019779.

Kolb, B. and Tees, R. C. (eds) (1990) *The cerebral cortex of the rat.*, *The cerebral cortex of the rat*. Cambridge, MA, US: The MIT Press.

Larremore, D. B. *et al.* (2014) ‘Inhibition causes ceaseless dynamics in networks of excitable nodes’, *Physical Review Letters*, 112(13), pp. 1–5. doi: 10.1103/PhysRevLett.112.138103.

Larremore, D. B., Shew, W. L. and Restrepo, J. G. (2011) ‘Predicting Criticality and Dynamic Range in Complex Networks: Effects of Topology’, *Physical Review Letters*, 106(5), pp. 1–4. doi: 10.1103/PhysRevLett.106.058101.

Lee, D. *et al.* (1998) ‘Variability and correlated noise in the discharge of neurons in motor and parietal areas of the primate cortex’, *Journal of Neuroscience*, 18(3), pp. 1–10. doi: 10.1523/JNEUROSCI.18-03-01161.1998.

Legendy, C. R. and Salcman, M. (1985) ‘Bursts and recurrences of bursts in the spike trains of spontaneously active striate cortex neurons’, *Journal of neurophysiology*. American Physiological Society Bethesda, MD, 53(4), pp. 926–939.

Lehmann, E. L. and Casella, G. (1998) *Theory of Point Estimation , Second Edition Springer Texts in Statistics, Springer*. doi: 10.2307/1270597.

Levina, A., Herrmann, J. M. and Geisel, T. (2007) 'Dynamical synapses causing self-organized criticality in neural networks', *Nature Physics*, 3(12), pp. 857–860. doi: 10.1038/nphys758.

Llinás, R. R. *et al.* (1999) 'Thalamocortical dysrhythmia: A neurological and neuropsychiatric syndrome characterized by magnetoencephalography', *Proceedings of the National Academy of Sciences*, 96(26), p. 15222 LP-15227. doi: 10.1073/pnas.96.26.15222.

Loreto, V. *et al.* (1995) 'Renormalization Group Approach to the Critical Behavior of the Forest-Fire Model', *Physical Review Letters*, 75(3), pp. 465–468. doi: 10.1103/PhysRevLett.75.465.

Lucas-Meunier, E. *et al.* (2009) 'Involvement of Nicotinic and Muscarinic Receptors in the Endogenous Cholinergic Modulation of the Balance between Excitation and Inhibition in the Young Rat Visual Cortex', *Cerebral Cortex*, 19(10), pp. 2411–2427. doi: 10.1093/cercor/bhn258.

Luczak, A., Barthó, P. and Harris, K. D. (2009) 'Spontaneous Events Outline the Realm of Possible Sensory Responses in Neocortical Populations', *Neuron*. Elsevier Ltd, 62(3), pp. 413–425. doi: 10.1016/j.neuron.2009.03.014.

Maffei, A. and Turrigiano, G. G. (2008) 'Multiple Modes of Network Homeostasis in Visual Cortical Layer 2/3', *The Journal of Neuroscience*, 28(17), p. 4377 LP-4384. doi: 10.1523/JNEUROSCI.5298-07.2008.

Mao, B. *et al.* (2001) 'Dynamics of spontaneous activity in neocortical slices', *Neuron*, 32(5), pp. 883–898. doi: 10.1016/S0896-6273(01)00518-9.

Markov, N. T. *et al.* (2014) 'A weighted and directed interareal connectivity matrix for macaque cerebral cortex', *Cerebral cortex (New York, N.Y. : 1991)*. 2012/09/25. Oxford University Press, 24(1), pp. 17–36. doi: 10.1093/cercor/bhs270.

Meinecke, D. L. and Peters, A. (1987) 'Gaba immunoreactive neurons in rat visual cortex', *Journal of Comparative neurology*, 261(3), pp. 388–404. doi: 10.1002/cne.902610305.

Meshulam, L. *et al.* (2018) 'Coarse-graining, fixed points, and scaling in a large population of neurons', *arXiv*, p. 1809.08461.

Miller, J. -e. K. *et al.* (2014) 'Visual stimuli recruit intrinsically generated cortical ensembles', *Proceedings of the National Academy of Sciences*, 111(38), pp. E4053–E4061. doi: 10.1073/pnas.1406077111.

Mitzenmacher, M. (2003) 'A Brief History of Generative Models for Power Law and Lognormal Distributions', *Internet Mathematics*, 1(2), pp. 226–251.

Monier, C. *et al.* (2003) 'Orientation and direction of synaptic inputs in visual cortical neurons', *Neuron*, 37(4), pp. 663–680. doi: 10.1016/S0896-6273(03)00064-3.

Nelson, S. B. and Valakh, V. (2015) ‘Excitatory/Inhibitory Balance and Circuit Homeostasis in Autism Spectrum Disorders’, *Neuron*. Elsevier Inc., 87(4), pp. 684–698. doi: 10.1016/j.neuron.2015.07.033.

Oh, S. W. *et al.* (2014) ‘A mesoscale connectome of the mouse brain’, *Nature*. Nature Publishing Group, 508(7495), pp. 207–214. doi: 10.1038/nature13186.

Ohl, F. W., Scheich, H. and Freeman, W. J. (2001) ‘Change in pattern of ongoing cortical activity with auditory category learning’, *Nature*. Macmillan Magazines Ltd., 412, p. 733. doi: 10.1038/35089076.

Okun, M. and Lampl, I. (2008) ‘Instantaneous correlation of excitation and inhibition during ongoing and sensory-evoked activities’, *Nature Neuroscience*. Nature Publishing Group, 11, p. 535. doi: 10.1038/nn.2105.

Petermann, T. *et al.* (2009) ‘Spontaneous cortical activity in awake monkeys composed of neuronal avalanches’, *Proceedings of the National Academy of Sciences*, 106(37), pp. 15921–15926. doi: 10.1073/pnas.0904089106.

Petersen, C. C. H. *et al.* (2003) ‘Interaction of sensory responses with spontaneous depolarization in layer 2/3 barrel cortex.’, *Proceedings of the National Academy of Sciences of the United States of America*, 100(23), pp. 13638–43. doi: 10.1073/pnas.2235811100.

Plenz, D., Niebur, E. and Schuster, H. G. (2014) *Criticality in Neural Systems*. Edited by D. Plenz, E. Niebur, and H. G. Schuster. Weinheim, Germany: Wiley.

Poil, S.-S. *et al.* (2012) ‘Critical-state dynamics of avalanches and oscillations jointly emerge from balanced excitation/inhibition in neuronal networks.’, *The Journal of neuroscience : the official journal of the Society for Neuroscience*, 32(29), pp. 9817–23. doi: 10.1523/JNEUROSCI.5990-11.2012.

Poo, C. and Isaacson, J. S. (2009) ‘Odor Representations in Olfactory Cortex: “Sparse” Coding, Global Inhibition, and Oscillations’, *Neuron*. Elsevier Ltd, 62(6), pp. 850–861. doi: 10.1016/j.neuron.2009.05.022.

Ramón y Cajal, S. (1894) ‘The Croonian lecture.—La fine structure des centres nerveux’, *Proceedings of the Royal Society of London*. The Royal Society London, 55(331–335), pp. 444–468.

Reed, W. J. and Hughes, B. D. (2002) ‘From gene families and genera to incomes and internet file sizes: why power laws are so common in nature.’, *Physical review. E, Statistical, nonlinear, and soft matter physics*, 66(6 Pt 2), p. 067103. doi: 10.1103/PhysRevE.66.067103.

Romano, S. A. *et al.* (2015) ‘Spontaneous neuronal network dynamics reveal circuit’s functional adaptations for behavior’, *Neuron*, 85(5), pp. 1070–1085. doi: 10.1016/j.neuron.2015.01.027.

Rossant, C. *et al.* (2016) ‘Spike sorting for large, dense electrode arrays.’, *Nature neuroscience*, 19(4), pp. 634–41. doi: 10.1038/nn.4268.

Rubenstein, J. L. and Merzenich, M. M. (2003) ‘Model of autism: increased ratio of excitation/inhibition in key neural systems’, *Genes, Brain and Behavior*, 2, pp. 255–267. doi: 10.1034/j.1601-183X.2003.00037.x.

Rubin, R., Abbott, L. F. and Sompolinsky, H. (2017) ‘Balanced Excitation and Inhibition are Required for High-Capacity, Noise-Robust Neuronal Selectivity’. doi: 10.1073/pnas.1705841114.

Sahara, S. *et al.* (2012) ‘The Fraction of Cortical GABAergic Neurons Is Constant from Near the Start of Cortical Neurogenesis to Adulthood’, *Journal of Neuroscience*, 32(14), pp. 4755–4761. doi: 10.1523/JNEUROSCI.6412-11.2012.

Sanseverino, E. R. *et al.* (1973) ‘Maintained activity of single neurons in striate and non-striate areas of the cat visual cortex’, *Brain research*. Elsevier, 54, pp. 225–242.

di Santo, S. *et al.* (2018) ‘Landau-Ginzburg theory of cortex dynamics: Scale-free avalanches emerge at the edge of synchronization’, (8). doi: 10.1073/pnas.1712989115.

Scarpetta, S. and de Candia, A. (2013) ‘Neural Avalanches at the Critical Point between Replay and Non-Replay of Spatiotemporal Patterns’, *PLOS Computational Biology*, 8(6), p. e64162. doi: 10.1371/journal.pone.0064162.

Scott, G. *et al.* (2014) ‘Voltage Imaging of Waking Mouse Cortex Reveals Emergence of Critical Neuronal Dynamics’, *Journal of Neuroscience*, 34(50), pp. 16611–16620. doi: 10.1523/JNEUROSCI.3474-14.2014.

Shannon, C. E. (1948) ‘A mathematical theory of communication’, *Bell system technical journal*. Wiley Online Library, 27(3), pp. 379–423. doi: 10.1002/j.1538-7305.1948.tb01338.x.

Shew, W. L. *et al.* (2009) ‘Neuronal Avalanches Imply Maximum Dynamic Range in Cortical Networks at Criticality’, *Journal of Neuroscience*, 29(49), pp. 15595–15600. doi: 10.1523/JNEUROSCI.3864-09.2009.

Shew, W. L. *et al.* (2011) ‘Information Capacity and Transmission Are Maximized in Balanced Cortical Networks with Neuronal Avalanches’, *Journal of Neuroscience*, 31(1), pp. 55–63. doi: 10.1523/JNEUROSCI.4637-10.2011.

Shew, W. L., Clawson, W. P., Pobst, J., Karimipanah, Y., Wright, N. C., *et al.* (2015) ‘Adaptation to sensory input tunes visual cortex to criticality’, *Nature Physics*, 11(8), pp. 659–663. doi: 10.1038/nphys3370.

Shew, W. L., Clawson, W. P., Pobst, J., Karimipanah, Y., Wright, N. C., *et al.* (2015) ‘Adaptation to sensory input tunes visual cortex to criticality’, *Nature Physics*, 11(8), pp. 659–663. doi: 10.1038/nphys3370.

Shew, W. L. and Plenz, D. (2013) ‘The functional benefits of criticality in the cortex’, *Neuroscientist*, 19(1), pp. 88–100. doi: 10.1177/1073858412445487.

Shriki, O. *et al.* (2013) ‘Neuronal Avalanches in the Resting MEG of the Human Brain’, *Journal of Neuroscience*, 33(16), pp. 7079–7090. doi: 10.1523/JNEUROSCI.4286-12.2013.

Shu, Y., Hasenstaub, A. and McCormick, D. A. (2003) ‘Turning on and off recurrent balanced cortical activity’, *Nature*. Macmillan Magazines Ltd., 423, p. 288. doi: 10.1038/nature01616.

Sitdikova, G. *et al.* (2014) ‘Isoflurane suppresses early cortical activity’, *Annals of Clinical and Translational Neurology*. John Wiley & Sons, Ltd, 1(1), pp. 15–26. doi: 10.1002/acn3.16.

Song, S. *et al.* (2005) ‘Highly nonrandom Features of Synaptic Connectivity in Local Cortical Circuits’, *PLoS biol.*, 3(3), p. e68. doi: 10.1371/journal.pbio.0030068.

Sornette, D. (1998) ‘Multiplicative processes and power laws’, *Physical Review E*, 57(4), pp. 4811–4813. doi: 10.1103/PhysRevE.57.4811.

Stanley, H. E. (1971) ‘Introduction to Phase Transitions and Critical Phenomena’, *American Journal of Physics*, 40(6), p. 927. doi: 10.1119/1.1986710.

Stanley, H. E. (1971) *Phase transitions and critical phenomena*. Clarendon Press, Oxford.

Stanley, H. E. (1999) ‘Scaling, universality, and renormalization: Three pillars of modern critical phenomena.’, *Rev. Mod. Phys.*, 71(2), p. S358.

Stringer, C. *et al.* (2016) ‘Inhibitory control of correlated intrinsic variability in cortical networks’, *eLife*, 5(DECEMBER2016), pp. 1–33. doi: 10.7554/eLife.19695.

Stumpf, M. P. H. and Porter, M. A. (2012) ‘Mathematics. Critical truths about power laws.’, *Science (New York, N.Y.)*, 335(6069), pp. 665–6. doi: 10.1126/science.1216142.

Swadlow, H. A. (1988) ‘Efferent neurons and suspected interneurons in binocular visual cortex of the awake rabbit: receptive fields and binocular properties’, *Journal of Neurophysiology*. American Physiological Society, 59(4), pp. 1162–1187. doi: 10.1152/jn.1988.59.4.1162.

Tagliazucchi, E. *et al.* (2012) ‘Criticality in large-scale brain fmri dynamics unveiled by a novel point process analysis’, *Frontiers in Physiology*, 3 FEB(February), pp. 1–12. doi: 10.3389/fphys.2012.00015.

Tan, A. Y. Y. *et al.* (2004) ‘Tone-Evoked Excitatory and Inhibitory Synaptic Conductances of Primary Auditory Cortex Neurons’, *Journal of Neurophysiology*. American Physiological Society, 92(1), pp. 630–643. doi: 10.1152/jn.01020.2003.

Tauber, U. C. (2014) *Critical Dynamics: A Field Theory Approach to Equilibrium and Non-equilibrium Scaling Behavior*. Cambridge: Cambridge University Press.

Terauchi, A. *et al.* (2010) ‘Distinct FGFs promote differentiation of excitatory and inhibitory synapses’, *Nature*. Macmillan Publishers Limited. All rights reserved, 465, p. 783. doi: 10.1038/nature09041.

Tsodyks, M. *et al.* (1999) 'Linking Spontaneous Activity of Single Cortical Neurons and the Underlying Functional Architecture', *Science*, 286(5446), p. 1943 LP-1946. doi: 10.1126/science.286.5446.1943.

Tsodyks, M. V *et al.* (1997) 'Paradoxical effects of external modulation of inhibitory interneurons', *Journal of neuroscience*. Soc Neuroscience, 17(11), pp. 4382–4388.

Turrigiano, G. (2011) 'Too Many Cooks? Intrinsic and Synaptic Homeostatic Mechanisms in Cortical Circuit Refinement', *Annual Review of Neuroscience*. Annual Reviews, 34(1), pp. 89–103. doi: 10.1146/annurev-neuro-060909-153238.

Turrigiano, G., Abbott, L. F. and Marder, E. (1994) 'Activity-dependent changes in the intrinsic properties of cultured neurons', *Science*, 264(5161), p. 974 LP-977. doi: 10.1126/science.8178157.

Vespignani, A., Zapperi, S. and Loreto, V. (1997) 'Dynamically driven renormalization group', *Journal of Statistical Physics*, 88(1–2), pp. 47–79. doi: 10.1007/BF02508464.

Vespignani, A., Zapperi, S. and Pietronero, L. (1995) 'Renormalization approach to the self-organized critical behavior of sandpile models', *Physical Review E*, 51(3), pp. 1711–1724. doi: 10.1103/PhysRevE.51.1711.

Vreeswijk, C. van and Sompolinsky, H. (1998) 'Chaotic Balanced State in a Model of Cortical Circuits', *Neural Computation*, 10(6), pp. 1321–1371. doi: 10.1162/089976698300017214.

Wang, Q., Sporns, O. and Burkhalter, A. (2012) 'Network Analysis of Corticocortical Connections Reveals Ventral and Dorsal Processing Streams in Mouse Visual Cortex', *The Journal of Neuroscience*, 32(13), p. 4386 LP-4399. doi: 10.1523/JNEUROSCI.6063-11.2012.

Wang, S.-J., Hilgetag, C. C. and Zhou, C. (2011) 'Sustained activity in hierarchical modular neural networks: self-organized criticality and oscillations.', *Frontiers in computational neuroscience*, 5(June), p. 30. doi: 10.3389/fncom.2011.00030.

Wassef, A., Baker, J. and Kochan, L. D. (2003) 'GABA and Schizophrenia: A Review of Basic Science and Clinical Studies', *Journal of Clinical Psychopharmacology*, 23(6). Available at: https://journals.lww.com/psychopharmacology/Fulltext/2003/12000/GABA_and_Schizophrenia__A_Review_of_Basic_Science.11.aspx.

Webb, A. C. (1976) 'The effects of changing levels of arousal on the spontaneous activity of cortical neurones II. Relaxation and alarm', *Proceedings of the Royal Society of London. Series B. Biological Sciences*. The Royal Society London, 194(1115), pp. 239–251.

Wehr, M. and Zador, A. M. (2003) 'Balance inhibition underlies tuning and sharpens spike timing in auditory cortex.', *Nature*, 426(Novermber), pp. 422–446. doi: 10.1038/nature02116.

Wilent, W. B. and Contreras, D. (2005) 'Dynamics of excitation and inhibition underlying stimulus selectivity in rat somatosensory cortex', *Nature Neuroscience*. Nature Publishing Group, 8, p. 1364.

William Moreau, A. *et al.* (2009) 'Serotoninergic Fine-Tuning of the Excitation–Inhibition Balance in Rat Visual Cortical Networks', *Cerebral Cortex*, 20(2), pp. 456–467. doi: 10.1093/cercor/bhp114.

Williams-García, R. V. *et al.* (2014) 'Quasicritical brain dynamics on a nonequilibrium Widom line', *Physical Review E - Statistical, Nonlinear, and Soft Matter Physics*, 90(6), pp. 1–8. doi: 10.1103/PhysRevE.90.062714.

Williams, G. V and Castner, S. A. (2006) 'Under the curve: Critical issues for elucidating D1 receptor function in working memory', *Neuroscience*, 139(1), pp. 263–276. doi: https://doi.org/10.1016/j.neuroscience.2005.09.028.

Wilson, K. G. (1975) 'The renormalization group: Critical phenomena and the Kondo problem', *Reviews of Modern Physics*, 47(4), pp. 773–840. doi: 10.1103/RevModPhys.47.773.

Wilson, K. G. (1979) 'Problems in Physics with many Scales of Length', *Scientific American*, 241(2), pp. 158–179. doi: 10.1038/scientificamerican0879-158.

Wu, G. K. *et al.* (2008) 'Lateral sharpening of cortical frequency tuning by approximately balanced inhibition', *Neuron*, 58(1), pp. 132–143. doi: 10.1016/j.neuron.2008.01.035.

Yang, D. P., Zhou, H. J. and Zhou, C. (2017) 'Co-emergence of multi-scale cortical activities of irregular firing, oscillations and avalanches achieves cost-efficient information capacity', *PLoS Computational Biology*, 13(2), pp. 1–28. doi: 10.1371/journal.pcbi.1005384.

Yao, H. *et al.* (2007) 'Rapid learning in cortical coding of visual scenes', *Nature Neuroscience*. Nature Publishing Group, 10, p. 772. doi: 10.1038/nn1895.

Yu, S. *et al.* (2017) 'Maintained avalanche dynamics during task-induced changes of neuronal activity in nonhuman primates', pp. 1–22.

Zagha, E. and McCormick, D. A. (2014) 'Neural control of brain state', *Current opinion in neurobiology*. Elsevier, 29, pp. 178–186. doi: 10.1016/j.conb.2014.09.010.

Zhang, Z., Jiao, Y.-Y. and Sun, Q.-Q. (2011) 'Developmental maturation of excitation and inhibition balance in principal neurons across four layers of somatosensory cortex', *Neuroscience*, 174, pp. 10–25. doi: 10.1016/j.neuroscience.2010.11.045.

APPENDIX

This section contains all relevant MATLAB scripts written in analysis of the projects mentioned in **Error! Reference source not found.**, **Error! Reference source not found.**and **Error! Reference source not found.**

Codes for Chapter 2

Functions

```
% function name-> Neural_activity
% Inputs-> N: size of network; T: Time duration of simulation
% trans: transient time steps; randlist: list of random numbers 1 to N
% alpha: fraction of inhibitory neurons, I,E: inhibitory and excitatory
weights
% B_in: Connectivity Matrix; sponr: rate of spontaneous activation
%Output: S, network activity time-series
function S=Neural_activity(N,T,trans,alpha,randlist,I,E,B_in,sponr)
imask1=randlist<=alpha*N; % logical indexing columns for inhibitory neurons
B_in(:,imask1)=-1*B_in(:,imask1);%set outgoing connection from inhibitory
neurons to be negative
B_in(:,imask1)=I*B_in(:,imask1);
B_in(:,~imask1)=E*B_in(:,~imask1);
nev=false(N,T);  %initialize matrix for storing activity
%%%%%%%% compute the activity of the network %%%%%%%%%%
%initial condition: activate Ni neurons in first timestep
nev(1:N/2,1)=1;
%evolve dynamics: probabilistic spike propagation
t=1;
while t<T  %stop computing if we reach T steps
    %determine which neurons fire in the next time step
    nev(:, t+1) = B_in*nev(:,t)>rand(N,1);
    %random activation at rate of one spike among all neurons every 100
timesteps
    nev(rand(N,1)<sponr,t+1)=1;
    t=t+1;
end
sumwtrans =sum(nev,1);% complete spike count series
S=sumwtrans(trans+1:end);% removing 1000 time steps of transience data

%To calculate the network entropy
% function: Entropy
% input-> Prob_den: Probability distribution of network activity S
% output-> H: Shannon Entropy
function H=Entropy(Prob_den)
H = - sum(Prob_den(Prob_den>0).*log2(Prob_den(Prob_den>0)));% shannon entropy

%To calculate the network entropy
% function: Connectivity_matrix
% input-> N: Network size; k: mean degree; randlist: random numbers from 1-N
% output-> B: connectivity matrix
function B=Connectivity_matrix(N,k,randlist)
```

```
% Setting up Connectivity Matrix
B=rand(N); % initialize as random matrix
imask=randlist<=0.1*N;       %setting fraction to set connectivity matrix at
criticality
B(:,imask)=-1*B(:,imask);   %set outgoing connection from inhibitory neurons
to be negative
B(rand(N)>k)=0;             %set mean degree
B=B/max(abs(eig(B)));       %enforce largest eigenvalue = 1
```

Main code

```
task=1;% Set 1 for figure 1 data; 2 for figure 2 and 3 for figure 3
rng('shuffle'); % randomize initial seed
N=10000;  %total number of neurons
T=21000; %duration of simulation
trans = 1000; % transient steps
%spontaneous activation rate
sponr=1/N/100; %one spike per 100 time steps among all neurons
k=0.01;%mean degree N*k
bins = linspace(0,1/N,1);% defining bin size for histogram of neural activity
[~,randlist] = sort(rand(1,N));% initiate random number list, preferably keep
it same
B=Connectivity_matrix(N,k,randlist); % Connectivity Matrix
B=abs(B); %make B non-negative to run inside alpha loop
if task==1
alphalist= 0.09:0.01:0.11;% list of alpha(fraction of inhibitory neurons)
Ifac= 1.25;% W_E(mean excitatory weight)
Efac= 1.25;%W_I(mean inhibitory weight)
for a=1:length(alphalist)
% Neural acitivity, S
S(:,a)=Neural_activity(N,T,trans,alphalist(a),randlist,Ifac,Efac,B,sponr)/N;
h = histc(S(:,a),bins); % make histogram to get S distribution
Prob(:,a) = h/(T-trans); % Probability P(S)
end
elseif task==2
% list of alpha(fraction of inhibitory neurons)
alphalist= [0.1,0.2]; % 0.01:0.01:0.36;
Efac= 1.25:0.25:3.25; % [1.5,2.5]; % W_E(mean excitatory weight)
Ifac= 1.25:0.25:3.25; % [1.5,2.5]; %W_I(mean inhibitory weight)
for a=1:length(alphalist)
for i=1:length(Ifac)
for e=1:length(Efac)
% Neural acitivity, S
S=Neural_activity(N,T,trans,alphalist(a),randlist,Ifac(i),Efac(e),B,sponr)/N;
h = histc(S,bins); % make histogram to get S distribution
Prob = h/(T-trans);% Probability P(S)
H(a,i,e) = Entropy(Prob); % Shannon entropy
end
end
end
elseif task==3
alphalist= 0.01:0.01:0.7;
Efac= 1.25:0.25:3.25;     % W_E(mean excitatory weight)
Ifac= 1.25:0.25:3.25;      %W_I(mean inhibitory weight)
for i=1:length(Ifac)
for e=1:length(Efac)
```

```
for a=1:length(alphalist)
% Neural acitivity, S
S=Neural_activity(N,T,trans,alphalist(a),randlist,Ifac(i),Efac(e),B,sponr)/N;
h = histc(S,bins); % make histogram to get S distribution
Prob = h/(T-trans);% Probability P(S)
H(a) = Entropy(Prob); % Shannon entropy
end
[MaxH(e,i),Max_idx] = max(H); % maximum entropy at fixed W_E and W_I
Alpha_crit(e,i) = alphalist(Max_idx);%critical alpha where entropy maximize
end
end
[Igrid,Egrid] = meshgrid(Efac,Ifac); % make grid-points
[nx,ny,nz] = surfnorm(Egrid,Igrid,A_crit);% normal vector at each grid point
%points normal*constant,c distance away
c=0.01;
% above normal
E1 = Egrid + nx*c; % excitatory weight
I1 = Igrid + ny*c; % inhibitory weight
A1 = A_crit + nz*c; % fraction of inhibitory neurons
% below normal
E2 = Egrid - nx*c; % excitatory weight
I2 = Igrid - ny*c; % inhibitory weight
A2 = A_crit - nz*c;% fraction of inhibitory neurons
% entropy values at both normal distances
for e=1:length(Efac)
for i=1:length(Ifac)
S=Neural_activity(N,T,trans,A1(e,i),randlist,I1(e,i),E1(e,i),B,sponr)/N;
h = histc(S,bins); % make histogram to get S distribution
Prob = h/(T-trans);% Probability P(S)
H1(e,i) = Entropy(Prob); % Shannon entropy
S=Neural_activity(N,T,trans,A2(e,i),randlist,I2(e,i),E2(e,i),B,sponr)/N;
h = histc(S,bins); % make histogram to get S distribution
Prob = h/(T-trans);% Probability P(S)
H2(e,i) = Entropy(Prob); % Shannon entropy
end
end
% fragility calculated at all W_E and W_I values
for e=1:length(Efac)
for i=1:length(Ifac)
Fragility(e,i)=((MaxH(e,i)-H1(e,i))+(MaxH(e,i)-H2(e,i)))/2;
end
end
else
disp('Enter 1, 2 or 3 only')
end
```

Codes for Chapter 3

Functions

```
%To calculate the dynamics of simple model
%Input-> l,b: lattice dimensions, Time: simulation time
%C: Coupling strength, p: probability of external activation
%Output-> lat: Lattice activity data as time series
%spkcnts: Spike counts time series
function [lat,spkcnts]=SimpleDynamics(l,b,Time,C,p)
nb_Con=[0 1 0; 1 1 1;0 1 0]; % Nearest-neighbor Connectivity
```

```
lat=false(l,b,Time); % neural network on 2D lattice (lXb) evolve over time
lat(:,:,1) = rand(l,b)<1; % initialize neural activity data matrix
spkcnts = single(zeros(l,b,Time)); % variable to store total spike input to a
neuron
for t=1:Time-1
% active neighbors based on the network activity
spkcnts(:,:,t)=conv2(squeeze(single(lat(:,:,t))),nb_Con,'same');
lat(:,:,t+1)=(1-(1-C).^spkcnts(:,:,t)*(1-p))>rand(l,b); % activation step
end

%To calculate the connectivity matrix for realistic model
%function: RealConnect
%Input-> l,b, dimensions of network lattice
%Output-> B: Connectivity Matrix
function B=RealConnect(l,b)
N=l*b; % Number of neurons
% short-range inhibition and long range excitation
xpos=[]; for i=1:l; xpos=[xpos; ones(l,1)*i]; end %x positions
ypos=[]; for i=1:b; ypos=[ypos; (1:b)']; end %y positions
dmat=squareform(pdist([xpos ypos])); %pairwise distances
Ilist = rand(N,1)<0.2;% 20% neurons set to inhibitory
C_E=2;C_I=3; %sigma for (ext./inh.) gaussian weight dist.
B=single(zeros(N));
B(:,~Ilist)=exp(-(dmat(:,~Ilist)/C_E).^2);% exct. weights
B(:,Ilist)=-exp(-(dmat(:,Ilist)/C_I).^2);% inh. weights
for bi=1:N
    B(bi,bi)=0;% no self-activation
end

%To calculate the dynamics of Realistic Model
%Input-> N: network size, Time: simulation time
%B: Connectivity Matrix
%Output-> nev: neural activity data as time series
%spkcnts: synaptic input time series
function [nev,syn_input]=RealisticDynamics(N,Time,B)
p_ext=5e-6;% external noise
Tau=80;% adaptation time constant
ref_parameter=1e-3; % refractory parameter
% Initialize variables
nev = false(N,Time); % variable to store neuronal activity
h=zeros(N,Time);% history time-series
syn_input = zeros(N,Time-1); % variable to store total spike input to a
neuron
nev(:,1) = rand(N,1)<1; % 1% activity
% initial simulation without adaptation
for t=1:490
syn_input(:,t)=(B*nev(:,t))+p_ext; % estimate synaptic input
nev(:,t+1)=syn_input(:,t)>rand(N,1); % activation based on synaptic input
end
% adaptation introduced after sufficient history is present
for t=491:Time-1
s_tau=sum(nev(:,t-Tau+1:t),2);
h(:,t)=s_tau+(s_tau==0); % estimate history of a neuron
syn_input(:,t)=((B*nev(:,t))./h(:,t))+p_ext; % synaptic input with adaptation
syn_input(nev(:,t),t)=ref_parameter*syn_input(nev(:,t),t); % refractory-ness
nev(:,t+1)=syn_input(:,t)>rand(N,1); % activation based on synaptic input
```

```
end

%To convert 1D neuron data to 2D lattice form
%Input-> nev: 1D time series; l,b: dimensions
%Output-> Lattice: 2D lattice time series
function lat = nev_to_lattice(nev,l,b)
for len=1:l
    for bre=1:b
        nev_pos = (len-1)*l + bre;
        lat(len,bre,:) = nev(nev_pos,:);% activity data in form of a lattice
    end
end

%PPMAKER Transform data into a point process
%   data is an (x,y,t) timeseries
%   zthresh is the number of SD to threshold above or below
%  Returns a thresholded version and a point process version.
%  NOTE: if zthresh is negative ALL DATA WILL BE INVERTED (data=-data)
%  to facilitate thresholding and also subsequent calculations of
%  magnitude
%  NOTE: amended by Greg to be more flexible
%  NOTE: "point process" has subtly different meaning in Enzo's paper,
%  i.e. whether a voxel is 'on' if it CROSSES from < to > 1SD, or whether
%  we just mean >1SD
function [ pp, thresh ] = ppmaker( data, zthresh )
if nargin <2
    zthresh = 1;
end
thresh = zeros(size(data));
zimg = zscore(data, 0, 3); % transform to zstats voxelwise
for t=1:size(data,3)
if zthresh < 0
thresh(:,:,t) = (zimg(:,:,t) < zthresh);
else
thresh(:,:,t) = (zimg(:,:,t) > zthresh);
end
end
% point process forces only the 'moment' threshold crossing occurs to be on
pp=cat(3, thresh(:,:,1), ...
    and( thresh(:,:,2:end), not(thresh(:,:,1:(end-1)))));
end

%To get data from expt readings and convert to lattice data
%function-> ExptData
%Input-> ExptNum, Experiment number 2 to 10,
%fileNum, file number for each expt.; zthresh: threshold on voltage signal
%Output-> lattice and (nev) 1D time series of point-process neural data
function [lattice,nev]=ExptData(ExptNum,fileNum,zthresh)
if exist('brainWindow')==0
    load('brain_window.mat');
end
fname = sprintf('%s%03d%s%d%s','Exp',ExptNum,'_',fileNum,'Data.mat');
load(fname);
% point process binary data and thresholded binary data
[ pp, thresh ] = ppmaker( ratioSequenceFiltered, zthresh);
pp=single(pp(:,:,201:end));
l=192;b=128;
```

```
Time=size(pp,3);
lattice=false(l,b,Time);
nev=false(l*b,Time);
% filtering the data by brain window
for t=1:Time
    pp_step1=logical(pp(:,:,t).*brainWindow);
    pp_step2=pp_step1(21:212,100:227);%;
    lattice(:,:,t)=pp_step2;
    % converting lattice to 1D data
    nev(:,t)=pp_step2(:);
end

% To estimate zeta_min and k,x0 corresponding to it
% function-> Zeta_calculation
% Input-> h_nume, h_deno: fine scale spike counts
% h_nume_k1, h_deno_k1: course scale spike counts
% k,x0: arrays for transformation scheme parameters
% task: choose option for simple model or others
function
[Zeta_min,k_zetamin,x0_zetamin]=Zeta_calculation(h_nume,h_deno,h_nume_k1,h_de
no_k1,k,x0,task)
bins=linspace(0,5,6); % n-counts bins
% activation probability at fine scale
for nn=1:length(bins)
if h_deno(nn)==0
phi(nn)= 0;
else
phi(nn)= h_nume(nn)/h_deno(nn);
end
end
% activation probability at coarse scale for different transformational
% scheme(different (k,x0) value combinations)
for ii=1:length(k)
for jj=1:length(x0)
for nn=1:length(bins)
if h_deno_k1(nn,ii,jj)==0
phi_k1(nn,ii,jj)= 0;
else
phi_k1(nn,ii,jj)= h_nume_k1(nn,ii,jj)/h_deno_k1(nn,ii,jj);
end
end
% zeta calculations from phi and phi_k1
for nn=1:length(bins)
zeta_n(nn) = abs(phi(nn)-phi_k1(nn,ii,jj));
end
if task==4
zeta(ii,jj) = sum(zeta_n);
else
zeta(ii,jj) = sum(zeta_n(2:end-1));
end
end
end
% minima of zeta
Zeta_min=min(min(zeta));
for ii=1:length(k)
for jj=1:length(x0)
if zeta(ii,jj)==Zeta_min
```

```
k_zetamin = k(ii); % k for zeta min
x0_zetamin = x0(jj); % x0 for zeta min
end
end
end

function [ dilatedvoxels ] = dilator2(voxels, sz)
% Faster version of dilator
    [x, y] = ind2sub(sz,voxels');
    xs = [ x-1, x, x+1, x-1,  x+1, x-1, x, x + 1];
    ys = [ y-1, y-1, y-1, y,  y, y+1, y+1, y+1];
    inx = (xs > 0) & (xs <= sz(1));
    iny = (ys > 0) & (ys <= sz(2));
    in = inx & iny;
    dilatedvoxels = unique([voxels', sub2ind(sz, xs(in), ys(in))])';
end

function C = fastintersect(A,B)
if ~isempty(A)&&~isempty(B)
   P = zeros(1, max(max(A),max(B)) ) ;
   P(A) = 1;
   C = B(logical(P(B)));
else
    C = [];
end

function [ ava cl ] = avalanche(pp)
%LOCALAVALANCHEFINDER Compute cluster and avalanche data from a point process
% pp is a (x,y,t) point process timecourse
%
% This function returns a description of clusters (cl)
% and avalanches (av) detected in pp
%
% cl.C is a cell array of clusters (connected components) at each t
% cl.AV is a cell array of active voxel ids at each t
% cl.Lab is a 4D timecourse where (x,y,z,t) is a cluster label
% cl.N is a vector of the number of clusters at each t
% cl.A is a vector of the number of active voxels at each t
% cl.P is a vector of the order parameter (size of the largest cluster) at
% each t
% cl.Pmag is a vector of the order parameter (size of the largest cluster)
% at each t based on MAGNITUDE of the values within it
% cl.S is a vector of the frequency of cluster sizes 1..(x*y*z)
% cl.D is a cell array of the fractal dimensions of clusters at each t
%   ** D is EXPERIMENTAL **
% ava.N is the number of avalanches detected in total
% ava.O is a vector of time of onset of each avalanche
% ava.L is a vector of the duration of each avalanche
% ava.S is a vector of the size of each avalanche
% ava.St is a cell array of the size of each avalanche over time
% ava.M is a vector of the maximum size
% ava.A{i}{t} is a cell array of the voxel ids belonging to each avalanche i
% at each time point for that avalanche
% by Gregory Scott (gregory.scott99@imperial.ac.uk)
% based on Tagliazucchi et al, Frontiers in Physiology, 2012
%-------------------------------------------------------------------------
```

```
% Cluster analysis
cl.ImageSize = [ size(pp,1) size(pp,2) ];
cl.S = zeros(size(pp,1) * size(pp,2),1); % create a frequency table for
cluster sizes in VOXELS
clusterim = zeros(size(pp(:,:,1))); % create a volume for box counting
for t=1:size(pp, 3) % iterate over pp timecourse
im = squeeze(pp(:,:,t)); % pull out image at this time point
ConComp = bwconncomp(im); % find connected components
cl.C{t} = ConComp; % store the clusters (connected components)
cl.N(t) = ConComp.NumObjects; % number of clusters
cl.A(t) = nnz(im); % number of active sites
cl.AV{t} = vertcat(ConComp.PixelIdxList{:}); % list of voxel ids
%cl.P(t) = 0; % size of largest cluster by VOXELS (start at zero)
%cl.Pmag(t) = 0; % size of largest cluster by AMPLITUDES
%cl.D{t} = []; % fractal dimensions
labelim = zeros(size(pp(:,:,1))); % create a volume for labelling
% iterate over each cluster, recording the statistics
for i=1:ConComp.NumObjects
sz = length(ConComp.PixelIdxList{i}); % size of cluster in VOXELS
% calculate size of cluster in MAGNITUDE
clMag{t,i} = sum(im(ConComp.PixelIdxList{i}));
cl.S(sz) = cl.S(sz) + 1; % update frequency counts for size
%cl.P(t) = max(cl.P(t), sz); % update size of largest cluster by VOXELS
%cl.Pmag(t) = max(cl.Pmag(t), clMag{t,i}); % update by MAGNITUDE
labelim(ConComp.PixelIdxList{i}) = i; % light up labels
%if(sz == 1) % box counting unnecessary if single voxel
%cl.D{t} = [ cl.D{t} 2 ]; % assume dimension = 3 (?)
%else % box counting and fractal dimension
%% light up voxels for this cluster in a temporary image
%clusterim(ConComp.PixelIdxList{i}) = 1;
%% fd = boxcounterik(trimmask(clusterim)); % box count
%clusterim(ConComp.PixelIdxList{i}) = 0; % turn off the cluster
%%   cl.D{t} = [ cl.D{t} fd ]; % store the fractal dimension
%end
end
cl.Lab(:,:,t) = labelim; % store cluster labelling for this time point
end
%-------------------------------------------------------------------------
% Avalanche analysis v2 - working backwards
%Let Cti be the ith cluster at time t. We consider a cluster i0 starting an
%avalanche at time t0 if for all j,
%Ct0?1j n Ct0i0 = 0 (i.e., no clusters were present in that region at the
previous timestep)
% An id is assigned to this avalanche and the same id is assigned to all
%clusters intersecting this cluster at the following time,this is all
%clusters i such that
%     Ct0i0 ? Ct0+1i != ?.
%The same procedure is applied recursively to all clusters satisfying the
%former condition until no more intersections are found. When this happens,
%all clusters labeled with this id constitute the avalanche.
ava.N = 0; % avalanche counter (and identifier)
for t=2:size(pp,3)
for i = 1:cl.C{t}.NumObjects
% iterate over clusters at this time point is this cluster the start of a new
%avalanche? to be one, all the voxels in the cluster must have been off in
%the previous time point AND ALL VOXELS ADJACENT TO THE CLUSTER (ELSE THEY
%WOULD HAVE BEEN IN THE AVALANCHE AND SO NOT MARK THE START OF A NEW AVA)
```

```
% Get the voxels in the cluster
voxels = cl.C{t}.PixelIdxList{i};
% dilate the cluster by one voxel
voxels2 = dilator2(voxels, cl.ImageSize);
% Test whether the cluster intersects with no active voxels at the previous
time point. TO DO: might be faster just to do something like
% img=pp(:,:,t-1); img(voxels) == 0;
if(isempty(fastintersect(voxels2, cl.AV{t-1})))
% this must be a new avalanche to track
ava.N = ava.N + 1; % increment avalanche counter
id = ava.N;
ava.O(id) = t; % record time of onset
ava.S(id) = length(voxels); % record number of VOXELS
%ava.Smag(id) = clMag{t,i}; % record size in MAGNITUDE
%ava.St{id}(1) = length(voxels);
%ava.L(id) = 1; % record duration (start at 1)
% TO DO: uncomment this if ever required (slow!)
% ava.A{id, 1} = voxels; % record ids of voxels at avalanche onset
% ava.Voxels{id} = voxels;
% track this avalanche through time and see which clusters intersect it and
%when it comes to an end
for t2 = (t+1):size(pp,3)
% see if there is any intersection of the voxels of the avalanche from the
%previous time point with any active voxels in the present dilate the
%avalanche by one voxel before checking for intersections
voxels = dilator2(voxels, cl.ImageSize);
% use the labelling lookup volume to find intersecting clusters
labelim = squeeze(cl.Lab(:,:,t2));
intersectingids = labelim(voxels);
% are any labels non-zero (i.e. clusters)?
if(any(intersectingids))
% the avalanche has survived this time point!
% ava.L(id) = t2 - t; % record new duration
% remove zeros (shouldnt be any) and duplicate labels
intersectingids = unique(intersectingids(intersectingids > 0));
%intersectingids is a list of unique clusters ids which have contiguity with
%the (dilated) avalanche, so we extend the avalanche to include all voxels in
%these clusters (i.e. the avalanche propagates)
newvoxels = vertcat(cl.C{t2}.PixelIdxList{intersectingids});
% TO DO: uncomment this if ever required (slow!)
% ava.A{id, (t2-t) + 1} = newvoxels; % store the new voxels
% ava.Voxels{id} = [ ava.Voxels{id}; newvoxels ];
% AVA SIZE USING NUMBER OF ACTIVE PIXELS IN AVA AT EVERY TIME POINT
ava.S(id) = ava.S(id) + length(newvoxels);
% Calculate new size in magnitude
%ava.Smag(id) = ava.Smag(id) + sum([clMag{t2,intersectingids}]);
% store the progression in size over time
% TO DO: this is duplicating the role of ava.A
% ava.St{id}((t2-t) + 1) = length(newvoxels);
voxels = newvoxels; % update the voxels for the next time point
else
%% NEW
%Calculate new ava S AVA SIZE USING UNIQUE PIXELS IN AVA AT ANY TIME POINT
%ava.S(id) = length(unique(ava.Voxels{id}));
%  ava.Voxels{id} = unique( ava.Voxels{id} );
break;
end
```

```
end
end
end
end
if ava.N == 0
ava.O = [];
ava.S = [];
% ava.St = [];
% ava.L = [];
ava.Voxels = [];
end
end
```

Main Code

```
task=1;
subtask=1;
rng('shuffle');
nb_Con=[0 1 0; 1 1 1;0 1 0];
if task==1
% Simple Model Avg S
% for spatiotemp. activity data call SimpleDynamics at C=0.2;0.23;0.3
C=0.15:0.01:0.35;
dim=400;%200
Time =1.6102e4; % simulation time
Trans=100;
%dimensions of initial lattice
l = dim; b = dim; N= l*b;
%Dynamical parameters
p = 0.001;
for Cstep=1:length(C)
[lattice,Spike_Counts]=SimpleDynamics(l,b,Time,C(Cstep),p);
AvgS(Cstep)=sum(sum(lattice(:,:,Trans+1:end)))/N;
end
elseif task==2
% Realistic Model mean correlation
% for spatiotemp. activity data call RealisticDynamics at I=0.01;0.65;2.0
Time = 1.65e4; % simulation time
dim=160;
l=dim;b=dim;N=l*b;
% Connectivity Matrix for realistic Model
B=RealConnect(l,b);
I=0.01:0.1:2.01;
for Istep=1:length(I)
% tuning inhibition
B_prime=B;
B_prime(:,Ilist)=I(Istep)*B_prime(:,Ilist);
[nev,synaptic_input]=RealisticDynamics(N,Time,B_prime);
subNev_spk=nev(:,501:end)';
CorrNev_spk=corr(subNev_spk);
MeanCor(Istep)= nanmean(abs(CorrNev_spk(:)));
S_spk(Istep)=mean(nev,1);
end
elseif task==3
% Expt Data lattice and mean correlation
% ExptNum: experiment number runs from 2 to 10; increasing time till drug
```

```
% FileNum: Multiple readings recorded at each ExptNum
ExptNum=2;FileNum=1;
load('brain_window.mat');
[lattice,nev]=ExptData(ExptNum,fileNum,zthresh,brainWindow);
S=squeeze(sum(sum(lattice,1),2));
% point process data correlation
subNev=nev';
CorrNev=corr(subNev);
CorrNev(isnan(CorrNev))=0;
MeanCor= nanmean(abs(CorrNev(:)));
elseif task==4
if subtask==1
% renormalization step
% done at each point in parameter space over 100 random realizations
% use the following piece to create data for 100 runs of same code
% combine all the data by running Zeta_calculation.m
% final answer calculated as zeta See equation.
dim=400;%200
Time =1.6102e4; % simulation time
Trans=100;
%dimensions of initial lattice
l = dim; b = dim; N= l*b;
% renormalization block length
%Dynamical parameters
p = 0.001;%0.01;0.0001;
C=0.23;%0.15:0.01:0.35;
% transformational scheme parameters
r=8;%4;16; % spatial dimension of transformational block
time_r=1;%2;4;8;16; % temporal dimension of transformational block
k=1:5:101; % steepness of transformation function f(S_b)
x0=0.01:0.02:1; % mid point of transfromation function f(S_b)
h_nume_k1=zeros(length(bins),length(k),length(x0));
h_deno_k1=zeros(length(bins),length(k),length(x0));
[Lattice,Spike_Counts]=SimpleDynamics(l,b,Time,C,p);
elseif subtask==2
Time = 1.65e4; % simulation time
dim=160;
l=dim;b=dim;N=l*b;
nb_Con=[0 1 0; 1 1 1;0 1 0]; % connectivity nearest-neighbor for activation
probability
%Dynamical parameters
I=0.6;%0.01:0.1:2.01
% transformational scheme parameters
r=8;%4;16; % spatial dimension of transformational block
time_r=1;%2;4;8;16; % temporal dimension of transformational block
k=1:5:101; % steepness of transformation function f(S_b)
x0=0.01:0.02:1; % mid point of transfromation function f(S_b)
% Connectivity Matrix for realistic Model
B=RealConnect(l,b);
% tuning inhibition
B(:,Ilist)=I*B(:,Ilist);
% initial simulation without adaptation
[nev,synaptic_input]=RealisticDynamics(N,Time,B);
% to use the spiking data for zeta calculation
Lattice=nev_to_lattice(nev(:,501:end),l,b); % convert data dimensions
% to use the continous synaptic data for zeta calculation
```

```
% %Syn_Lattice=nev_to_lattice(synaptic_input(:,501:end),l,b); % convert data
dimensions
% %zthresh=0.5;
% %Lattice=ppmaker(Syn_Lattice , zthresh);
% active neighbors based on the network activity
Spike_Counts=convn(squeeze(single(Lattice(:,:,1:end-1))),nb_Con,'same');
elseif subtask==3
ExptNum=2;FileNum=1;
load('brain_window.mat');
[Lattice,nev]=ExptData(ExptNum,fileNum,zthresh,brainWindow);
Spike_Counts=convn(squeeze(single(Lattice(:,:,1:end-1))),nb_Con,'same');
end
[h_nume,h_deno]=nt_counts(Spike_Counts(:,:,Trans+1:end-
1),Lattice(:,:,Trans+2:end));
for ii=1:length(k)
for jj=1:length(x0)
[h_nume_k1(:,ii,jj),h_deno_k1(:,ii,jj)]=Renormalization(lattice(:,:,Trans+1:e
nd),r,time_r,k(ii),x0(jj),nb_Con);
end
end
%%%%%%%%%%%%%%%%%%%%%%%%%%%%zeta_min calculation%%%%%%%%%%%%%%%%
mean_h_nume=squeeze(mean(h_nume,2));
mean_h_deno=squeeze(mean(h_deno,2));
mean_h_nume_k1=squeeze(mean(h_nume_k1,2));
mean_h_deno_k1=squeeze(mean(h_deno_k1,2));
[Zeta_min,k_zetamin,x0_zetamin]=Zeta_calculation(mean_h_nume,mean_h_deno,mean
_h_nume_k1,mean_h_deno_k1,k,x0,task);
elseif task==5
% avalanche distribution and kappa calculation
% for realistic model model resuse the second half
% with Lattice generated from codes already explained
C=0.15:0.01:0.25;
dim=400;%200
Time =1.6102e4; % simulation time
Trans=100;
%dimensions of initial lattice
l = dim; b = dim; N= l*b;
% renormalization block length
%Dynamical parameters
p = 0.001;
for Cstep=1:length(C)
[lattice,~]=SimpleDynamics(l,b,Time,C(Cstep),p);
%%% %%%%%%%%Second half: avalanche distribution%%%% size and duration%%%%%
data=lattice(:,:,Trans+1:end);
[avalanche,~]=avalanche(data);
avsz=avalanche.S;
nav=avalanche.N;
xmin=min(avsz);
xmax=max(avsz);
dat=avsz(avsz>=xmin);
n=length(dat);
expon=1.5;
refcdf=((xmin:xmax).^(1-expon)-xmin^(1-expon))/(xmax^(1-expon)-xmin^(1-
expon)); %reference CDF
datcdf = cumsum(hist(dat,xmin:xmax)./n); %data CDF
ndiff=10;
xlist=round(logspace(log10(xmin*1.1),log10(xmax/1.1),ndiff));
```

```
kappa=1+sum(refcdf(xlist-xmin+1)-datcdf(xlist-xmin+1))/ndiff;
%plot avalanche size PDF
binv=unique(round(logspace(log10(xmin),log10(xmax),20*log10(xmax/xmin))));
nb=length(binv)-1;
num=histc(avsz,binv);
Avalanche_data{Cstep}=avsz;
Kappa_data(Cstep)=kappa;
if Cstep==1
loglog(binv(1:nb)+diff(binv),num(1:nb)./diff(binv)/nav,'k')
hold on;
elseif Cstep==2
loglog(binv(1:nb)+diff(binv),num(1:nb)./diff(binv)/nav,'r')
hold on;
elseif Cstep==3
loglog(binv(1:nb)+diff(binv),num(1:nb)./diff(binv)/nav,'b')
hold on;
elseif Cstep==4
loglog(binv(1:nb)+diff(binv),num(1:nb)./diff(binv)/nav,'g')
hold on;
elseif Cstep==5
loglog(binv(1:nb)+diff(binv),num(1:nb)./diff(binv)/nav,'c')
hold on;
end
clear avalanche
end
else
    disp('Enter between 1 to 6 only');
end
```

Codes for Chapter 4

Experimental data-analysis code

```
load('SpikeData.mat');
load('FirstHalfEndTime.mat')
for i=1:20
    if i~=15
       r0= sum(Spike_bicd_Rat3{i}(:,1:floor(TimeSecRat3(i,1))),2);
       r1= sum(Spike_bicd_Rat3{i}(:,ceil(TimeSecRat3(i,1))+1:end),2);
       Delta.Rat3.bicd.SpikeRate{i}=(r1-r0)./(r1+r0);
       Delta.Rat3.bicd.TotalSpikeRate{i}=(sum(r1)-
sum(r0))./(sum(r1)+sum(r0));
    end
end
for i=1:20
       r0= sum(Spike_muscd_Rat3{i}(:,1:floor(TimeSecRat3(i,2))),2);
       r1= sum(Spike_muscd_Rat3{i}(:,ceil(TimeSecRat3(i,2))+1:end),2);
       Delta.Rat3.muscd.SpikeRate{i}=(r1-r0)./(r1+r0);
       Delta.Rat3.muscd.TotalSpikeRate{i}=(sum(r1)-
sum(r0))./(sum(r1)+sum(r0));
end
for i=1:12
       r0= sum(Spike_bicd_Rat4{i}(:,1:floor(TimeSecRat4(i,1))),2);
       r1= sum(Spike_bicd_Rat4{i}(:,ceil(TimeSecRat4(i,1))+1:end),2);
       Delta.Rat4.bicd.SpikeRate{i}=(r1-r0)./(r1+r0);
```

```
        Delta.Rat4.bicd.TotalSpikeRate{i}=(sum(r1)-
sum(r0))./(sum(r1)+sum(r0));
end
for i=1:12
        r0= sum(Spike_muscd_Rat4{i}(:,1:floor(TimeSecRat4(i,2))),2);
        r1= sum(Spike_muscd_Rat4{i}(:,ceil(TimeSecRat4(i,2))+1:end),2);
        Delta.Rat4.muscd.SpikeRate{i}=(r1-r0)./(r1+r0);
        Delta.Rat4.muscd.TotalSpikeRate{i}=(sum(r1)-
sum(r0))./(sum(r1)+sum(r0));
end
for i=1:11
        r0= sum(Spike_bicd_Rat1{i}(:,1:floor(TimeSecRat1(i,1))),2);
        r1= sum(Spike_bicd_Rat1{i}(:,ceil(TimeSecRat1(i,1))+1:end),2);
        Delta.Rat1.bicd.SpikeRate{i}=(r1-r0)./(r1+r0);
        Delta.Rat1.bicd.TotalSpikeRate{i}=(sum(r1)-
sum(r0))./(sum(r1)+sum(r0));
end
for i=1:11
    if i~=6
         r0= sum(Spike_muscd_Rat1{i}(:,1:floor(TimeSecRat1(i,2))),2);
         r1= sum(Spike_muscd_Rat1{i}(:,ceil(TimeSecRat1(i,2))+1:end),2);
         Delta.Rat1.muscd.SpikeRate{i}=(r1-r0)./(r1+r0);
         Delta.Rat1.muscd.TotalSpikeRate{i}=(sum(r1)-
sum(r0))./(sum(r1)+sum(r0));
    end
end
Concentrations=[20,40,80,160,320,640,1280];
%%%%%%%%%%%%%%%%%%%%%%%%Delta calculations using quarter of spike data
% Delta for Nodrug 1st half and Nodrug 2nd half
for i=1:20
    if i~=15

T1=TimeSecRat3(i,1)/2;T2=TimeSecRat3(i,1);T3=TimeSecRat3(i,1)+(size(Spike_bic
d_Rat3{i},2)-ceil(TimeSecRat3(i,1)))/2;
        r0_1q= sum(Spike_bicd_Rat3{i}(:,1:floor(T1)),2);
        r0_2q= sum(Spike_bicd_Rat3{i}(:,ceil(T1):floor(T2)),2);
        r1_3q= sum(Spike_bicd_Rat3{i}(:,ceil(T2):floor(T3)),2);
        r1_4q= sum(Spike_bicd_Rat3{i}(:,ceil(T3):end),2);
        Delta.Rat3.bicd.SpikeRate13{i}=(r1_3q-r0_1q)./(r1_3q+r0_1q);
        Delta.Rat3.bicd.SpikeRate23{i}=(r1_3q-r0_2q)./(r1_3q+r0_2q);
        Delta.Rat3.bicd.SpikeRate14{i}=(r1_4q-r0_1q)./(r1_4q+r0_1q);
        Delta.Rat3.bicd.SpikeRate24{i}=(r1_4q-r0_2q)./(r1_4q+r0_2q);
        Delta.Rat3.bicd.TotalSpikeRate13{i}=(sum(r1_3q)-
sum(r0_1q))./(sum(r1_3q)+sum(r0_1q));
        Delta.Rat3.bicd.TotalSpikeRate23{i}=(sum(r1_3q)-
sum(r0_2q))./(sum(r1_3q)+sum(r0_2q));
        Delta.Rat3.bicd.TotalSpikeRate14{i}=(sum(r1_4q)-
sum(r0_1q))./(sum(r1_4q)+sum(r0_1q));
        Delta.Rat3.bicd.TotalSpikeRate24{i}=(sum(r1_4q)-
sum(r0_2q))./(sum(r1_4q)+sum(r0_2q));
    end
end
for i=1:20

T1=TimeSecRat3(i,2)/2;T2=TimeSecRat3(i,2);T3=TimeSecRat3(i,2)+(size(Spike_mus
cd_Rat3{i},2)-ceil(TimeSecRat3(i,2)))/2;
    r0_1q= sum(Spike_muscd_Rat3{i}(:,1:floor(T1)),2);
```

```
    r0_2q= sum(Spike_muscd_Rat3{i}(:,ceil(T1):floor(T2)),2);
    r1_3q= sum(Spike_muscd_Rat3{i}(:,ceil(T2):floor(T3)),2);
    r1_4q= sum(Spike_muscd_Rat3{i}(:,ceil(T3):end),2);
    Delta.Rat3.muscd.SpikeRate13{i}=(r1_3q-r0_1q)./(r1_3q+r0_1q);
    Delta.Rat3.muscd.SpikeRate23{i}=(r1_3q-r0_2q)./(r1_3q+r0_2q);
    Delta.Rat3.muscd.SpikeRate14{i}=(r1_4q-r0_1q)./(r1_4q+r0_1q);
    Delta.Rat3.muscd.SpikeRate24{i}=(r1_4q-r0_2q)./(r1_4q+r0_2q);
    Delta.Rat3.muscd.TotalSpikeRate13{i}=(sum(r1_3q)-
sum(r0_1q))./(sum(r1_3q)+sum(r0_1q));
    Delta.Rat3.muscd.TotalSpikeRate23{i}=(sum(r1_3q)-
sum(r0_2q))./(sum(r1_3q)+sum(r0_2q));
    Delta.Rat3.muscd.TotalSpikeRate14{i}=(sum(r1_4q)-
sum(r0_1q))./(sum(r1_4q)+sum(r0_1q));
    Delta.Rat3.muscd.TotalSpikeRate24{i}=(sum(r1_4q)-
sum(r0_2q))./(sum(r1_4q)+sum(r0_2q));
end
for i=1:12

T1=TimeSecRat4(i,1)/2;T2=TimeSecRat4(i,1);T3=TimeSecRat4(i,1)+(size(Spike_bic
d_Rat4{i},2)-ceil(TimeSecRat4(i,1)))/2;
    r0_1q= sum(Spike_bicd_Rat4{i}(:,1:floor(T1)),2);
    r0_2q= sum(Spike_bicd_Rat4{i}(:,ceil(T1):floor(T2)),2);
    r1_3q= sum(Spike_bicd_Rat4{i}(:,ceil(T2):floor(T3)),2);
    r1_4q= sum(Spike_bicd_Rat4{i}(:,ceil(T3):end),2);
    Delta.Rat4.bicd.SpikeRate13{i}=(r1_3q-r0_1q)./(r1_3q+r0_1q);
    Delta.Rat4.bicd.SpikeRate23{i}=(r1_3q-r0_2q)./(r1_3q+r0_2q);
    Delta.Rat4.bicd.SpikeRate14{i}=(r1_4q-r0_1q)./(r1_4q+r0_1q);
    Delta.Rat4.bicd.SpikeRate24{i}=(r1_4q-r0_2q)./(r1_4q+r0_2q);
    Delta.Rat4.bicd.TotalSpikeRate13{i}=(sum(r1_3q)-
sum(r0_1q))./(sum(r1_3q)+sum(r0_1q));
    Delta.Rat4.bicd.TotalSpikeRate23{i}=(sum(r1_3q)-
sum(r0_2q))./(sum(r1_3q)+sum(r0_2q));
    Delta.Rat4.bicd.TotalSpikeRate14{i}=(sum(r1_4q)-
sum(r0_1q))./(sum(r1_4q)+sum(r0_1q));
    Delta.Rat4.bicd.TotalSpikeRate24{i}=(sum(r1_4q)-
sum(r0_2q))./(sum(r1_4q)+sum(r0_2q));
end
for i=1:12

T1=TimeSecRat4(i,2)/2;T2=TimeSecRat4(i,2);T3=TimeSecRat4(i,2)+(size(Spike_mus
cd_Rat4{i},2)-ceil(TimeSecRat4(i,2)))/2;
    r0_1q= sum(Spike_muscd_Rat4{i}(:,1:floor(T1)),2);
    r0_2q= sum(Spike_muscd_Rat4{i}(:,ceil(T1):floor(T2)),2);
    r1_3q= sum(Spike_muscd_Rat4{i}(:,ceil(T2):floor(T3)),2);
    r1_4q= sum(Spike_muscd_Rat4{i}(:,ceil(T3):end),2);
    Delta.Rat4.muscd.SpikeRate13{i}=(r1_3q-r0_1q)./(r1_3q+r0_1q);
    Delta.Rat4.muscd.SpikeRate23{i}=(r1_3q-r0_2q)./(r1_3q+r0_2q);
    Delta.Rat4.muscd.SpikeRate14{i}=(r1_4q-r0_1q)./(r1_4q+r0_1q);
    Delta.Rat4.muscd.SpikeRate24{i}=(r1_4q-r0_2q)./(r1_4q+r0_2q);
    Delta.Rat4.muscd.TotalSpikeRate13{i}=(sum(r1_3q)-
sum(r0_1q))./(sum(r1_3q)+sum(r0_1q));
    Delta.Rat4.muscd.TotalSpikeRate23{i}=(sum(r1_3q)-
sum(r0_2q))./(sum(r1_3q)+sum(r0_2q));
    Delta.Rat4.muscd.TotalSpikeRate14{i}=(sum(r1_4q)-
sum(r0_1q))./(sum(r1_4q)+sum(r0_1q));
    Delta.Rat4.muscd.TotalSpikeRate24{i}=(sum(r1_4q)-
sum(r0_2q))./(sum(r1_4q)+sum(r0_2q));
```

```
end
for i=1:11

T1=TimeSecRat1(i,1)/2;T2=TimeSecRat1(i,1);T3=TimeSecRat1(i,1)+(size(Spike_bic
d_Rat1{i},2)-ceil(TimeSecRat1(i,1)))/2;
    r0_1q= sum(Spike_bicd_Rat1{i}(:,1:floor(T1)),2);
    r0_2q= sum(Spike_bicd_Rat1{i}(:,ceil(T1):floor(T2)),2);
    r1_3q= sum(Spike_bicd_Rat1{i}(:,ceil(T2):floor(T3)),2);
    r1_4q= sum(Spike_bicd_Rat1{i}(:,ceil(T3):end),2);
    Delta.Rat1.bicd.SpikeRate13{i}=(r1_3q-r0_1q)./(r1_3q+r0_1q);
    Delta.Rat1.bicd.SpikeRate23{i}=(r1_3q-r0_2q)./(r1_3q+r0_2q);
    Delta.Rat1.bicd.SpikeRate14{i}=(r1_4q-r0_1q)./(r1_4q+r0_1q);
    Delta.Rat1.bicd.SpikeRate24{i}=(r1_4q-r0_2q)./(r1_4q+r0_2q);
    Delta.Rat1.bicd.TotalSpikeRate13{i}=(sum(r1_3q)-
sum(r0_1q))./(sum(r1_3q)+sum(r0_1q));
    Delta.Rat1.bicd.TotalSpikeRate23{i}=(sum(r1_3q)-
sum(r0_2q))./(sum(r1_3q)+sum(r0_2q));
    Delta.Rat1.bicd.TotalSpikeRate14{i}=(sum(r1_4q)-
sum(r0_1q))./(sum(r1_4q)+sum(r0_1q));
    Delta.Rat1.bicd.TotalSpikeRate24{i}=(sum(r1_4q)-
sum(r0_2q))./(sum(r1_4q)+sum(r0_2q));
end
for i=1:11
    if i~=6

T1=TimeSecRat1(i,2)/2;T2=TimeSecRat1(i,2);T3=TimeSecRat1(i,2)+(size(Spike_mus
cd_Rat1{i},2)-ceil(TimeSecRat1(i,2)))/2;
        r0_1q= sum(Spike_muscd_Rat1{i}(:,1:floor(T1)),2);
        r0_2q= sum(Spike_muscd_Rat1{i}(:,ceil(T1):floor(T2)),2);
        r1_3q= sum(Spike_muscd_Rat1{i}(:,ceil(T2):floor(T3)),2);
        r1_4q= sum(Spike_muscd_Rat1{i}(:,ceil(T3):end),2);
        Delta.Rat1.muscd.SpikeRate13{i}=(r1_3q-r0_1q)./(r1_3q+r0_1q);
        Delta.Rat1.muscd.SpikeRate23{i}=(r1_3q-r0_2q)./(r1_3q+r0_2q);
        Delta.Rat1.muscd.SpikeRate14{i}=(r1_4q-r0_1q)./(r1_4q+r0_1q);
        Delta.Rat1.muscd.SpikeRate24{i}=(r1_4q-r0_2q)./(r1_4q+r0_2q);
        Delta.Rat1.muscd.TotalSpikeRate13{i}=(sum(r1_3q)-
sum(r0_1q))./(sum(r1_3q)+sum(r0_1q));
        Delta.Rat1.muscd.TotalSpikeRate23{i}=(sum(r1_3q)-
sum(r0_2q))./(sum(r1_3q)+sum(r0_2q));
        Delta.Rat1.muscd.TotalSpikeRate14{i}=(sum(r1_4q)-
sum(r0_1q))./(sum(r1_4q)+sum(r0_1q));
        Delta.Rat1.muscd.TotalSpikeRate24{i}=(sum(r1_4q)-
sum(r0_2q))./(sum(r1_4q)+sum(r0_2q));
    end
end
DeltaLowConc.bicd.SpikeRate=Delta.Rat1.bicd.SpikeRate13{1};
DeltaLowConc.muscd.SpikeRate=Delta.Rat1.muscd.SpikeRate13{1};
DeltaLowConc.bicd.TotalSpikeRate=Delta.Rat1.bicd.TotalSpikeRate13{1};
DeltaLowConc.muscd.TotalSpikeRate=Delta.Rat1.muscd.TotalSpikeRate13{1};
for i=2:8

DeltaLowConc.bicd.SpikeRate=[DeltaLowConc.bicd.SpikeRate;Delta.Rat1.bicd.Spik
eRate13{i}];

DeltaLowConc.muscd.SpikeRate=[DeltaLowConc.muscd.SpikeRate;Delta.Rat1.muscd.S
pikeRate13{i}];
```

```
DeltaLowConc.bicd.TotalSpikeRate=[DeltaLowConc.bicd.TotalSpikeRate;Delta.Rat1
.bicd.TotalSpikeRate13{i}];

DeltaLowConc.muscd.TotalSpikeRate=[DeltaLowConc.muscd.TotalSpikeRate;Delta.Ra
t1.muscd.TotalSpikeRate13{i}];
end
for i=1:8

DeltaLowConc.bicd.SpikeRate=[DeltaLowConc.bicd.SpikeRate;Delta.Rat1.bicd.Spik
eRate14{i};Delta.Rat1.bicd.SpikeRate23{i};Delta.Rat1.bicd.SpikeRate24{i}];

DeltaLowConc.muscd.SpikeRate=[DeltaLowConc.muscd.SpikeRate;Delta.Rat1.muscd.S
pikeRate14{i};Delta.Rat1.muscd.SpikeRate23{i};Delta.Rat1.muscd.SpikeRate24{i}
];

DeltaLowConc.bicd.TotalSpikeRate=[DeltaLowConc.bicd.TotalSpikeRate;Delta.Rat1
.bicd.TotalSpikeRate14{i};Delta.Rat1.bicd.TotalSpikeRate23{i};Delta.Rat1.bicd
.TotalSpikeRate24{i}];

DeltaLowConc.muscd.TotalSpikeRate=[DeltaLowConc.muscd.TotalSpikeRate;Delta.Ra
t1.muscd.TotalSpikeRate14{i};Delta.Rat1.muscd.TotalSpikeRate23{i};Delta.Rat1.
muscd.TotalSpikeRate24{i}];
end
for i=1:6

DeltaLowConc.bicd.SpikeRate=[DeltaLowConc.bicd.SpikeRate;Delta.Rat4.bicd.Spik
eRate13{i};Delta.Rat4.bicd.SpikeRate14{i};Delta.Rat4.bicd.SpikeRate23{i};Delt
a.Rat4.bicd.SpikeRate24{i}];

DeltaLowConc.muscd.SpikeRate=[DeltaLowConc.muscd.SpikeRate;Delta.Rat4.muscd.S
pikeRate13{i};Delta.Rat4.muscd.SpikeRate14{i};Delta.Rat4.muscd.SpikeRate23{i}
;Delta.Rat4.muscd.SpikeRate24{i}];

DeltaLowConc.bicd.TotalSpikeRate=[DeltaLowConc.bicd.TotalSpikeRate;Delta.Rat4
.bicd.TotalSpikeRate13{i};Delta.Rat4.bicd.TotalSpikeRate14{i};Delta.Rat4.bicd
.TotalSpikeRate23{i};Delta.Rat4.bicd.TotalSpikeRate24{i}];

DeltaLowConc.muscd.TotalSpikeRate=[DeltaLowConc.muscd.TotalSpikeRate;Delta.Ra
t4.muscd.TotalSpikeRate13{i};Delta.Rat4.muscd.TotalSpikeRate14{i};Delta.Rat4.
muscd.TotalSpikeRate23{i};Delta.Rat4.muscd.TotalSpikeRate24{i}];
end
for i=1:6

DeltaLowConc.bicd.SpikeRate=[DeltaLowConc.bicd.SpikeRate;Delta.Rat3.bicd.Spik
eRate13{i};Delta.Rat3.bicd.SpikeRate14{i};Delta.Rat3.bicd.SpikeRate23{i};Delt
a.Rat3.bicd.SpikeRate24{i}];

DeltaLowConc.muscd.SpikeRate=[DeltaLowConc.muscd.SpikeRate;Delta.Rat3.muscd.S
pikeRate13{i};Delta.Rat3.muscd.SpikeRate14{i};Delta.Rat3.muscd.SpikeRate23{i}
;Delta.Rat3.muscd.SpikeRate24{i}];

DeltaLowConc.bicd.TotalSpikeRate=[DeltaLowConc.bicd.TotalSpikeRate;Delta.Rat3
.bicd.TotalSpikeRate13{i};Delta.Rat3.bicd.TotalSpikeRate14{i};Delta.Rat3.bicd
.TotalSpikeRate23{i};Delta.Rat3.bicd.TotalSpikeRate24{i}];

DeltaLowConc.muscd.TotalSpikeRate=[DeltaLowConc.muscd.TotalSpikeRate;Delta.Ra
```

```
t3.muscd.TotalSpikeRate13{i};Delta.Rat3.muscd.TotalSpikeRate14{i};Delta.Rat3.
muscd.TotalSpikeRate23{i};Delta.Rat3.muscd.TotalSpikeRate24{i}];
end
DeltaHighConc.bicd.SpikeRate=Delta.Rat1.bicd.SpikeRate13{9};
DeltaHighConc.muscd.SpikeRate=Delta.Rat1.muscd.SpikeRate13{9};
DeltaHighConc.bicd.TotalSpikeRate=Delta.Rat1.bicd.TotalSpikeRate13{9};
DeltaHighConc.muscd.TotalSpikeRate=Delta.Rat1.muscd.TotalSpikeRate13{9};
for i=10:11

DeltaHighConc.bicd.SpikeRate=[DeltaHighConc.bicd.SpikeRate;Delta.Rat1.bicd.Sp
ikeRate13{i}];

DeltaHighConc.muscd.SpikeRate=[DeltaHighConc.muscd.SpikeRate;Delta.Rat1.muscd
.SpikeRate13{i}];

DeltaHighConc.bicd.TotalSpikeRate=[DeltaHighConc.bicd.TotalSpikeRate;Delta.Ra
t1.bicd.TotalSpikeRate13{i}];

DeltaHighConc.muscd.TotalSpikeRate=[DeltaHighConc.muscd.TotalSpikeRate;Delta.
Rat1.muscd.TotalSpikeRate13{i}];
end
for i=9:11

DeltaHighConc.bicd.SpikeRate=[DeltaHighConc.bicd.SpikeRate;Delta.Rat1.bicd.Sp
ikeRate14{i};Delta.Rat1.bicd.SpikeRate23{i};Delta.Rat1.bicd.SpikeRate24{i}];

DeltaHighConc.muscd.SpikeRate=[DeltaHighConc.muscd.SpikeRate;Delta.Rat1.muscd
.SpikeRate14{i};Delta.Rat1.muscd.SpikeRate23{i};Delta.Rat1.muscd.SpikeRate24{
i}];

DeltaHighConc.bicd.TotalSpikeRate=[DeltaHighConc.bicd.TotalSpikeRate;Delta.Ra
t1.bicd.TotalSpikeRate14{i};Delta.Rat1.bicd.TotalSpikeRate23{i};Delta.Rat1.bi
cd.TotalSpikeRate24{i}];

DeltaHighConc.muscd.TotalSpikeRate=[DeltaHighConc.muscd.TotalSpikeRate;Delta.
Rat1.muscd.TotalSpikeRate14{i};Delta.Rat1.muscd.TotalSpikeRate23{i};Delta.Rat
1.muscd.TotalSpikeRate24{i}];
end
for i=7:12

DeltaHighConc.bicd.SpikeRate=[DeltaHighConc.bicd.SpikeRate;Delta.Rat4.bicd.Sp
ikeRate13{i};Delta.Rat4.bicd.SpikeRate14{i};Delta.Rat4.bicd.SpikeRate23{i};De
lta.Rat4.bicd.SpikeRate24{i}];

DeltaHighConc.muscd.SpikeRate=[DeltaHighConc.muscd.SpikeRate;Delta.Rat4.muscd
.SpikeRate13{i};Delta.Rat4.muscd.SpikeRate14{i};Delta.Rat4.muscd.SpikeRate23{
i};Delta.Rat4.muscd.SpikeRate24{i}];

DeltaHighConc.bicd.TotalSpikeRate=[DeltaHighConc.bicd.TotalSpikeRate;Delta.Ra
t4.bicd.TotalSpikeRate13{i};Delta.Rat4.bicd.TotalSpikeRate14{i};Delta.Rat4.bi
cd.TotalSpikeRate23{i};Delta.Rat4.bicd.TotalSpikeRate24{i}];

DeltaHighConc.muscd.TotalSpikeRate=[DeltaHighConc.muscd.TotalSpikeRate;Delta.
Rat4.muscd.TotalSpikeRate13{i};Delta.Rat4.muscd.TotalSpikeRate14{i};Delta.Rat
4.muscd.TotalSpikeRate23{i};Delta.Rat4.muscd.TotalSpikeRate24{i}];
end
for i=7:20
```

```
DeltaHighConc.bicd.SpikeRate=[DeltaHighConc.bicd.SpikeRate;Delta.Rat3.bicd.Sp
ikeRate13{i};Delta.Rat3.bicd.SpikeRate14{i};Delta.Rat3.bicd.SpikeRate23{i};De
lta.Rat3.bicd.SpikeRate24{i}];

DeltaHighConc.muscd.SpikeRate=[DeltaHighConc.muscd.SpikeRate;Delta.Rat3.muscd
.SpikeRate13{i};Delta.Rat3.muscd.SpikeRate14{i};Delta.Rat3.muscd.SpikeRate23{
i};Delta.Rat3.muscd.SpikeRate24{i}];

DeltaHighConc.bicd.TotalSpikeRate=[DeltaHighConc.bicd.TotalSpikeRate;Delta.Ra
t3.bicd.TotalSpikeRate13{i};Delta.Rat3.bicd.TotalSpikeRate14{i};Delta.Rat3.bi
cd.TotalSpikeRate23{i};Delta.Rat3.bicd.TotalSpikeRate24{i}];

DeltaHighConc.muscd.TotalSpikeRate=[DeltaHighConc.muscd.TotalSpikeRate;Delta.
Rat3.muscd.TotalSpikeRate13{i};Delta.Rat3.muscd.TotalSpikeRate14{i};Delta.Rat
3.muscd.TotalSpikeRate23{i};Delta.Rat3.muscd.TotalSpikeRate24{i}];
end
bins=linspace(-1,1,11);
h.LowConc.bicd.SpikeRate=hist(DeltaLowConc.bicd.SpikeRate,bins)/length(DeltaL
owConc.bicd.SpikeRate);
h.LowConc.muscd.SpikeRate=hist(DeltaLowConc.muscd.SpikeRate,bins)/length(Delt
aLowConc.muscd.SpikeRate);
h.LowConc.bicd.TotalSpikeRate=hist(DeltaLowConc.bicd.TotalSpikeRate,bins)/len
gth(DeltaLowConc.bicd.TotalSpikeRate);
h.LowConc.muscd.TotalSpikeRate=hist(DeltaLowConc.muscd.TotalSpikeRate,bins)/l
ength(DeltaLowConc.muscd.TotalSpikeRate);
h.HighConc.bicd.SpikeRate=hist(DeltaHighConc.bicd.SpikeRate,bins)/length(Delt
aHighConc.bicd.SpikeRate);
h.HighConc.muscd.SpikeRate=hist(DeltaHighConc.muscd.SpikeRate,bins)/length(De
ltaHighConc.muscd.SpikeRate);
h.HighConc.bicd.TotalSpikeRate=hist(DeltaHighConc.bicd.TotalSpikeRate,bins)/l
ength(DeltaHighConc.bicd.TotalSpikeRate);
h.HighConc.muscd.TotalSpikeRate=hist(DeltaHighConc.muscd.TotalSpikeRate,bins)
/length(DeltaHighConc.muscd.TotalSpikeRate);
subplot(2,2,1)
Column(:,1)=h1stHalf.All.bicd.SpikeRate;
Column(:,2)=hLC160.LowConc.bicd.SpikeRate;
Column(:,3)=hHC160.HighConc.bicd.SpikeRate;
imagesc(1:1:3,bins,Column);
title('bicd-Single Neuron Spike Rate')
subplot(2,2,2)
Column(:,1)=h1stHalf.All.muscd.SpikeRate;
Column(:,2)=hLC160.LowConc.muscd.SpikeRate;
Column(:,3)=hHC160.HighConc.muscd.SpikeRate;
imagesc(1:1:3,bins,Column);
title('muscd-Single Neuron Spike Rate')
subplot(2,2,3)
Column(:,1)=h1stHalf.All.bicd.TotalSpikeRate;
Column(:,2)=hLC160.LowConc.bicd.TotalSpikeRate;
Column(:,3)=hHC160.HighConc.bicd.TotalSpikeRate;
imagesc(1:1:3,bins,Column);
title('bicd-Total Neuron Spike Rate')
subplot(2,2,4)
Column(:,1)=h1stHalf.All.muscd.TotalSpikeRate;
Column(:,2)=hLC160.LowConc.muscd.TotalSpikeRate;
Column(:,3)=hHC160.HighConc.muscd.TotalSpikeRate;
imagesc(1:1:3,bins,Column);
```

```
title('muscd-Total Neuron Spike Rate');
%%%%%%%%%%%%%%%%%%%%%%%%%%%%%%%%%%%%
subplot(2,2,1)
Column(:,1)=h1stHalf.All.bicd.SpikeRate;
Column(:,2)=hLC80.LowConc.bicd.SpikeRate;
Column(:,3)=hHC80.HighConc.bicd.SpikeRate;
imagesc(1:1:3,bins,Column);
title('bicd-Single Neuron Spike Rate')
subplot(2,2,2)
Column(:,1)=h1stHalf.All.muscd.SpikeRate;
Column(:,2)=hLC80.LowConc.muscd.SpikeRate;
Column(:,3)=hHC80.HighConc.muscd.SpikeRate;
imagesc(1:1:3,bins,Column);
title('muscd-Single Neuron Spike Rate')
subplot(2,2,3)
Column(:,1)=h1stHalf.All.bicd.TotalSpikeRate;
Column(:,2)=hLC80.LowConc.bicd.TotalSpikeRate;
Column(:,3)=hHC80.HighConc.bicd.TotalSpikeRate;
imagesc(1:1:3,bins,Column);
title('bicd-Total Neuron Spike Rate')
subplot(2,2,4)
Column(:,1)=h1stHalf.All.muscd.TotalSpikeRate;
Column(:,2)=hLC80.LowConc.muscd.TotalSpikeRate;
Column(:,3)=hHC80.HighConc.muscd.TotalSpikeRate;
imagesc(1:1:3,bins,Column);
title('muscd-Total Neuron Spike Rate')

[~,bic_idx]=sort(Delta.Rat3.bicd.SpikeRate{2},'descend');
[~,musc_idx]=sort(Delta.Rat3.muscd.SpikeRate{3},'descend');
subplot(1,2,1)
imagesc(5:5:5*size(Spike_bicd_Rat3{2},2),1:1:size(Spike_bicd_Rat3{2},1),Spike
_bicd_Rat3{2}(bic_idx,:)/5)
subplot(1,2,2)
imagesc(5:5:5*size(Spike_muscd_Rat3{3},2),1:1:size(Spike_muscd_Rat3{3},1),Spi
ke_muscd_Rat3{3}(musc_idx,:)/5)


subplot(2,1,1)
imagesc(5:5:5*size(Spike_bicd_Rat3{2},2),1,mean(Spike_bicd_Rat3{2})/5)
subplot(2,1,2)
imagesc(5:5:5*size(Spike_muscd_Rat3{3},2),1,mean(Spike_muscd_Rat3{3})/5)

subplot(1,2,1)
plot(sort(Delta.Rat3.bicd.SpikeRate{2},'descend'),1:1:length(Delta.Rat3.bicd.
SpikeRate{2}));
hold on;
plot(ones(length(Delta.Rat3.bicd.SpikeRate{2}),1)*Delta.Rat3.bicd.TotalSpikeR
ate{2},1:1:length(Delta.Rat3.bicd.SpikeRate{2}),'--r');
subplot(1,2,2)
plot(sort(Delta.Rat3.muscd.SpikeRate{3},'descend'),1:1:length(Delta.Rat3.musc
d.SpikeRate{3}));
hold on;
plot(ones(length(Delta.Rat3.muscd.SpikeRate{3}),1)*Delta.Rat3.muscd.TotalSpik
eRate{3},1:1:length(Delta.Rat3.muscd.SpikeRate{3}),'--r');

for i=1:20
```

```
     if i~=15
plot(1/length(Delta.Rat3.bicd.SpikeRate{i}):1/length(Delta.Rat3.bicd.SpikeRat
e{i}):1,sort(Delta.Rat3.bicd.SpikeRate{i},'descend'));
          hold on;
     end
end

for i=1:20
plot(1/length(Delta.Rat3.muscd.SpikeRate{i}):1/length(Delta.Rat3.muscd.SpikeR
ate{i}):1,sort(Delta.Rat3.muscd.SpikeRate{i},'descend'));
          hold on;
end

for i=1:20
    Delta.Rat3.bicd.NeuronCount(i)=length(Delta.Rat3.bicd.SpikeRate{i});
    Delta.Rat3.muscd.NeuronCount(i)=length(Delta.Rat3.muscd.SpikeRate{i});
end
for i=1:11
    Delta.Rat1.bicd.NeuronCount(i)=length(Delta.Rat1.bicd.SpikeRate{i});
    Delta.Rat1.muscd.NeuronCount(i)=length(Delta.Rat1.muscd.SpikeRate{i});
end
for i=1:12
    Delta.Rat4.bicd.NeuronCount(i)=length(Delta.Rat4.bicd.SpikeRate{i});
    Delta.Rat4.muscd.NeuronCount(i)=length(Delta.Rat4.muscd.SpikeRate{i});
end
```

Model analysis-Function

```
%To simulate model dynamics for paradoxical change
%function: Connectivity_Matrix
%Input->N: size of network; p: connection probability
%Weights of "Inh_subfrac" fraction of inhibitory neurons  are increased
%by factor of Inh_Incre
%Output-> B: Connectivity matrix
function B=Connectivity_Matrix(N,p,Inh_subfrac,Inh_Incre)
Xe=[rand(N*N*0.8*p,1);zeros(N*N*0.8*(1-p),1)]; % random ext. weights
Xi=-[rand((N*N*0.2*p),1);zeros(N*N*0.2*(1-p),1)];% random inh. weights
Xe=Xe(randperm(N*N*0.8)); %reaarranging exct. entries
Xi=Xi(randperm(N*N*0.2)); %reaarranging inh. entries
Ye=reshape(Xe,[N,0.8*N]); % reshape 1D to 2D
Yi=reshape(Xi,[N,0.2*N]);
Y=[Ye,Yi]; % combine Exct. and Inh. columns
B=Y./max(abs(eig(Y))); % set max eigenvalue 1
B(:,800:800+Inh_subfrac)=Inh_Incre*B(:,800:800+Inh_subfrac);% create
inhomogeneity in inh. Weights

%To simulate model dynamics for paradoxical change
%function: ModelDynamics
%Input->T: simulation time; Trans: transient steps
%Del_I: change in inhibition factor; B: connectivity matrix
%Output-> nev: 1D Model time-series
function nev=ModelDynamics(T,Trans,extr,Del_I,B)
N=size(B,1);% size of network
imask=sum(B,1)<0; % index array for inhibitory neurons
```

```
nev=false(N,T);
%evolve dynamics
for t=1:Trans+(T-Trans)/2
    inp = B*nev(:,t)+extr; % synaptic input
    nev(:,t+1)= inp>rand(N,1); % activation step
end
B(:,imask)=B(:,imask)*Del_I; % changing all inhibitory weights
for t=1+Trans+(T-Trans)/2:T-1
    %determine who spikes at time t+1
    inp = B*nev(:,t)+extr; % synaptic input
    nev(:,t+1)= inp>rand(N,1); % activation step
end

%To calculate Delta from spike counts data
%function Delta
%input-> spkcnt: spike counts
%output-> delSpike,delTSpike: Delta values for neurons and population
function [delSpike,delTSpike]=Delta(spkcnt)
r1=sum(spkcnt(:,round(size(spkcnt,2)/2)+1:end),2);
r0=sum(spkcnt(:,1:round(size(spkcnt,2)/2)),2);
delSpike=(r1-r0)./(r1+r0);
delTSpike=(sum(r1)-sum(r0))./(sum(r1)+sum(r0));

%To generate Motif data from connectivity and delta data
%function Ilist_gen
%Input-> B: connectivity matrix, D: Delta values of neurons
%dset: index of target neurons
%Output-> Ilist_new: raw Motif data
function Ilist_new=Ilist_gen(dset,B,D)
Ilist=false(0,6);
q1=1;
wthresh=0.5; %threshold for deciding if a synapse is weak or strong
for i=dset
    inset=find(B(i,:)~=0);
    for j=inset
        inset2=find(B(j,:)~=0);
        for k=inset2
            Ilist(q1,1:2)=[B(i,j) B(j,k)]>0; %E or I (1 or 0)synapse weights
            Ilist(q1,3:4)=D([j k])>0; %delta + or - (1 or 0)
            Ilist(q1,5:6)=abs([B(i,j) B(j,k)])>wthresh; %synapse strong or
weak (1 or 0)
            q1=q1+1;
        end
    end
end
% readjusting Motif Matrix
Ilist_new(1)=Ilist(1);
Ilist_new(2)=Ilist(3);
Ilist_new(3)=Ilist(5);
Ilist_new(4)=Ilist(2);
Ilist_new(5)=Ilist(4);
Ilist_new(6)=Ilist(6);

%To estimate motif probabilities based on raw motif data
%function MotifP_calculation
%Input-> Ilist: raw motif data; All_Motifs: All possible motifs
%ens_count: number of realizations
```

```
function MotifProb=MotifP_calculation(Ilist,All_Motifs,ens_count)
MotifProb=zeros(64,ens_count);
for trials=1:ens_count
    [C,~,IC]=unique(Ilist,'rows');
    PMotif=histc(IC,1:max(IC))/sum(histc(IC,1:max(IC)));
    for i=1:64
        for j=1:size(C,1)
            if C(j,:)==All_Motifs(i,:)
                MotifProb(i)=PMotif(j);
            end
        end
    end
end

%Transform All_Motif matrix to fit the figure representation
function All_Motif_new=AllMotif_transform(All_Motifs)
All_Motif_new(:,1)=All_Motifs(:,6);
All_Motif_new(:,4)=All_Motifs(:,5);
All_Motif_new(:,2)=All_Motifs(:,4);
All_Motif_new(:,5)=All_Motifs(:,3);
All_Motif_new(:,3)=All_Motifs(:,2);
All_Motif_new(:,6)=All_Motifs(:,1);
All_Motif_new=double(All_Motif_new);
All_Motif_new((All_Motif_new(:,1)==1),1)=2;
All_Motif_new((All_Motif_new(:,1)==0),1)=1;
All_Motif_new((All_Motif_new(:,4)==1),4)=2;
All_Motif_new((All_Motif_new(:,4)==0),4)=1;
All_Motif_new((All_Motif_new(:,2)==0),2)=3;
All_Motif_new((All_Motif_new(:,2)==1),2)=4;
All_Motif_new((All_Motif_new(:,5)==0),5)=3;
All_Motif_new((All_Motif_new(:,5)==1),5)=4;
All_Motif_new((All_Motif_new(:,3)==0),3)=5;
All_Motif_new((All_Motif_new(:,3)==1),3)=6;
All_Motif_new((All_Motif_new(:,6)==0),6)=5;
All_Motif_new((All_Motif_new(:,6)==1),6)=6;
```

Main Code

```
rng('shuffle');
N=1000;% size of network
extr=0.8; %probability of firing due to random external input
times=50; %factor by which subset of inhibitory neuron weights are increased
T=1.1e5; %simulation time
Trans=1e4; % transient steps
p=0.01; %connection probability
InhNeuronEnhc=100; % subset of inhibitory neuron whose weights are increased
tbins=1:500:(T-Trans); % bins of 500 time steps over which spike count is
calculated
if task==1
Del_I=5;%0.5 %Overall network's Inhibitory signal modulation
B=Connectivity_Matrix(N,p,InhNeuronEnhc,times); % create connectivity matrix
nev=ModelDynamics(T,Trans,extr,Del_I,B); % simulate the dynamics
% estimate spike counts in 500 steps of timebins
spkcnt=zeros(N,length(tbins));
for i=1:N
spkcnt(i,:)=histc(find(nev(i,Trans+1:end)),tbins);
end
```

```
[deltaSpike,deltaTotalSpike]=Delta(spkcnt);% calculate delta values
% Plotting data for single cases
[~,idx]=sort(deltaSpike,'descend');
subset=(sum(isnan(deltaSpike))+1):1:1000;
subplot(2,1,1)
imagesc(500:500:500*tbins,subset-
sum(isnan(deltaSpike)),spkcnt(idx(subset),:));
subplot(2,1,2)
imagesc(500:500:500*tbins,1,sum(spkcnt(:,1:199))/N);
figure
plot(sort(deltaSpike,'descend'),1:1:1000);
hold on;
plot(ones(length(deltaSpike),1)*deltaTotalSpike,1:1:N,'--r');
elseif task==2
Del_I=[1,5,25,125];%[1,0.5,0.2,0.04,0.008];%
Deltabins=linspace(-1,1,11);% bins for Delta values to estimate probabilities
ens_count=100;% number of random network realizations
for trials=1:ens_count
B=Connectivity_Matrix(N,p,InhNeuronEnhc,times);
for j=1:length(Del_I)
nev=ModelDynamics(T,Trans,extr,Del_I(j),B);
spkcnt=zeros(N,length(tbins));
for i=1:N
spkcnt(i,:)=histc(find(nev(i,Trans+1:end)),tbins);
end
[deltaSpike(:,trials,j),deltaTotalSpike(trials,j)]=Delta(spkcnt);
end
end
% estimating delta probabilities for neurons and populations
for j=1:length(Del_I)
DeltaSpikeList=deltaSpike(:,:,j);
DeltaSpikeList=DeltaSpikeList(~isnan(DeltaSpikeList));
h_SpikeRate(:,j)=hist(DeltaSpikeList,Deltabins)/length(DeltaSpikeList);
DeltaTotalSpikeList=deltaTotalSpike(:,j);
DeltaTotalSpikeList=DeltaTotalSpikeList(~isnan(DeltaTotalSpikeList));

h_TotalSpikeRate(:,j)=hist(DeltaTotalSpikeList,Deltabins)/length(DeltaTotalSp
ikeList);
end
subplot(2,1,1)
imagesc(Del_I,Deltabins,h_SpikeRate);
title('Delta neuron spike rate');
subplot(2,1,2)
imagesc(Del_I,Deltabins,h_TotalSpikeRate);
title('Delta Population spike rate');
elseif task==3
%64 possible motifs (binary representation)
% 1 : EE, D=++, W=ss
% 2 : EE, D=++, W=sw
% 3 : EE, D=++, W=ws
% 4 : EE, D=++, W=ww
% 5 : EE, D=+-, W=ss
% 6 : EE, D=+-, W=sw
% 7 : EE, D=+-, W=ws
% 8 : EE, D=+-, W=ww
Del_I=5;%0.5
Deltabins=linspace(-1,1,11);
```

```
ens_count=1000;
for trials=1:ens_count
B=Connectivity_Matrix(N,p,InhNeuronEnhc,times);
nev=ModelDynamics(T,Trans,extr,Del_I,B);
spkcnt=zeros(N,length(tbins));
for i=1:N
spkcnt(i,:)=histc(find(nev(i,Trans+1:end)),tbins);
end
[deltaSpike(:,trials),deltaTotalSpike(trials)]=Delta(spkcnt);
%delta vector
D=deltaSpike(:,trials)';
dset=find(D>0.5);
%dset=find(D<-0.5);
randlist=randperm(N);
dset_random=randlist(1:length(dset));
Ilist{trials}=Ilist_gen(dset,B,D);% generate Input motif data from
paradoxical neurons
Ilist_rand{trials}=Ilist_gen(dset_random,B,D);% generate Input motif data
from randomly selected neurons
%find unique motifs and count them
for i=1:64
All_Motifs(i,:)=logical(de2bi(i-1,6)); % all possible input motifs cases
end
All_Motifs=flipud(All_Motifs);% adjustment of matrix
All_Motifs=fliplr(All_Motifs);
% calculate motif probabilities for Input to paradoxical neurons
MotifProb(:,trials)=MotifP_calculation(Ilist{trials},All_Motifs,ens_count);
% calculate motif probabilities for Input to randomly selected neurons
MotifProb_rand(:,trials)=MotifP_calculation(Ilist_rand{trials},All_Motifs,ens
_count);
end
% mean motif probabilities
meanMotifProb=mean(MotifProb,2);
meanMotifProb_rand=mean(MotifProb_rand,2);
%Kullback-Leibler KL Divergence using motif probabilities
KL_value=-meanMotifProb.*log(meanMotifProb_rand./meanMotifProb);
% ttest rejects the null hypothesis at the 5% significance level or p-value
<0.05.
% null hypothesis is for ttest(x,y) mean(x)=mean(y) without assuming equal
% variances
for i=1:64
[hvalue(i),pvalue(i)]=ttest2(MotifProb(i,:),MotifProb_rand(i,:),'Vartype','un
equal');
end
% Plotting data for top 95% of motif probabilites that exist in network
[Sorted,SortedLabel]=sort(abs(meanMotifProb),'descend');
for i=1:length(Sorted)
if (sum(Sorted(1:i))>=0.95)
i_final=i-1;
break;
end
end
meanMotifProb_Plot=meanMotifProb(SortedLabel(1:i_final));
meanMotifProb_rand_Plot=meanMotifProb_rand(SortedLabel(1:i_final));
KL_value_Plot=KL_value(SortedLabel(1:i_final));
All_Motifs_Plot=All_Motifs(SortedLabel(1:i_final),:);
SortedLabel_Plot=SortedLabel(1:i_final);
```

```
p_Plot=pvalue(SortedLabel(1:i_final));
All_Motif_new=AllMotif_transform(All_Motifs);
All_Motif_new_Plot=AllMotif_transform(All_Motifs_Plot);
figure
map=([1 0 0;0.4 0 0; 0 1 0;0 0.4 0;0 0 1;0 0 0.4]);
figure
subplot(2,1,1)
bar([meanMotifProb,meanMotifProb_rand]);
subplot(2,1,2)
imagesc(All_Motif_new');
colormap(map)
figure
subplot(2,1,1)
bar(KL_value_Plot);
subplot(2,1,2)
imagesc(All_Motif_new_Plot');
colormap(map)
else
disp('Enter 1,2 or 3 only')
end
```